

Spontaneous Symmetry Breaking in Projected Entangled Pair State models

Von der Fakultät für Mathematik, Informatik und
Naturwissenschaften der RWTH Aachen University zur Erlangung
des akademischen Grades eines Doktors der Naturwissenschaften
genehmigte Dissertation

vorgelegt von

Manuel Rispler, M.Sc.

aus Aachen

Berichter: Priv.-Doz. Dr. rer. nat. Norbert Schuch
Prof. Dr. rer. nat. Barbara M. Terhal

Tag der mündlichen Prüfung: 13. Juni 2017

Diese Dissertation ist auf den Internetseiten der
Hochschulbibliothek online verfügbar.

An meine Großeltern

*Elisabeth und Franz,
Rudolf und Gerhilde*

Abstract

In this thesis, we consider projected entangled pair state (PEPS) models as a framework for two-dimensional strongly-correlated quantum many body systems, where the global properties of the system are concisely encoded in one local tensor. While it was well known how to construct PEPS models with desired symmetries by manifestly encoding the symmetry in the local tensor, our goal in this work is to investigate whether this manifestly encoded symmetry can be spontaneously broken. By defining long-range order as a good criterion for symmetry breaking in a finite volume PEPS, we answer this question in the affirmative. A particularly attractive feature of PEPS models is that they have an exact holographic mapping, which is to say that the large system behavior is described by the “PEPS boundary”, given by the fixed point(s) of the so called transfer operator. We investigate the implications of long-range order and prove that it leads to a particular symmetry breaking pattern in the fixed point space. We find this pattern by first proving that long-range order implies an asymptotic degeneracy in the transfer operator and then identifying the symmetry breaking mechanism as the one which, from all possible boundary (-matrix) configurations, selects the configurations that correspond to *positive-semi-definite* matrices, i.e. one-dimensional *virtual* quantum states. We prove that these correspond to boundary configurations that do not mix under arbitrary perturbations and are thus stable. We study the entanglement properties of these virtual quantum states and show that they can be described by local entanglement Hamiltonians, establishing that also in phases with symmetry breaking, gapped quantum phases have an associated *local* entanglement Hamiltonian.

Zusammenfassung

In der vorliegenden Arbeit beschäftigen wir uns mit sogenannten PEPS Modellen (PEPS, engl. “projizierte verschränkte Paarzustände”) als Werkzeug zur Beschreibung und Analyse von stark korrelierten Quantenvielteilchensystemen. PEPS Modelle kodieren die *globalen* (Verschränktheits-)Eigenschaften in einem *lokalen* Tensor, insbesondere inklusive der Symmetrieeigenschaften. Ziel der vorliegenden Arbeit ist es, zu untersuchen, ob diese manifest kodierte Symmetrie spontan gebrochen werden kann. Indem wir langreichweitige Ordnung als geeignetes Kriterium für Symmetriebrechung in einem PEPS mit endlichem Volumen identifizieren, beantworten wir diese Frage affirmativ. Eine besonders attraktive Eigenschaft von PEPS Modellen ist, dass sie eine exakte holographische Abbildung ermöglichen, in der das zwei-dimensionale “Bulk“-System durch einen ein-dimensionalen “PEPS Rand” beschrieben wird, der auf dem Fixpunktraum des sogenannten Transferoperators lebt. Wir untersuchen die Implikationen von langreichweitiger Ordnung und beweisen, dass diese zu einem eindeutigen Symmetriebrechungsmuster im Fixpunktraum führt. Wir finden dieses Muster explizit, indem wir zunächst beweisen, dass langreichweitige Ordnung zu einer asymptotischen Entartung im Transferoperator führt, um dann den Symmetriebrechungsmechanismus als denjenigen zu identifizieren, der aus allen möglichen Randzuständen (Matrizen) diejenigen auswählt, die zu *positiv-semi-definiten* Matrizen korrespondieren, also ein-dimensionalen *virtuellen* Quantenzuständen. Wir beweisen, dass dies genau diejenigen Randkonfigurationen sind, die unter beliebigen Störungen nicht mischen und somit stabil sind. Wir untersuchen die Verschränktheitseigenschaften dieser virtuellen Quantenzustände und zeigen, dass diese durch lokale Verschränktheitshamiltonians beschrieben werden können, womit wir etablieren, dass Quantenphasen auch in Phasen mit Symmetriebrechung einen assoziierten Verschränktheitshamiltonian besitzen.

Contents

Abstract	v
Zusammenfassung	vii
1 Introduction	1
2 Entanglement in quantum many body systems	5
2.1 Entanglement	6
2.2 Area law and PEPS	9
3 Projected Entangled Pair State models	13
3.1 From mean field theory to PEPS	14
3.2 PEPS models: Hamiltonians and symmetry	18
3.3 Perturbations of PEPS	20
3.4 Examples: Ising and “RK-PEPS”	21
3.5 Matrix Product States: correlations, transfer operator, symmetry	22
3.6 PEPS transfer operator, fixed points and symmetry	27
3.7 Perturbations in the transfer operator	29
3.8 Isomorphism: Transfer operator and quantum channels	30
3.9 Spectral decomposition of channels	33
3.10 Fixed points of quantum channels	35
4 Long-range order and symmetry breaking	41
4.1 Long-range order	42
4.2 Stability of fixed points in the presence of degeneracy	47
4.3 Construction of symmetry broken states	48
4.4 Algebraic derivation of symmetry breaking states	54

5	Numerical methods	57
5.1	Contractions of tensor networks	57
5.2	The power method and the Arnoldi algorithm	58
5.3	The infinite matrix product state (iMPS) algorithm	62
6	Prototype models: Ising, AKLT and q-state Potts PEPS	67
6.1	Ising PEPS	68
6.2	AKLT model with “nematic” field	74
6.3	Potts PEPS	81
7	Entanglement Hamiltonians	93
7.1	The Li-Haldane conjecture	93
7.2	Bulk-boundary isometry, Boundary Hamiltonians	95
7.3	Locality analysis of extended Hermitian operators	97
7.4	Entanglement Hamiltonians for symmetry broken PEPS	100
8	Conclusions and Outlook	107
A	Appendix	109
A.1	Perturbation theory for transfer operators	109
A.2	Formal definition of the limit in a two-dimensional PEPS with long-range order	111
A.3	Taking the thermodynamic limit in the long-range order expression	112
A.4	Gell-Mann matrices for locality analysis	114
	Bibliography	117

Chapter 1

Introduction

This thesis is concerned with projected entangled pair state models as a framework for quantum many body systems in two dimensions. Our key interest will be the interplay between local and global *entanglement* and *symmetry* properties of these systems. At low temperatures, quantum correlations, i.e. entanglement, lead(s) to novel effects and exotic states of so-called *quantum matter* [61]. The quantum mechanical description of a many body system is given by a *global* wave-function that encompasses a macroscopic number of particles, which interact by a *local* Hamiltonian. These particles mathematically live on a tensor product space, typically arranged on some lattice structure. In order to explore these quantum correlations, we have to find the wave-function and when trying to do so, we are quickly faced with the very basic problem that the underlying Hilbert space, on which the many body state lives, grows exponentially with the number of constituents (i.e. the size of the lattice), while at the same time, the Hamiltonian describing these systems is typically local and translation invariant and can be specified with very few parameters. It turns out that the states of interest, ground states, low-lying excitations and thermal states only occupy a small subset of the many body Hilbert space. Parametrizing this “physical corner of Hilbert space” is the central effort of PEPS [74, 45]. The key insight is, that the states of interest follow a very peculiar entanglement scaling, which is known as the area law scaling. PEPS encode this global entanglement scaling property locally in the *PEPS tensor* and they have been proven to describe the low-energy landscape of local Hamiltonians well [40]. This leads us to taking a “bottom-up” model-building approach to PEPS: the definition of a single *local tensor* allows us to effectively and compactly define an entire

many body model, consisting of a Hamiltonian, the corresponding ground-state and low-energy landscape. The question we are concerned with in this work is, how much information about the global, *emergent*, properties of a system can be locally encoded in the PEPS tensor. As we have seen above, this worked for the area law, which for PEPS is “built-in” in the local tensor. The same holds for symmetries: it is well known, how to locally encode symmetries in the PEPS tensor, that lead to global symmetries in the model. The question we are concerned with in this work is: can PEPS models host systems, where this locally encoded symmetry is, globally, spontaneously broken? Spontaneous symmetry breaking is a prime example of an emergent phenomenon, which in fact can only happen in the thermodynamic limit. Remarkably, we will find that we can indeed observe spontaneous symmetry breaking in PEPS. After showing that long-range order is the suitable criterion to detect emergent (“hidden”) symmetry breaking in finite systems, we will study its implications for PEPS models. We will show how the stability of symmetry broken states leads us to a *unique* symmetry breaking pattern on the entanglement degrees of freedom of the system, which in a PEPS model are given by the fixed points of the so-called transfer operator. We will prove this uniqueness and explicitly determine the corresponding symmetry broken states. We will then construct prototype PEPS models, which fulfill the requirements, we set out earlier. We extensively study their properties numerically and successfully extract the signatures of symmetry breaking from finite PEPS data. Thanks to an exact holographic mapping, the entanglement degrees of freedom in a PEPS model can be described by another quantum system living on the boundary of the two-dimensional model. Having established the “true”, symmetry broken, nature of this boundary, we study its entanglement structure by the use of so called entanglement Hamiltonians, where we establish that also phases with symmetry breaking have an associated *local* entanglement Hamiltonian.

In chapter 2, we will start by discussing entanglement in many body systems. We explain what is meant by entanglement scaling and the area law. In chapter 3, we show how trying to encode entanglement locally naturally leads to PEPS. We pave the way for PEPS models, introducing parent Hamiltonians, perturbations and symmetries and give a general recipe for the construction of PEPS models. We then show how correlations in PEPS are encoded in the transfer operator, which renders this the central object for the study of long-range order and symmetry breaking, thereby necessitating a number of analytical techniques

needed to tackle transfer operators and their eigenstates (fixed points), which we are concerned with in the second half of chapter 3. We then are ready for chapter 4, where we present long-range order (opposed to an order parameter) as the suitable criterion for symmetry breaking in PEPS. We prove, that long-range order implies an emergent degeneracy in the largest eigenvalue of the transfer operator. Defining the notion of symmetry broken states as the ones stable under arbitrary perturbations, we then prove that the set of symmetry broken fixed points is uniquely defined as the ones corresponding to virtual density matrices. We manage to construct these states explicitly from the states that defined the original (unbroken) model. We then move on to chapter 5, in which we present the numerical techniques we need in order to be able to study and simulate PEPS models on the computer. We put these techniques to extensive use in chapter 6, where we use the mentioned recipe for PEPS model building to study three prototypical PEPS models, from which we are able to extract the signatures of symmetry breaking. We conclude with chapter 7, where we study the entanglement structure of the PEPS boundary and show that the boundary of PEPS with spontaneous symmetry breaking is described by a local entanglement Hamiltonian.

Publications

Parts of the ideas presented here have been published in the following two publications:

- Manuel Rispler, Kasper Duivenvoorden and Norbert Schuch, "Long-range order and symmetry breaking in Projected Entangled Pair State models" *Phys. Rev. B*, 92:155133 , 2015
- Manuel Rispler, Kasper Duivenvoorden and Norbert Schuch, " \mathbb{Z}_N symmetry breaking in Projected Entangled Pair State models", *Journal of Physics A: Mathematical and Theoretical* 50(36):365001 , 2017

Chapter 2

Entanglement in quantum many body systems

The most crucial insight from the theory of entanglement, which has shed light on the structure of quantum many body states of local Hamiltonians, is known as the area law [20, 5]. Let us use this chapter to describe what is meant by that and how this motivates us to model quantum many body systems by their entanglement degrees of freedom, eventually leading to PEPS models.

The postulates of quantum mechanics tell us, that a physical system is described by states $|\psi\rangle \in \mathcal{H}$ and observables $\mathcal{A} \in \mathcal{B}(\mathcal{H})$ on a Hilbert space \mathcal{H} [70]. The latter are operators acting on the former. The density matrix for pure states is given by $\rho = |\psi\rangle\langle\psi|$ and the Born rule tells us, that expectation values of observables are computed by $\langle\mathcal{O}\rangle = \text{tr}(\mathcal{O}\rho)$. The operation we need in order to talk about systems built from subsystems, is the tensor product. Both the states and by extension the operators on these states can be furnished with a tensor product, which is denoted by \otimes , to allow for a system with more than one constituent: $\mathcal{H} = \mathcal{H}_1 \otimes \mathcal{H}_2$. While this is known to be plagued with problems for infinite systems and one in principle has to resort to formulate the theory in terms of algebras of observables and functionals on them, we will take the pragmatic standpoint that we can always work with a large but finite system when it is convenient and remind ourselves of these subtleties, whenever it is due. We formulate our theory on the lattice, where the Hilbert space is large

but finite

$$\mathcal{H} = \bigotimes_{i=1}^N \mathcal{H}_i. \quad (2.1)$$

Assuming, that we have a local orthonormal basis at hand, the quantum state living on this space is parametrized by

$$|\psi\rangle = \sum_{i_1 \dots i_N} c_{i_1 \dots i_N} |i_1 \dots i_N\rangle. \quad (2.2)$$

Notice, that while the basis elements have a product structure, they are just the tensor product of the local bases, the state itself does not necessarily have this product property. This leads to the concept of *entanglement*.

2.1 Entanglement

Non-classical effects in strongly correlated quantum many body systems are intricately related to the phenomenon of entanglement. The notion of entanglement is defined as follows: We call a pure quantum state

$$|\psi\rangle \in \mathcal{H}_A \otimes \mathcal{H}_B, \quad (2.3)$$

(bipartite-)entangled, if it is *not separable*, i.e. there exist no $|\phi_A\rangle \in \mathcal{H}_A$ and $|\phi_B\rangle \in \mathcal{H}_B$, such that $|\psi\rangle$ is a product state:

$$|\psi\rangle \neq |\phi\rangle_A \otimes |\phi\rangle_B. \quad (2.4)$$

The relevance of this phenomenon was put forward by Einstein, Podolsky and Rosen in 1935 [19], who realized that the fact that the quantum state of a composite system may sometimes not be a composition of independent descriptions of the subsystems has unexpected implications. While this led them to doubt that quantum theory was correct, it was Schrödinger, who coined the term “entanglement” and understood the fundamental change this phenomenon would lead to [64]:

“[...] I would not call that *one* but rather *the* characteristic trait of quantum mechanics, the one that enforces its entire departure from classical lines of thought. By the interaction the two representatives (or ψ -functions) have become entangled. [...]”

Entanglement is at the heart of quantum theory and has profound implications for its very foundation. Most notably, John Bell introduced a bound on the possible outcomes of a certain measurement procedure (“the Bell inequality”), above which a theory cannot be local-realistic and found that quantum mechanics violates this bound [6]. The states that maximally violate these assumptions as called maximally entangled states, or Bell states in the case of two-level systems. Our representative shall be

$$|\psi^+\rangle = \frac{1}{\sqrt{2}}(|00\rangle + |11\rangle), \quad (2.5)$$

noting that there are three other Bell-states, which are equivalent under local unitaries. Experiments to this day maintain that quantum theory is correct and nature violates the Bell inequality. So called loophole-free Bell tests were published as recent as 2015 and closed all “reasonable” loopholes [29]. Entanglement is rather poorly understood beyond the pure bipartite case and subject to many ongoing debates. A review on entanglement theory can be found in [31]. Our approach could be summarized as asking, what implications does this “quantumness” of entanglement have for many body systems? How is this “quantum matter” related to entanglement of many body systems and what can we learn from entanglement theory in order to find good descriptions of these systems?

The modern understanding of entanglement is that of a resource theory. Entanglement is a non-local resource, which is hard to produce in contrast to the cheap transformations local operations and classical communication between the two parties (“LOCC”). Entanglement is useful in order to complete non-trivial tasks and in the process we consume it. The meaning of resource can be quite literally that of a thing that we need in order to produce a desired other thing, which would be for example quantum communication or teleportation, dense coding, entanglement distillation etc. but it can also be more abstract, like the ability of a material to allow for non-local correlations and (quasi-)particles, as would be the case for anyonic excitations in topologically ordered condensed matter systems for example.

In the case of bipartite pure states, entanglement is well understood, thanks to the existence of entanglement monotones, which were defined by Vidal [77] and

comprise the necessary criteria for entanglement measures. It is straightforward to certify, whether a given state is entangled, to compare the amount of entanglement between two states and to decide whether one state can be converted into the other under LOCC. The most powerful mathematical tool for bipartite entanglement is the singular value decomposition, which in this context is called the Schmidt decomposition:

Given a rectangular matrix $M \in \mathbb{C}^m \times \mathbb{C}^n$, it is always possible to perform a singular value decomposition (SVD), which is to find matrices U , S and V , such that

$$M = USV^\dagger, \quad (2.6)$$

where U is a unitary $m \times m$ matrix, S is a $m \times n$ rectangular matrix with non-negative diagonal entries and V is a unitary $n \times n$ matrix. If we now take a bipartition of a quantum state

$$|\psi\rangle = \sum_{ij} c_{ij} |\psi_i\rangle_A \otimes |\psi_j\rangle_B, \quad (2.7)$$

apply this to the wave-function coefficient and absorb the unitaries in the local basis sets, we arrive at the Schmidt normal form:

$$|\psi\rangle = \sum_k s_k |\phi_k^{[A]}\rangle |\phi_k^{[B]}\rangle \quad (2.8)$$

Note, that this normal form is unique in terms of the singular values. The two parties A and B (against Alice and Bob) can apply local unitaries to their subsystem, which is reflected in the unitary freedom to choose the local basis, but the singular values cannot be changed by one party alone, which already indicates, that this is a good measure of entanglement.

This has an effect on the ability to compute expectation values via the Born rule given above. Suppose the observable we want to compute only acts on A , then we are tracing out B . This motivates us to define the reduced density matrix, which is given by the partial trace over system B :

$$\rho_A = \text{tr}_B(\rho) = \sum_k (\mathbb{1}_A \otimes \langle k|_B) [\rho] (\mathbb{1}_A \otimes |k\rangle_B), \quad (2.9)$$

where $|k\rangle$ is some complete basis for subsystem B . From the Schmidt normal form, we learn that the reduced state is pure, if and only if A and B are not entangled. If they are entangled, the reduced state is a mixed state and mea-

suring the amount of entanglement is equivalent to measuring the "mixedness" of the reduced density matrix. This is done by entropies, so we define the Rényi entropies as

$$S_\alpha(X) = \frac{1}{1-\alpha} \text{tr}(X^\alpha) \quad (2.10)$$

There are additional natural requirements for a good measure of entanglement: besides invariance/monotonicity under local unitaries, the measure should be additive (under tensoring of states) and continuous in the input state [77]. It turns out that for pure bipartite entanglement the von Neumann entropy of the reduced state is a unique measure of entanglement:

$$S(\rho_A) = -\text{tr}(\rho_A \log(\rho_A)) = -\sum_k s_k^2 \log(s_k^2) \quad (2.11)$$

2.2 Area law and PEPS

So far we have been only concerned with entanglement between two parties. The natural question is how to take this to a many body setting. In principle, one could go to the theory of multipartite entanglement and try to find measures for this, however the study of multipartite entanglement is very challenging and for the most part an open problem [3]. We will therefore focus on bipartite entanglement, which is far better understood. This means that in order to speak about bipartite entanglement, we group the system at hand into two parts, ascribing one connected region of the lattice to a subsystem R , which corresponds to A in the above setting but is now extended in space) and the complement region to subsystem \bar{R} , which corresponds to B . We call this an entanglement cut, depicted in Fig. 2.1. The many body aspect will come into play in the form of the scaling of entanglement when changing the sizes of the two regions in this bipartition. As in the two particle case in the previous section, the entanglement entropy is again our measure of entanglement. Given a generic many body state, we would have a maximally mixed reduced state and thus have an entropy which is proportional to its volume.

However, this disregards the fact that we are typically interested in very special class of states: Ground states, low excitations and thermal states of local Hamiltonians. These typically have a finite correlation length. In order to get some intuition, let us take a very naïve approach for a moment and treat entanglement somewhat analogous to correlations. The entanglement entropy measures the correlation between the two subsystems of the bipartition. Together with

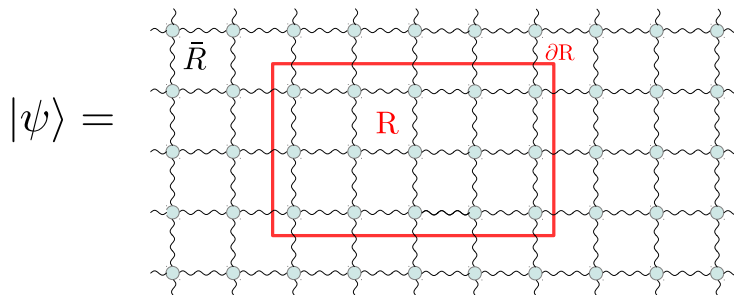


Figure 2.1: Example of a bipartition of a many body quantum state. Nodes depict the particles on the lattice (e.g. spins) and wiggly lines indicate correlations. We partition into subsystems R and \bar{R} and anything on subsystem R is described by the reduced density matrix ρ_R , which we compute by tracing out system B . The entropy of this reduced state ρ_R is related to the entanglement between subsystems R and \bar{R} . When the entropy is proportional to the boundary ∂R , we say that the system follows an area law.

the finite correlation length, this implies that only things which are not further away from the bipartition cut, than the correlation length, can contribute to the entropy, which means that the latter is proportional to the length of the bipartition cut length, denoted as the boundary of the subsystem(s). It is slightly ironic, that the area law is nowadays mostly used in lower-dimensional systems, where it is not an area but rather a constant or a perimeter, but the name, which was originally inspired by black hole thermodynamics, which deals with the boundary of three-dimensional objects and thus areas in the usual sense, has stuck.

In one dimensional systems, it has been proven that the ground states of gapped local Hamiltonians fulfil an area law [28]. Also the relation, that exponentially decaying correlations imply an area law, which we use in our vague intuition building in the preceding paragraph, has been proven rigorously for one-dimensional systems [8]. Let us take this point, to mention tensor networks and PEPS for the first time: The one-dimensional version, known as matrix product states (MPS), naturally have an area law built in and indeed Hastings [28] also proved that the ground states of local gapped Hamiltonians have MPS form. In higher dimensions, the situation is less clear and open to debate. Understanding the area law is an important problem in the field of Hamiltonian complexity [46], i.e. the question of how difficult it is to simulate a physical system. While the

area law structure was a strong motivation to study generalizations of matrix product states, which are then called projected entangled pair states (PEPS) and will be the subject of this thesis, the current status can be summarized as follows: On the one hand, there exist states in two dimensions, which have an area law and cannot be described by tensor networks [25]. On the other hand, it was proven in [40], that the ground state of a local gapped Hamiltonian has a PEPS description, if one makes a moderate assumption on the scaling of the density of states. The latter does not initially rely on an area law structure, which suggests that we can leave the potential complications of the area law discussion aside and take from this, that PEPS are very well suited for two-dimensional local gapped Hamiltonians. We continue in the next chapter with defining PEPS and showing, how we get to *PEPS models*.

Chapter 3

Projected Entangled Pair State models

As alluded to in the previous chapter, projected entangled pair states provide a systematic way for the construction of many body wave functions with a desired entanglement scaling [74, 45]. In this chapter, we will define what a PEPS is and how we can use it to construct PEPS models and identify their relevant properties. We will start by showing how one can introduce entanglement degrees of freedom in a local description of a many body system and how this leads to the definition of the PEPS tensor. In a second step, we will reveal the entanglement properties of the state we construct and how it automatically leads to area law states. We show how the tensor defines an entire model with an associated Hamiltonian, including a presentation of how to build symmetries in these models. We then give a prescription how to construct PEPS models from classical statistical models. We show how to analyze these models by their transfer operator and derive an exact holographic mapping between the bulk and the boundary state. We conclude the chapter with the most important properties of transfer operators, largely relying on a strong link to the theory of quantum channels.

3.1 From mean field theory to PEPS

A particularly simple ansatz to solve the many body problem on the lattice is to just assume that it is a product of independent wave-functions on every lattice site. As we will always assume translation invariance, specifying the *local* wave-function then immediately defines the *global* wave-function. This is quite useful in many cases and is a good example of how to get a local description of the many body system, where by local we mean that we only have to specify the wave-function on one site to describe the entire system. This ansatz is known as mean field theory [10] and works quite well in many cases, however it completely discards the entanglement structure of wave-functions right from the start. Our goal now will be to find a local ansatz, that nevertheless lets us encode entanglement properties. The key idea is to take the local Hilbert space describing one lattice site and attaching extra degrees of freedom to it, so called *fiducial* states, which are entangled with the physical particle. These will in a later step then take care of entangling the site with the rest of the system. From a quantum information perspective, this process can be viewed as entanglement swapping. To distinguish the two types of local degrees of freedom, the original degree of freedom will be called *physical* degree of freedom and the fiducial states will be called entanglement or *virtual* degrees of freedom. We will use a square lattice for simplicity, even though the construction works for any lattice. The new, “hybrid” local state thus lives on the Hilbert space $\mathcal{H}_{\text{physical}} \otimes (\mathcal{H}_{\text{virtual}})^{\otimes 4}$. The dimension of the physical Hilbert space is dependent on the problem we are trying to describe and is conventionally denoted $\dim(\mathcal{H}_{\text{physical}}) = d$. The dimensions of the virtual spaces are arbitrary, we choose them all equal and call this dimension the bond dimension, denoted by $\dim(\mathcal{H}_{\text{virtual}}) = D$. As we will see in a moment, this bond dimension is directly related to the entanglement we can capture with this construction. Let all spaces be spanned by some orthonormal basis sets in the computational basis, then the hybrid state on the lattice site can be expanded in that basis. We refer to the indices corresponding to the virtual spaces as virtual indices, usually given a Greek letter index and the one corresponding to the physical space as the physical index, usually given a Latin letter index. We depict this tensor graphically by a five-legged object (Fig. 3.1).

We now define the procedure how to get from this local object to the global wave-function. This process is called contraction and works by putting one

$$\begin{aligned}
 \begin{array}{c} \bullet \\ \bullet \\ \bullet \\ \bullet \\ \bullet \end{array} &= \sum_{\alpha, \beta, \gamma, \delta} \alpha \begin{array}{c} i \\ \diagup \quad \diagdown \\ \beta \end{array} \gamma \delta \quad |i\alpha\beta\gamma\delta\rangle \\
 A_{\alpha\beta\gamma\delta}^i &= \begin{array}{c} i \\ \diagup \quad \diagdown \\ \beta \end{array} \gamma \delta
 \end{aligned}$$

Figure 3.1: We model the many body wave-function by defining a local object, which is a hybrid state consisting of one physical (red dot) and four virtual (black dots) Hilbert spaces. Expanding this state in a basis immediately leads to the definition of the PEPS tensor A . Its graphical representation conventionally has the physical index (Latin letter) pointing up and the four virtual indices (Greek letters) point lie in plane (left, front, right, back).

hybrid state on every lattice site and taking the inner product over adjacent virtual states. Since we assumed (wlog) the virtual spaces to be spanned by orthonormal bases, this is equivalent to putting the indices corresponding to adjacent sites equal and summing over this index. As an example we contract two PEPS tensors by writing out the tensors in eq. 3.1:

$$\sum_{\gamma} (A_{\alpha\beta\gamma\delta}^{i_1} A_{\gamma\mu\nu\rho}^{i_2}) |i_1 i_2\rangle \langle \alpha\beta\delta\mu\nu\rho|. \tag{3.1}$$

We then perform the same operation diagrammatically by graphically representing the tensors as boxes with legs, as done in in fig. 3.2.

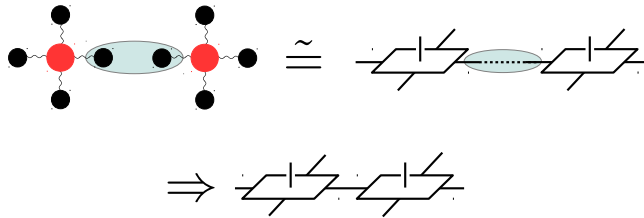


Figure 3.2: The fusion of two hybrid states is done by taking the inner product on the virtual spaces belonging to neighboring sites. This is equivalent to setting the indices in the corresponding PEPS tensor equal and summing over them. This process is called contraction of an index and is graphically depicted by connecting the two legs. This shows the advantage of the diagrammatic manipulations, when compared to the the formula 3.1, where it is hard to keep track of which index goes where.

The full wave-function is given by contracting out all the virtual indices over the lattice, where we either close the boundary periodically or choose some virtual boundary configuration. This leaves us with a quantum state living on $(\mathcal{H}_{\text{physical}})^{\otimes N}$, as desired.

The diagram illustrates the contraction of virtual indices in a PEPS tensor network. On the left, the quantum state $|\psi\rangle$ is shown. This is equated to a tensor network where multiple layers of tensors are connected. The horizontal lines represent physical indices, while the vertical and diagonal lines represent virtual indices. The virtual indices are contracted between adjacent layers, forming a lattice-like structure. The boundaries of the virtual indices are shown as dashed lines, indicating a specific virtual boundary condition. The overall structure represents the contraction of all virtual indices, leaving only the physical indices as the final quantum state.

Figure 3.3: Contracting out the virtual indices gives the physical quantum state after choosing an appropriate virtual boundary condition.

We have thus completed the description of a procedure how to get a global quantum state from a local tensor in a “bottom-up” approach to wave-functions. The presented viewpoint with fiducial states emphasizes the character of PEPS as “mean field with entanglement”. In order to understand its entanglement properties, we will now present the more standard PEPS construction, which works in a somewhat reverse fashion to the above approach. For this, let us imagine again a square lattice, however now a priori without any physical degrees of freedom. Let the virtual degrees of freedom form maximally entangled pairs of the form

$$|\omega\rangle_{m,n} = \sum_{k=0}^{D-1} |k\rangle_m |k\rangle_n, \quad (3.2)$$

which are nothing but generalized Bell states. By m and n we denote lattice sites, which are nearest neighbors. We thus have a square lattice, where on every node there are four incident halves of a Bell state shared with every nearest neighbor. We denote the full state by

$$|\Omega\rangle = \bigotimes_{l \in \text{links}} |\omega\rangle_l \quad (3.3)$$

In order to eventually describe one physical degree of freedom per lattice site, we apply a linear map on every node, which is commonly referred to as the projector \mathcal{P} .

As shown in figure 3.4, the linear map has four states as input and one state as output. This map is specified by an array with five indices and we arrive at

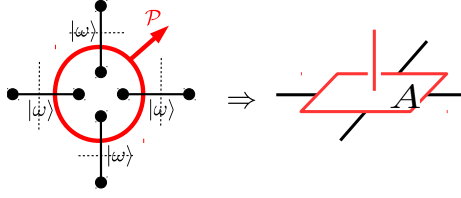


Figure 3.4: PEPS construction from maximally entangled virtual states. The linear map \mathcal{P} takes as input one part of the two-party maximally entangled states $|\omega\rangle$ and has the physical Hilbert space as its target space.

the definition of the PEPS tensor, which is completely equivalent to our above construction that resulted in eq. 3.1:

$$\mathcal{P} : (\mathcal{H}_{\text{virtual}})^{\otimes 4} \rightarrow \mathcal{H}_{\text{physical}} \quad (3.4)$$

$$\mathcal{P} = \sum_{i\alpha\beta\gamma\delta} A_{\alpha\beta\gamma\delta}^i |i\rangle \langle\alpha\beta\gamma\delta|. \quad (3.5)$$

We thus interpret the virtual states as an input and the physical state as an output of a linear map. As we constructed the state from applying a projector (actually a linear map) on (maximally) entangled pair states, this explains the name projected entangled pair state. This interpretation is very insightful, because we know the amount of entanglement in the virtual links, their entanglement is simply given by $S(\text{tr}_B |\omega\rangle \langle\omega|) = \log D$, i.e. by tracing out one side of the maximally entangled state, as defined in eq. 2.9. The quantum state is then given by applying the linear map on every node of the network of maximally entangled virtual states:

$$|\psi\rangle = (\mathcal{P} \otimes \dots \otimes \mathcal{P})(|\Omega\rangle). \quad (3.6)$$

If we now make an entanglement cut on this quantum state, i.e. bipartition it into two regions (cf. fig. 2.1), the above equation immediately gives us an upper bound on the entanglement, this bipartition can have. The key insight is that the linear map acts locally and as was alluded to in chapter 1, the entanglement entropy is non-increasing under local operations. The entanglement entropy is thus upper bounded by the entanglement entropy of the virtual state. Computing the entanglement entropy of the virtual state is almost trivial. The cut will bipartition, which means it cuts through the virtual maximally entangled pairs along the boundary of the region. Only these states that are cut in half,

contribute to the entanglement and the entropy is simply given by

$$S(\text{tr}_{\bar{R}} |\psi\rangle \langle \psi|) \leq S(\text{tr}_{\bar{R}} |\Omega\rangle \langle \Omega|) = L \log(D), \quad (3.7)$$

where L denotes the length of the boundary, which is equal to the number of bonds we cut. We thus learn, that PEPS have an area law structure built into the way we construct them. By varying the bond dimension, we can increase the amount of entanglement that can be captured by the PEPS wave-function. Let us mention as a side-remark, that this class is also complete, any quantum state can be written as a PEPS, albeit one has to allow for arbitrary bond dimensions, which makes this rather useless in practice. However it has turned out that already at very small bond dimensions PEPS states can host very intriguing phenomena and provide a fruitful analytical and numerical framework [75].

3.2 PEPS models: Hamiltonians and symmetries

PEPS and tensor networks in general are state-centered, i.e. they construct the quantum state directly. To emphasize the model-building character of PEPS, and to ensure that we are actually dealing with a physical model, let us (a) relate this state to a Hamiltonian and (b) show how to encode symmetries in the tensor. For the first part, let us construct a Hamiltonian from the PEPS tensor, which is designed such that the PEPS wave-function is the ground-state of this Hamiltonian. We again view the tensor as a linear map from virtual spaces to physical space $\mathcal{A} : (\mathbb{C}^D)^{\otimes 4} \rightarrow \mathbb{C}^d$. Similarly, we define \mathcal{A}_R as the linear map from the virtual boundary of a region R to the physical bulk space of R by taking $|R|$ copies of \mathcal{A} and contracting the inner indices. The parent Hamiltonian [50] is given by

$$H = \sum_R h_R, \quad (3.8)$$

where h_R is the projector onto the orthogonal complement of the image of (\mathcal{A}_R) . Depending on the particular PEPS tensor, we might have to define bigger patches R before this becomes a non-trivial operator, however the area law property gives a counting argument that this will happen, since the image space grows with the volume and the domain only with the size of the boundary. We

see, that h_R are defined purely by the tensor, thus its spectral properties will be determined by the properties of the tensor. At this point, a few remarks about the main results on parent Hamiltonians are in order: If we view the local tensor as a linear map from virtual to physical space, we see from simple dimension counting, that it will be typically a mapping from many to fewer degrees of freedom. This implies that the mapping cannot be injective. However, we can block several sites together and again owing to the area law structure, the size of the image of this map will grow faster than the preimage, which means that after a finite number of blocking steps, we can expect that the linear map will generically be injective. By “generic” we mean, that *almost all* maps are injective, which can be seen by the fact that a map is injective if it has full rank and the set of rank-deficit matrices is a very special set with constraints and thus lives on a lower-dimensional subspace of the space of all matrices. Given a rank-deficit matrix, a small perturbation will always steer it away and render it full-rank. Thus, if we for example draw random PEPS according to some probabilistic process, we will draw an injective PEPS with probability one. In the case of MPS, injectivity has very strong implications. An injective MPS always describes the unique ground state of its parent Hamiltonian, which additionally has a gap above [65]. In the two-dimensional PEPS case, this is not true anymore in this generality. It has been proven [24], that an injective PEPS is the unique ground-state. However the one-to-one relation between injectivity and “gappedness” is lost, such that the parent Hamiltonian might be gapless (thermodynamic limit) or there might be a non-injective PEPS with a gapped parent Hamiltonian. While this is a weaker result, it allows for richer physics: It implies that PEPS could (and in fact can) host second order phase-transitions.

We thus learn that the PEPS tensor defines a Hamiltonian and its ground state and the low-energy theory above it. If we now make the PEPS tensor parameter-dependent, this defines not only one state but an entire family of states and parent Hamiltonians:

$$\begin{aligned} A &\rightarrow A(\theta) \\ H &\rightarrow H(\theta) \\ |\psi\rangle &\rightarrow |\psi(\theta)\rangle. \end{aligned} \tag{3.9}$$

The last property missing to have a PEPS model are symmetries, which we will incorporate in the following. This can be achieved by a local encoding of the

symmetry in the tensor. The goal is to build (N -body) wave-functions, that are invariant under the action of some unitary group representation with elements u_g , labeled by group elements $g \in G$, i.e.

$$(u_g)^{\otimes N} |\psi\rangle = |\psi\rangle. \quad (3.10)$$

In the PEPS picture, this has the u_g acting on the physical index of every lattice site. We can achieve the desired invariance of the wave-function, if acting on the physical index with u_g is equivalent to acting with a (potentially different) unitary representation V_g in a conjugating fashion, see fig. 3.5. Acting on the virtual indices in a conjugate way, such that the physical state is the same is called a gauge transformation.

$$\begin{array}{c} u_g \\ \diagup \quad \diagdown \\ \text{---} \quad \text{---} \\ \diagdown \quad \diagup \end{array} = V_g \begin{array}{c} V_g \\ \diagup \quad \diagdown \\ \text{---} \quad \text{---} \\ \diagdown \quad \diagup \\ V_g^\dagger \end{array} V_g^\dagger$$

Figure 3.5: Constructing tensors A , such that the depicted relation holds, leads to PEPS tensors (models) with symmetry, as the symmetry is absorbed in a gauge transformation the virtual legs, where it cancels out in the contraction process.

The parent Hamiltonian directly inherits this symmetry and we thus arrived at symmetric PEPS models.

3.3 Perturbations of PEPS

We can probe the neighborhood of a PEPS tensor by applying perturbations on the local tensor. This notion of perturbation will be very useful later, as symmetry breaking is closely related to stability under perturbations. The most general perturbation one could think of would be

$$A(\epsilon) = A + \epsilon C \quad |C| = 1. \quad (3.11)$$

However, this turns out to be too general since it can lead to discontinuities in the parent Hamiltonian. The perturbations corresponding to perturbations of the parent Hamiltonian are given by purely perturbing the physical index of the PEPS tensor [15].

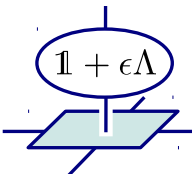
$$A^i \rightarrow (\mathbb{1} + \epsilon\Lambda)_{ij} A^j =$$


Figure 3.6: Perturbations are given by so called deformations of the physical index. These correspond to smooth deformations of the parent Hamiltonian

3.4 Examples: Ising and “RK-PEPS”

In the spirit of our model building approach to PEPS, we define a parameter-dependent local tensor with a symmetry. Remarkably, there is a general recipe how to construct such model tensors, which is inspired by Rokhsar-Kivelson wave-functions [59]. The simplest example is the so called “Ising-PEPS”, which we define as

$$A^0 = |0\rangle \langle \theta|^{\otimes 4} \quad A^1 = |1\rangle \langle \bar{\theta}|^{\otimes 4}, \quad (3.12)$$

where $|\theta\rangle = \cos(\theta)|0\rangle + \sin(\theta)|1\rangle$ and $|\bar{\theta}\rangle = X|\theta\rangle = \sin(\theta)|0\rangle + \cos(\theta)|1\rangle$.

Let us compare this to the partition function of the classical Ising Hamiltonian $H = -\sum_{\langle i,j \rangle} \sigma_i \sigma_j$, which is given by

$$Z = \text{tr} e^{-\beta H} = \sum_{\{\sigma\}} e^{\sum_{\langle i,j \rangle} \beta \sigma_i \sigma_j} = \sum_{\{\sigma\}} \prod_{\langle i,j \rangle} e^{\beta \sigma_i \sigma_j}, \quad (3.13)$$

with the Ising variable $\sigma_i \in \{+1, -1\}$. For every configuration $\{\sigma\}$, across any “bond”, the weight in the partition function only depends on the relative sign of the two variables and is given by $e^{\beta \sigma_i \sigma_j} = e^{\pm\beta}$. If we now in comparison evaluate $\langle \psi | \psi \rangle$ for the Ising PEPS, this will be a big superposition over all possible lattice configurations analogous to $\{\sigma\}$. Notice, that the edges coming out of any vertex are either all $|\theta\rangle$ or all $|\bar{\theta}\rangle$ on both ket and bra layer and hence the overlap with a neighboring site is either $\langle \theta | \bar{\theta} \rangle^2 = \sin^2(2\theta)$ or 1. We can therefore identify $\sin(2\theta) = e^{-\beta}$. Furthermore, all σ_z -correlation functions in the Ising PEPS are in one-to-one correspondence with thermal correlation functions in the classical square lattice Ising model. In particular, we know the exact value of the critical temperature, due to the self-duality of the Ising model, which was found by Kramers and Wannier [36] to be $\beta_c = \log(1 + \sqrt{2})/2$, which

we can directly translate to the (quantum) critical point of the Ising PEPS:

$$\theta_c = \frac{1}{2} \arcsin(e^{-\beta_c}) = \frac{1}{2} \arcsin\left(\frac{1}{\sqrt{1+\sqrt{2}}}\right) \approx 0.3496 \quad (3.14)$$

As mentioned above, the construction of the Ising PEPS is a particular example of a general recipe known as RK-wave-functions. Rokhsar and Kivelson [59] invented a way to construct quantum states from a classical model (classical Hamiltonian):

$$|\psi\rangle = \sum_{\sigma_1 \dots \sigma_N} e^{-\beta H_{cl}(\sigma_1, \dots, \sigma_N)/2} |\sigma_1, \dots, \sigma_N\rangle \quad (3.15)$$

An expectation value of an arbitrary (potentially extended) operator over this quantum state reads

$$\langle O \rangle = \sum_{\sigma_1 \dots \sigma_N, \sigma'_1 \dots \sigma'_N} \langle \sigma_1, \dots, \sigma_N | e^{-\beta H_{cl}(\sigma_1, \dots, \sigma_N)/2} O e^{-\beta H_{cl}(\sigma'_1, \dots, \sigma'_N)/2} | \sigma'_1, \dots, \sigma'_N \rangle, \quad (3.16)$$

which tells that in the case of $[O, H_{cl}] = 0$ we get the corresponding thermal expectation value of the classical model:

$$\langle \psi | O | \psi \rangle = \text{tr} (O e^{-\beta H_{cl}}) \quad (3.17)$$

This construction is very useful for building toy-models for PEPS quantum phases [75]: We can just take a classical Hamiltonian, which we know to have certain desired properties, in particular a (thermal) phase transition and encode its partition function in the virtual bonds of the PEPS. This then gets mapped to a quantum phase transition in the RK construction, which means that in order to study a certain transition type, it is sufficient to know a corresponding classical model.

3.5 Matrix Product States: correlations, transfer operator, symmetry

We started this chapter by motivating and defining the PEPS tensor, the central object of this thesis and how this leads to the study of PEPS models. In order to develop methods to tackle these systems, let us now take one step back and see what we can learn from the one-dimensional case, which is far better understood

[22, 63, 65, 13, 50]. In one dimension, we only have to deal with two virtual indices per site. With the contraction rule from above, this will immediately lead to products over matrices and the states being nothing but the well known matrix product states. We use the tensors $A_{\alpha\beta}^i$ and put them on a chain and contract the adjacent indices. This applies to every bond and we eventually arrive at the well known MPS form

$$|\psi\rangle = \sum \text{tr} (A^{i_1} A^{i_2} \dots A^{i_N}) |i_1 \dots i_N\rangle, \quad (3.18)$$

depicted in fig. 3.7.

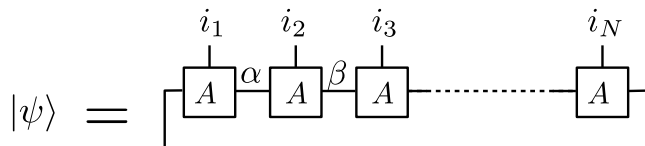


Figure 3.7: The matrix product state representation (shown with periodic boundary)

We thus showed, that the PEPS construction in one dimension naturally leads to an MPS like structure. The wave-functions we get from tensor network methods are always unnormalized. Let us demonstrate how to compute the norm of an MPS, which naturally leads to the concept of transfer operators (transfer matrices). For this we have to take two copies of the wave-function where one copy is a bra and one is a ket vector, which leads to the terminology of bra- and ket-layer in the MPS and later the PEPS diagrammatics. We evaluate the correlator in a diagram in fig. 3.8. This diagram gives a very crucial insight into the structure of MPS and PEPS. If we would have to first construct the entire wave-function from the tensor, this would result in an intermediate tensor, whose size grows with the number of sites. The tensor A has size dD^2 and thus the tensor describing a chain of length L would have $d^L D^2$ entries, i.e. growing exponentially with the length. The lesson to learn is that we can avoid this by first contracting ket- and bra-layer for one site, which gives a matrix of size $D^2 \times D^2$. We then only have to perform matrix multiplication on objects of fixed size, *independent* of the length of the chain. This object is very crucial in the analytical (and numerical) study of MPS and is called the transfer operator \mathbb{T} . From its definition given in figs. 3.8, 3.9, it follows, that the norm is given by $\langle\psi|\psi\rangle = \text{tr}(\mathbb{T}^N)$.

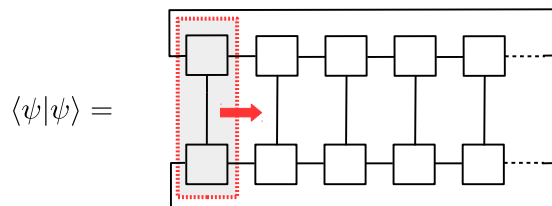


Figure 3.8: Computing the norm of an MPS wave-function. We define the transfer operator by contracting the physical index on one site, which gives the tensor in the red box (see below, fig. 3.9). The norm is then just given by the trace over a matrix product.

$$\mathbb{T} = \sum_i A^i \otimes \bar{A}^i =:$$

Figure 3.9: Definition of the MPS transfer operator. It is a matrix from virtual ket and bra layer to virtual ket and bra layer. We use a bar to indicate complex conjugation.

We now show, how a symmetry of the tensor leads to a symmetry in the transfer operator, which will be crucial in the rest of this work. The key insight is that the representations, with which we require the tensor to transform, are unitary and thus the physical symmetry operation cancels out. The transfer operator is thus invariant under a symmetry operation of the form depicted in fig. 3.10.

$$\begin{array}{c}
 \begin{array}{c} u_g \\ | \\ \square \\ | \\ \square \end{array} = V_g \begin{array}{c} | \\ \square \\ | \\ \square \end{array} V_g^\dagger \\
 \Downarrow \\
 \begin{array}{c} \square \\ | \\ \square \end{array} = \bar{V}_g \begin{array}{c} | \\ \square \\ | \\ \square \end{array} \bar{V}_g^\dagger \\
 = \\
 \begin{array}{c} \square \\ | \\ \square \end{array} = V_g \begin{array}{c} | \\ \square \\ | \\ \square \end{array} V_g^\dagger
 \end{array}$$

Figure 3.10: The symmetry of the tensor leads to a symmetry in the transfer operator.

Applying the symmetry on both sides of the equation in fig. 3.10, we learn that

the symmetry commutes with the transfer operator:

$$(V_g \otimes \bar{V}_g)\mathbb{T} = \mathbb{T}(V_g \otimes \bar{V}_g) \quad (3.19)$$

$$[\mathbb{T}, (V_g \otimes \bar{V}_g)] = 0. \quad (3.20)$$

We will generally assume that the transfer operator is diagonalizable, note that a priori it is not Hermitian and we thus have left and right eigenvectors and complex eigenvalues $\lambda_k \in \mathbb{C}$. The above commutation with the symmetry (eq. 3.20) allows us to label the eigenvectors by that symmetry (splitting up a simple counting label into a symmetry label k and a degeneracy label ν)

$$\mathbb{T} = \sum_{k,\nu} \lambda_{k,\nu} |r_{k,\nu}\rangle \langle l_{k,\nu}|. \quad (3.21)$$

The eigenvectors corresponding to the largest magnitude eigenvalues are called left and right fixed points of \mathbb{T} . We can (wlog) re-scale the eigenvalues by the largest eigenvalue, such that all eigenvalues lie within the complex unit disc. The fixed point space of \mathbb{T} is then described by the operator

$$\mathbb{T}^\infty = \lim_{n \rightarrow \infty} T^n = \sum_{k,\nu} |r_{k,\nu}\rangle \langle l_{k,\nu}|. \quad (3.22)$$

This property of the transfer operator allows us to do a particularly interesting entanglement cut (cf. fig. 2.1). We can go to very large (infinite) system size and describe the reduced density matrix on a finite patch of the chain simply by the MPS tensor on the patch with the boundary condition being the fixed point space of the transfer operator.

Let us take a closer look at the two point correlation function $\langle O^{[i]} O^{[j]} \rangle$. This will be given by

$$\langle O^{[i]} O^{[j]} \rangle = \frac{\langle \psi | O^{[i]} O^{[j]} | \psi \rangle}{\langle \psi | \psi \rangle}. \quad (3.23)$$

Note that the MPS wave-function is in principle unnormalized, which is why we have to carry $\langle \psi | \psi \rangle$, given by $\text{tr } \mathbb{T}^L$. The numerator can be evaluated almost in the same fashion, except for the sites i and j , where the observables sit. For these, we define a dressed transfer operator

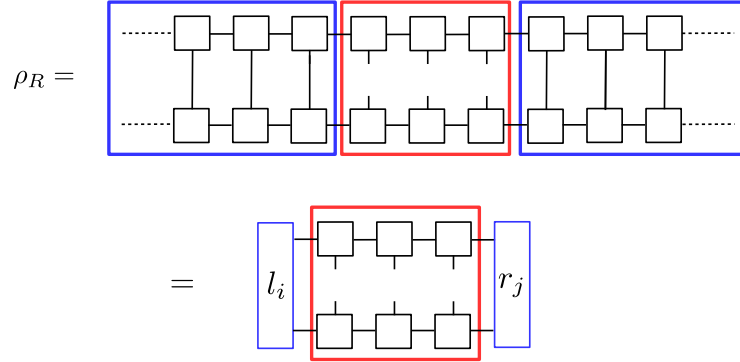


Figure 3.11: The “environment” of a finite patch of an MPS is given by the fixed points of the transfer operator, which serve as boundary conditions to the MPS. In case of degenerate fixed points we would get linear combinations of fixed points as the environment.

$$\mathbb{T}_O := \begin{array}{c} \text{---} \bar{A} \text{---} \\ | \\ \text{---} O \text{---} \\ | \\ \text{---} A \text{---} \end{array} = \sum_i O_{ij} A^i \otimes \bar{A}^j. \quad (3.24)$$

Now, the correlator is given by

$$\langle O^{[i]} O^{[j]} \rangle = \frac{\text{tr} \{ \mathbb{T}_O \mathbb{T}^{|i-j|} \mathbb{T}_O \mathbb{T}^{L-|i-j|-2} \}}{\text{tr} \{ \mathbb{T}^L \}}. \quad (3.25)$$

Let us assume for a moment, that the largest eigenvalue is unique, i.e. $\mathbb{T} = \sum_k \lambda_k |r_k\rangle\langle l_k|$, where $|\lambda_0| > |\lambda_1| \geq \dots$, then $\mathbb{T}^L \rightarrow \lambda_0^L |r_0\rangle\langle l_0|$ and the above expression simplifies to

$$\langle O^{[i]} O^{[j]} \rangle = \sum_k \left(\frac{\lambda_k}{\lambda_0} \right)^{|i-j|-2} (l_0 | \mathbb{T}_O | r_k) (l_k | \mathbb{T}_O | r_0). \quad (3.26)$$

This shows that correlations decay exponentially and the correlation length ξ is determined by the eigenvalues of the transfer operator.

$$\xi = -\frac{1}{\log(|\lambda_1/\lambda_0|)}. \quad (3.27)$$

In the case of exact degeneracy, the MPS has long-range correlations. In order to incorporate algebraically decaying correlations, we would have to let the bond-

dimension grow with system size, which is not viable for large (thermodynamic limit) systems. An MPS with fixed bond dimension cannot describe critical systems.

3.6 PEPS transfer operator, fixed points and symmetry

As we have seen above, the transfer operator encodes the correlations of the system. We therefore generalize the definition to two-dimensional PEPS. To that end, we put the two-dimensional system on a cylinder (torus) of size $N_v \times N_h$ and then treat the vertical one dimension of it as a (now size-dependent) “quasi-MPS”, which we denote by B_i , see fig. 3.12, where $i \equiv (i_1, \dots, i_{N_v})$ is a multi-index along the vertical slice of the cylinder.

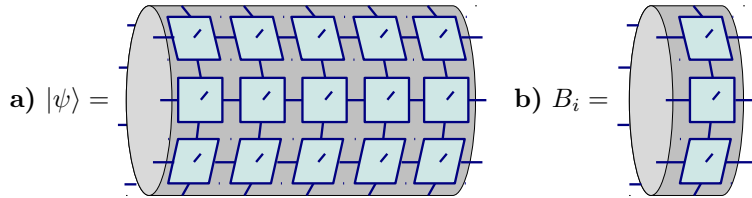


Figure 3.12: We put the system on a cylindrical geometry, which is most convenient for the thermodynamic limit and lets us define a transfer operator in terms of the “quasi-MPS” B_i

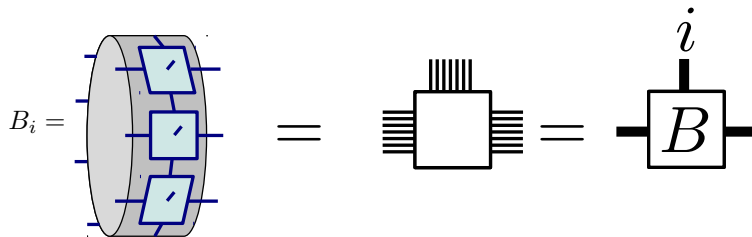


Figure 3.13: One slice of the quantum state can be viewed as a “quasi-MPS” with hybrid indices running over the vertical direction of the lattice, i.e. the dimensions of the MPS grow with N_v .

This compactification allows us to define a transfer operator for PEPS, in the spirit of the transfer operator for MPS. It will now be an extended object in

the vertical direction and act on an entire column “slice” of the cylinder. It is a mapping from bra and ket-layer to another bra- and ket layer:

$$\mathbb{T} : \mathcal{H}^{\otimes N_v} \otimes \mathcal{H}^{\otimes N_v} \rightarrow \mathcal{H}^{\otimes N_v} \otimes \mathcal{H}^{\otimes N_v} \quad (3.28)$$

$$\mathbb{T} = \sum_i B_i \otimes \bar{B}_i. \quad (3.29)$$

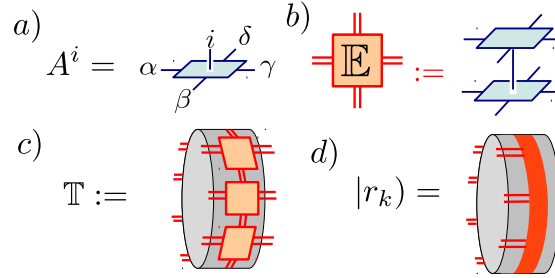


Figure 3.14: Construction of the PEPS transfer operator and its fixed points from (a) the local tensor. (b) Locally contracting bra- and ket-layer gives the “double-tensor” \mathbb{E} (c) contracting one column gives the transfer operator. (d) Its eigenvectors (incl. the fixed points) are extended along the vertical direction and define the PEPS environment analogous to fig. 3.11.

Correspondingly, its eigenvectors are now extended in the vertical direction on N_v sites. While it is in principle an extension of (and thus a different object) than the MPS transfer operator, we still use the same symbol, since we will only be concerned with the PEPS transfer operator and most properties we laid out earlier, carry over to the new transfer operator. Correlations in the horizontal direction are mediated by \mathbb{T} in complete analogy with the MPS case. Most importantly, the fixed points of this PEPS transfer operator now define the *PEPS environment*, exactly as in fig. 3.11. The fact, that the transfer operator itself has a substructure, which most importantly depends on the vertical dimension, leads to new features. On the one hand, taking the thermodynamic limit is non-trivial, unlike the MPS case. On the other hand, this will allow the PEPS to describe critical systems with finite bond dimension, as for example in the models presented in section 3.4.

The symmetry property (fig. 3.5) leads to a commutation of the transfer operator with the virtual symmetry operation applied on both layers simultaneously,

shown in fig. 3.15, which is expressed by

$$[\mathbb{T}, (V_g \otimes \bar{V}_g)^{\otimes N_v}] = 0. \quad (3.30)$$

Analogous to eq. 3.21, we can label the eigenpairs by the symmetry, with the only difference that the symmetry operation and the eigenvectors are now extended along N_v :

$$\mathbb{T} = \sum_{k,\nu} \lambda_{k,\nu} |r_{k,\nu}\rangle \langle l_{k,\nu}|. \quad (3.31)$$

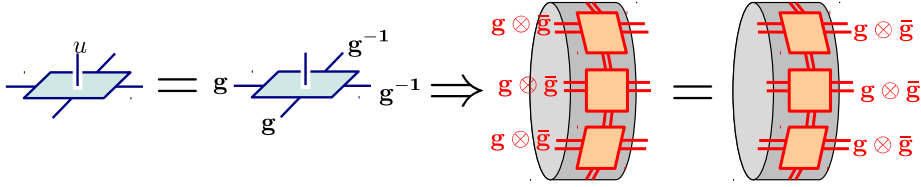


Figure 3.15: By inheriting the local symmetry of the tensor (left equation), the transfer operator commutes with the symmetry by construction. (We identify V_g with g for readability of the diagram.)

3.7 Perturbations in the transfer operator

We now define the notion of a dressed transfer operator in analogy to eq. 3.24, which is the usual transfer operator with an additional operator Λ acting on *one* physical index at site $[k]$:

$$\Lambda := \text{[Diagram]} \Rightarrow \mathbb{T}_\Lambda^{[k]} := \text{[Diagram]} \quad (3.32)$$

This lets us expand the transfer operator of a perturbed model in terms of the unperturbed model as

$$\mathbb{T}_{(\mathbb{1} + \epsilon \Lambda)} = \mathbb{T} + \epsilon \sum_{k=1}^{N_v} \mathbb{T}_\Lambda^{[k]} + \mathcal{O}(\epsilon^2). \quad (3.33)$$

As we derive in detail in the appendix (see A.1), one can use an approach very similar to (degenerate) Rayleigh-Schrödinger perturbation theory to expand the

eigenstates of the perturbed transfer operator in terms of the non-perturbed one. The correction to the eigenvalues is given by evaluating the perturbation T_Λ in the fixed points (“ground state”) of \mathbb{T} ,

$$\lambda_k^{(1)} = (l_k^{(0)} | T_\Lambda | r_k^{(0)}), \quad (3.34)$$

where we denote the order of the expansion by round brackets (n). In case of degeneracy, we have to diagonalize the corresponding matrix, which tells us whether the degeneracy is lifted. The correction to the eigenstates (fixed points) is given by the matrix elements of T_Λ between all excited states and the ground-states (ground-state subspace S)

$$|r_{k,\alpha}^{(1)}\rangle = \sum_{m \notin S} \frac{1}{\lambda_k^{(0)} - \lambda_m^{(0)}} |r_m^{(0)}\rangle (l_m^{(0)} | T_\Lambda | r_{k,\alpha}^{(0)}). \quad (3.35)$$

These expressions will be useful later to test the stability of the fixed points of the transfer operator.

3.8 Isomorphism: Transfer operator and quantum channels

A key tool for us will be to use results from quantum channel theory, one of the cornerstones of quantum information theory. Many key properties of channels are described in [79]. The relation might seem a bit surprising at first sight, so we spend some time to develop it. A quantum channel \mathcal{E} is the most general operation possible on a quantum state. Since it is an operation on the quantum state, which is itself an operator, it goes under the name of superoperator and is a mapping of the form

$$\mathcal{E} : \mathcal{B}(\mathcal{H}) \rightarrow \mathcal{B}(\mathcal{H}). \quad (3.36)$$

Assuming that the input is a quantum state in the first place, i.e. $\rho \in \mathcal{B}(\mathcal{H})$ with $\rho^\dagger = \rho$ and $\rho \geq 0$. The question then is, what kind of \mathcal{E} can we operate with on ρ within the realm of quantum mechanics. Foremost, the operation has to be linear, $\mathcal{E}(A + B) = \mathcal{E}(A) + \mathcal{E}(B)$. A first, rather obvious limitation is, that $\mathcal{E}(\rho) \geq 0$, otherwise we are not left with a quantum state anymore. This restricts it to be what is called a positive map. The last requirement is called *complete* positivity, which is the requirement that when we are given a system

in a state ρ and only act with a channel on some part of a system while leaving the other part of the system unchanged, the resulting global state must also be a quantum state (a density matrix). This condition is written as

$$(\mathbb{1}_k \otimes \mathcal{E})(\rho) \geq 0 \quad \forall k, \quad (3.37)$$

where $\mathbb{1}_k$ acts on degrees of freedom the channel \mathcal{E} does not act on, which can be of arbitrary size. Operators, which also fulfill this additional requirement, are called completely positive and thus the study of quantum operations is called the study of completely positive maps. We like to point out here, that this is a subject of great interest and intricately related to the study of entanglement. For example, a great problem in quantum information science is to find ways to decide whether a given quantum state is entangled or not. The famous Peres-Horodecki criterion says, that the transpose operation is a positive but not completely positive map, if it is acting on entangled states [49]. We allow ourselves to use ancillary degrees of freedom which we are free to discard again in the end. This is called Naimark extension (sometimes with reference to the broader Stinespring dilation theorem, see [42]), or as coined by John Smolin, “going to the church of the larger Hilbert space.” This extension point of view has several useful consequences. First, the concept of purification, which tells us that given a mixed state ρ_A of a system at hand, it is always possible, to find a (in fact classes of states, due to unitary equivalence) pure state $|\psi\rangle$, “the purification”, on a larger system, which describes exactly the same state, if we trace out the additional degrees of freedom with a partial trace.

$$\rho_A = \sum_k p_k |k\rangle_A \langle k| = \text{tr}_B \{ |\psi\rangle \langle \psi| \} \quad (3.38)$$

$$\text{with } |\psi\rangle = \sum_a \sqrt{p_a} |a\rangle_A |a\rangle_B \quad (3.39)$$

We know from the Schrödinger equation, that pure state evolution is unitary. Hence the quantum operation is a unitary on the bigger system:

$$\mathcal{E}(\rho) = \text{tr}_B [U(\rho \otimes |0\rangle_B \langle 0|)U^\dagger]. \quad (3.40)$$

We evaluate this equation by carrying out the partial trace and choosing orthonormal bases (ρ is positive, Hermitian and thus diagonalizable).

$$= \sum_{ijkl} |i\rangle \langle i| \otimes \langle j| U |k0\rangle p_k \langle k0| U^\dagger |l\rangle \langle l| \otimes |j\rangle \quad (3.41)$$

$$= \sum_{ijkl} |i\rangle \langle l| \langle ij| U |k0\rangle p_k \langle k0| U^\dagger |ij\rangle. \quad (3.42)$$

We now arrange the numbers $\langle ij| U |k0\rangle =: A_{ik}^j$ into matrices A , called Kraus operators, with indices i , k and the superscript j . We arrive at the operator sum representation of quantum channels [42]:

$$\mathcal{E}(\rho) = \sum_j A^j \rho A^{j\dagger}. \quad (3.43)$$

(Note that this *not* the PEPS tensor. When talking about channels, A will denote the Kraus operators, as this is the convention in this field. We will see that it is equivalent to the MPS tensor and it will always be clear from the context, which object we are talking about.) Due to unitarity of U and completeness of the basis set $|k\rangle$, it can be seen that

$$\sum_j A^{j\dagger} A^j = \mathbb{1}, \quad (3.44)$$

which is a property called trace preservation, as by this condition, the trace is unchanged:

$$\text{tr}(\mathcal{E}(\rho)) = \text{tr}\left(\sum_j A^j \rho A^{j\dagger}\right) = \text{tr}(\mathbb{1}\rho) = \text{tr}\rho. \quad (3.45)$$

Trace-preservation is more easily handled by introducing the concept of dual channels. For any channel $\mathcal{E}(\rho)$, there is a channel $\mathcal{E}^*(\rho)$ called its dual, which is defined implicitly via the Hilbert-Schmidt inner product

$$\text{tr}(X\mathcal{E}(Y)) = \text{tr}(\mathcal{E}^*(X)Y) \quad (3.46)$$

and can be seen as the Hermitian conjugate under the inner product. By virtue of this definition, a channel is trace-preserving if and only if its dual has the property $\mathcal{E}^*(\mathbb{1}) = \mathbb{1}$, which is a property called *unitality*. If we allow for arbitrary A^i , i.e. $\sum_i A^{i\dagger} A^i \neq \mathbb{1}$, the channel is no longer trace-preserving. We can interpret a decrease in the trace as a “lossy” channel, which discards cer-

tain states. The interpretation of opposite case of increasing trace is not as straightforward.

“Bra-to-ket” isomorphism

We now get to the point, why we are interested in quantum channels and their properties. The Kraus representation of the channel takes as input a (square) matrix

$$\rho = \sum_{a,b=0}^{D-1} \rho_{ab} |a\rangle \langle b|. \quad (3.47)$$

Now for every ρ , we make the identification $|a\rangle \langle b| \rightarrow |a\rangle |b\rangle$, which is nothing but vectorizing the matrix $\rho \rightarrow |\rho\rangle$. The action of the channel

$$\rho \rightarrow \sum_i A^i \rho A^{i\dagger} \quad (3.48)$$

translates to

$$|\rho\rangle \rightarrow \sum_i A^i \otimes A^{i\dagger T} |\rho\rangle, \quad (3.49)$$

where the transpose arises due to the right action being translated into a left action under the above introduced “Bra-flipping” (also known as column (row) stacking). We observe, that this is exactly equation (3.9):

$$\mathbb{T} = \sum_i A^i \otimes \bar{A}^i, \quad (3.50)$$

from which we conclude that we can identify the Kraus operators with the MPS matrices and there is a one-to-one mapping between quantum channels and transfer operators. We may use the concepts transfer operator and quantum channel interchangeably. In cases where we distinguish, \mathbb{T} will denote the operator acting on vectors and T the superoperator acting on matrices.

3.9 Spectral decomposition of channels

As we will work on large systems, we have to deal with high powers of transfer operators, which makes it desirable to find a spectral decomposition of \mathbb{T} . Note, that Hermitian conjugation on the matrix level $\mathbb{T}^\dagger = \sum_i A^{i\dagger} \otimes \bar{A}^{i\dagger}$ of a channel gives rise to the dual channel. Hence, unless we have the special case of a self-dual channel with $A^{i\dagger} = A^i$, we learn that the transfer operator \mathbb{T} is *not* a

Hermitian operator, which makes its analysis more demanding than the study of Hermitian operators. We have to deal with complex eigenvalues as well as left and right eigenvectors and could moreover, in principle, end up with Jordan blocks:

$$\mathbb{T} = X \left(\bigoplus_{k=1}^K J_k(\lambda_k) \right) X^{-1} \quad J_k(\lambda_k) = \begin{pmatrix} \lambda_k & 1 & 0 & \dots \\ 0 & \ddots & \ddots & 0 \\ & & \lambda_k & 1 \\ 0 & & \dots & \lambda_k \end{pmatrix} \quad (3.51)$$

In the case of no Jordan blocks, the diagonal form would look like

$$\mathbb{T} = \sum_k \lambda_k |r_k\rangle\langle l_k|, \quad (3.52)$$

where we use round bracket notation for the eigenvectors to remind ourselves, that these vectors live on the “doubled” space $\mathcal{H} \otimes \mathcal{H}$ of bra and ket together. While we can still find a bi-orthonormal Eigendecomposition with $\langle l_i | r_j \rangle = \delta_{ij}$, we lose normalization of the eigenvectors themselves.

For the evaluation of any physical quantity, i.e. expectation value, we always deal with normalized expressions (cf. eq. 3.23). From this, we take the freedom to normalize the spectrum of the transfer operator, which appears both in the numerator and the denominator of these expressions and choose to divide by the eigenvalue with the largest magnitude, which forces all eigenvalues inside the unit circle, $|\lambda_k| \leq 1$. Eigenvalues, which have $|\lambda_k| = 1$ are called peripheral. Using the arguments of [79], we will show that the peripheral spectrum has no Jordan blocks for unital CP maps. Based on the observation, that $\text{tr}(AT^n(B))$ is finite and independent of n , we can show a contradiction with the existence of Jordan blocks on the peripheral spectrum. On the one hand, the Hölder inequality tells us, that

$$\|AT^n(B)\|_1 \leq \|A\|_\infty \|T^n(B)\|_1 \leq \|A\|_\infty \|B\|_\infty \|\mathbf{1}\|_1 = \|A\|_\infty \|B\|_\infty d, \quad (3.53)$$

which is bounded for bounded operators and has no dependency on the power n . On the other hand, just assuming a single Jordan block gives

$$J_k(\lambda) = \begin{pmatrix} \lambda & 1 \\ 0 & \lambda \end{pmatrix} \Rightarrow (J_k)^n = \begin{pmatrix} \lambda^n & n\lambda^{n-1} \\ 0 & \lambda^n \end{pmatrix} \quad (3.54)$$

and thus a term growing unboundedly with n , which is the desired contradiction. We conclude, that there are no Jordan blocks on the peripheral spectrum of a unital transfer operator.

3.10 Fixed points of quantum channels

A key theorem about (component-wise) positive matrices, which is pivotal for the study of stochastic matrices and is due to Oscar Perron and Georg Frobenius, states that the spectral radius of a entry-wise positive matrix is attained by an eigenvector, which is moreover itself entry-wise positive [30]. This theorem has been carried over to positive maps by Evans and Høegh-Krohn [21]. It is fundamental to the study of transfer operators and has been dubbed the Quantum Perron-Frobenius theorem. We define the notion of irreducibility: a (completely positive) map $T : \mathcal{M}_d(\mathbb{C}) \rightarrow \mathcal{M}_d(\mathbb{C})$ is called irreducible, iff there is no Hermitian projector $P \notin \{0, \mathbb{1}\}$, such that $T(P\mathcal{M}_dP) \subset PT(\mathcal{M}_d)P$.

For an irreducible positive map T , the spectral radius $r(T)$ is attained by a non-degenerate eigenvalue with a corresponding positive definite eigenstate: $T(X) = rX$, with $X > 0$

While the original proof [21] is quite a tour de force, we cite the much more straightforward proof by Wolf [79]: First, we establish, that irreducibility is equivalent to

$$(\mathbb{1} + T)^{d-1}(X) > 0, \quad (3.55)$$

for all $X \geq 0$ and d the dimension of the space. This can be seen from the positivity property, since this implies that T cannot decrease the rank of $(\mathbb{1} + T)(X)$ and thus $\ker((\mathbb{1} + T)(X)) \subseteq \ker(X)$. Furthermore, irreducibility in the original formulation was defined as T having no proper invariant subspace, which implies that the map $\mathbb{1} + T$ has to be rank increasing. Since a positive-semi-definite matrix has to have at least rank one, it follows that after at most $d - 1$ applications, the resulting matrix must be full rank and hence strictly positive. We now look at the following expression:

$$(\mathbb{1} + T)^{d-1}(T - \lambda\mathbb{1})(X) = (T - \lambda\mathbb{1})(X)(\mathbb{1} + T)^{d-1}. \quad (3.56)$$

Let us now specifically choose $\lambda = r$ and X as the largest eigenpair, then by

commuting the two terms and using the above relation, we learn that X must be strictly positive for the largest eigenvalue. Note, that as described in section 3.9, we can wlog assume $r = 1$.

Fixed points of unital channels

As stated above, unitality and trace preservation are dual concepts. Unitality is algebraically much easier to deal with. Let us prove the following two statements:

- The fixed point set of a unital channel forms an algebra, if the dual map has a full rank fixed point
- All fixed points of a unital channel can then be chosen positive semi-definite

A channel $T(\rho) = \sum_k A_k \rho A_k^\dagger$ is *unital*, if it preserves the identity element:

$$T(\mathbf{1}) = \mathbf{1}. \quad (3.57)$$

Let us assume that the dual channel admits a full rank fixed point [38]:

$$\exists \sigma > 0 \Rightarrow T^*(\sigma) = \sigma \quad (3.58)$$

Note, that we can always meet this assumption by projecting onto the maximal support of the dual fixed point space. From this we can show, that the fixed point space forms an algebra. This goes as follows: If X is a fixed point of T , then let us show that for unital channels this implies that $X^\dagger X$ is also a fixed point (trivially, X^\dagger is also a fixed point, which is true for any channel). This can be seen by the following expression:

$$\text{tr}(\sigma[T(XX^\dagger) - XX^\dagger]) = \text{tr}(T^*(\sigma)XX^\dagger - \sigma XX^\dagger) = 0 \quad (3.59)$$

The Schwarz inequality holds for any CP map, i.e. $T(XX^\dagger) - XX^\dagger \geq 0$ (for a proof see 3.10). This means that we have a trace over a positive *definite* matrix multiplied with a positive semi-definite matrix. This can only be zero, if the latter matrix is the zero matrix. We thus proved, that

$$T(XX^\dagger) = XX^\dagger, \quad (3.60)$$

which means XX^\dagger is a fixed point. This is crucial for the next step. Observe that

$$\sum_i [A_i, X][A_i, X]^\dagger = T(XX^\dagger) - T(X)X^\dagger - XT(X^\dagger) + XT(\mathbb{1})X^\dagger. \quad (3.61)$$

Now, owing to the unitality property $T(\mathbb{1}) = \mathbb{1}$, and thanks to XX^\dagger , X^\dagger and X all being fixed points, the right hand side of eq. 3.61 is identically zero. The left hand side is positive semi-definite, which implies it must be the zero operator [4]. This can be the case, if and only if

$$[X, A_i] = 0 \quad \forall X, A_i \quad (3.62)$$

This result is called generalized Lüders theorem (cf. [9], who prove it for self-dual channels and [62], where the unitality condition was neglected): For a unital completely positive map, all fixed points must commute with the Kraus operators. Now the algebra property follows almost trivially. Given two fixed points X and Y , we have $[X, A_i] = [Y, A_i] = 0$. This directly implies $[XY, A_i] = 0$, which means XY is a fixed point, since commuting with the Kraus operators is sufficient. Hence,

$$T(XY) = T(X)T(Y) = XY, \quad (3.63)$$

i.e. the fixed point space of a unital CP map, whose dual admits a full rank fixed point, is an algebra.

Schwarz inequality for CP maps

Every CP map satisfies an operator type Schwarz inequality [14]. To see this, note that any CP map can be written with an isometry V as (called Stinepring dilation) [79]

$$T(X) = V(X \otimes \mathbb{1})V^\dagger \quad (3.64)$$

Hence,

$$T(X^\dagger)T(X) = V(X \otimes \mathbb{1})V^\dagger V(X \otimes \mathbb{1})V^\dagger \quad (3.65)$$

Now $V^\dagger V = \Pi$ is an orthogonal projector, since the V 's are isometries. We can thus write

$$T(X^\dagger)T(X) = V(X \otimes \mathbb{1})\mathbb{1}(X \otimes \mathbb{1})V^\dagger - V(X \otimes \mathbb{1})(\mathbb{1} - \Pi)(X \otimes \mathbb{1})V^\dagger = T(X^\dagger X) - M^\dagger M, \quad (3.66)$$

where $M = (\mathbf{1} - \Pi)(X \otimes \mathbf{1})V^\dagger$. Regrouping, we thus have

$$T(X^\dagger X) \geq T(X^\dagger)T(X) \quad (3.67)$$

Fixed points of unital channel can all be chosen positive

A channel is a linear map on a finite dimensional vector space. Brouwer's fixed point theorem tells us it has at least one fixed point $T(X) = X$. From the Kraus representation of the channel, we know that this implies $T(X^\dagger) = X^\dagger$. Note that we can then write the fixed point as

$$X = \frac{1}{2}[X + X^\dagger] - \frac{i}{2}[i(X - X^\dagger)] = Y_1 + iY_2, \quad (3.68)$$

which is a (complex) linear combination of Hermitian objects, which are all fixed points. We can further decompose a Hermitian matrix Y as

$$Y = \frac{1}{2}[(\sqrt{Y^2} + Y) - (\sqrt{Y^2} - Y)]. \quad (3.69)$$

Since Y was Hermitian, Y^2 is positive and thus has a unique positive square root. However, this decomposition is only useful, if the new objects are also fixed points. Y was already a fixed point, but what about $\sqrt{Y^2}$? To verify that this is also a fixed point, we take again the Lüders property: a fixed point of a unital channel must commute with all Kraus operators. Thus

$$[Y, A_i] = 0 \Rightarrow [Y^2, A_i] = 0 \quad (3.70)$$

$$\Rightarrow [\sqrt{Y^2}\sqrt{Y^2}, A_i] = \sqrt{Y^2}[\sqrt{Y^2}, A_i] + [\sqrt{Y^2}, A_i]\sqrt{Y^2} = 0 \quad (3.71)$$

Now we take the (complete!) eigenbasis of $\sqrt{Y^2} = \sum_i \lambda_i |i\rangle \langle i|$. Note, that crucially this was the (unique) positive root, i.e. $\lambda_i \geq 0$

$$\langle i | \sqrt{Y^2}[\sqrt{Y^2}, A_i] + [\sqrt{Y^2}, A_i]\sqrt{Y^2} |j\rangle = (\lambda_i + \lambda_j) \langle i | [\sqrt{Y^2}, A_i] |j\rangle = 0 \quad (3.72)$$

The first term can only be zero if $\lambda_i = \lambda_j = 0$ simultaneously, which however implies $\langle i | [\sqrt{Y^2}, A_i] |j\rangle = 0$. For any other λ_i, λ_j , the commutator must vanish for the equation to hold. We thus showed that any matrix element has to vanish, which means that $[\sqrt{Y^2}, A_i] = 0$ and by virtue of this $\sqrt{Y^2}$ is again a fixed point. We thus proved, that any fixed point of a unital channel, whose dual has a full rank fixed point, can be decomposed into a complex linear combination

of positive semi-definite fixed points [62].

Fixed point set of trace preserving transfer operators

While in the above we characterized unital channels, let us now state properties of the fixed point space of the dual map, i.e. a trace preserving channel. The following theorem characterizes the fixed point space of a trace preserving completely positive map. Let $T : \mathcal{M}_d(\mathbb{C}) \rightarrow \mathcal{M}_d(\mathbb{C})$, be a trace-preserving CP map. Then there is a unitary U and a set of positive semi-definite density matrices $R_k \in \mathcal{M}_{m_k}(\mathbb{C})$ such that the fixed point set is given by

$$\mathcal{F}_T = U \left(\bigoplus_{k=1}^K \mathcal{M}_{d_k} \otimes R_k \right) U^\dagger. \quad (3.73)$$

\mathcal{M}_{d_k} stands for the full algebra of complex matrices and the dimensionalities of the spaces being tensored together match the dimensionality of the fixed point space: $m_k \cdot d_k = d$. This theorem will be of great utility to us, since the characterization of the fixed point set is crucial in understanding the mechanism of symmetry breaking in PEPS. It is due to [38, 7, 79].

Chapter 4

Long-range order and symmetry breaking

Spontaneous symmetry breaking is the prime example of global order emerging from local interactions in quantum systems at zero temperature. In a general sense, we speak of spontaneous symmetry breaking when the ground states of a system “lose” the symmetry of the underlying Hamiltonian in the thermodynamic limit [71]. In this chapter, we will develop the description of an analogous mechanism in the PEPS framework. The analogy will be on the one hand between the PEPS transfer operator and the Hamiltonian, which are both formulated in a manifestly symmetric fashion, and on the other hand between the ground states (of the Hamiltonian) and the fixed points (of the transfer operator), which, as it will turn out, both can lose the symmetry of their underlying theory spontaneously. In both cases, the symmetry broken states are “physical” in a specific sense. Finding the correct description of these symmetry broken states is challenging, because on a finite system, the symmetry breaking is “obscured” by quantum fluctuations, which restore the symmetry [32, 35] and we have to develop techniques to capture the correct behavior and find a description of the physical, symmetry broken states in a finite system.

This chapter will be outlined as follows: We will start by showing how long-range order, unlike an order parameter, is a good criterion for the presence of symmetry breaking in finite systems. We will then prove, that long-range order leads to an asymptotic degeneracy in the PEPS transfer operator. We show how

in the presence of this degeneracy, a stability requirement leads to symmetry breaking. We prove that the symmetry breaking pattern is uniquely specified, allowing us to construct the symmetry broken states directly from the model defining ones. We will be concerned with finite abelian symmetry \mathbb{Z}_N throughout this chapter.

4.1 Long-range order

Let us start by demonstrating why order parameters are a problematic way to describe symmetry breaking in finite systems. Given a (finite) lattice Ω of size $|\Omega|$ and a Hamiltonian $H_\Omega = \sum_k E_k |\psi_k\rangle \langle \psi_k|$, which is invariant under some unitary symmetry operation u , i.e. $[H_\Omega, u] = 0$, we would like to detect symmetry breaking with some order parameter \hat{O} . We require from an order parameter that it does not commute with the symmetry, i.e. $[\hat{O}, u] \neq 0$. If we are in a situation, where this Hamiltonian is asymptotically degenerate, the order parameter on *any* finite system cannot detect symmetry breaking. This follows from the fact that due to the degeneracy only being asymptotic, the eigenstates of the Hamiltonian on a finite system all transform trivially under the (*unitary*) symmetry:

$$u |\psi_k\rangle = e^{i\phi_k} |\psi_k\rangle. \quad (4.1)$$

Assuming, that the order parameter takes a non-zero expectation value on any of these finite-volume states then immediately leads to a contradiction,

$$\langle \psi_k | \hat{O} | \psi_k \rangle = \langle \psi_k | u^\dagger \hat{O} u | \psi_k \rangle \neq \langle \psi_k | u^\dagger u \hat{O} | \psi_k \rangle = \langle \psi_k | \hat{O} | \psi_k \rangle, \quad (4.2)$$

from which we conclude that it cannot acquire a non-zero expectation value and is thus unable to detect symmetry breaking. The standard way to resolve this, is to add a perturbation to the Hamiltonian that couples to the order parameter, e.g. $H_\Omega(B) = H_\Omega + B \sum_{i \in \Omega} O_i$. This will select the eigenstates that diagonalize the perturbation, i.e. the symmetry broken states. Let $\langle \cdot \rangle_{B, \Omega}$ denote the expectation value in the ground state of this perturbed Hamiltonian. Then the usual order parameter (e.g. the spontaneous magnetization) is defined as:

$$m := \lim_{B \rightarrow 0} \lim_{|\Omega| \rightarrow \infty} \frac{1}{|\Omega|} \langle O \rangle_\Omega. \quad (4.3)$$

Using this procedure will not tell us anything about symmetric PEPS, since

the PEPS of the perturbed model will be non-symmetric and finding out how it could be related to the symmetric PEPS on a finite system seems an impossible task. What turns out to be a much more viable and insightful procedure on a finite system is to use long-range order instead, which is measured by the two-point correlator

$$\sigma := \lim_{|\Omega| \rightarrow \infty} \frac{1}{|\Omega|} \sqrt{\langle O^\dagger O \rangle_{0, \Omega}}, \quad (4.4)$$

for some suitably chosen magnetization operator $O = \sum_{i \in \Omega} Z_i$ (with local operators Z_i). It has been shown in a number of cases that $m \geq \sigma$, i.e., long-range order implies a non-zero spontaneous magnetization [32, 35]. Note that long-range order does not suffer from the same problem as the order parameter above, since it is an even function. This implies that a symmetric PEPS wave-function built from a symmetric local tensor can acquire long-range order. It is for this reason that we consider PEPS wave-functions with long-range order (which we will use interchangeably with symmetry breaking in the following); our goal will be on the one hand to understand the conditions under which long-range order occurs, and on the other hand to identify the wave-functions describing the corresponding symmetry broken states (i.e., those obtained as ground states of $H_\Omega(B)$ in the limit $B \rightarrow 0$). Specifically, in the case of a \mathbb{Z}_N symmetry considered here, long-range order will denote a non-zero σ for some Z obeying

$$u^\dagger Z u = \omega^\alpha Z, \quad (4.5)$$

for some $\alpha = 0 \dots N-1$ and again $\omega = \exp(\frac{2\pi i}{N})$. The $\alpha = 1$ case we will refer to as full symmetry breaking since Z does not commute with any symmetry operation u^n . In that case, the above condition could for example be fulfilled by the so called clock matrices $Z = \sum_k \omega^k |k\rangle \langle k|$. On the other hand, if $\gcd(\alpha, N) > 1$, then the symmetry is only partially broken since Z commutes with $u^{N/\gcd(\alpha, N)}$. Evaluating σ can be done using a symmetric PEPS: we will do so on a closed manifold (periodic boundary conditions) such that the full state is symmetric.

Let us now turn towards the study of PEPS. For a PEPS $|\Psi\rangle$, we have that $\sigma^2 = \lim_{N_h, N_v \rightarrow \infty} \sigma_{N_v, N_h}^2$ where

$$\sigma_{N_v, N_h}^2 = \frac{1}{N_h^2 N_v^2} \sum_{ij} \frac{\langle \Psi | Z_i Z_j^\dagger | \Psi \rangle}{\langle \Psi | \Psi \rangle}. \quad (4.6)$$

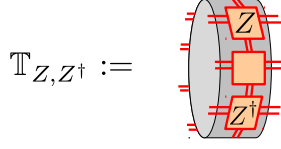


Figure 4.1: The transfer operator $\mathbb{T}_{Z,Z^\dagger}^{[i,j]}$ dressed on two physical sites, where the full operator is given by all permutations

In what follows, we will normalize Z_i such that its operator norm $\|Z_i\|_{\text{op}} \leq 1$. We will decompose the above sum over i and j into two parts: either $i_y \neq j_y$ or $i_y = j_y$. For the first part, define $\mathbb{T}_Z := \frac{1}{N_v} \sum_{k=1}^{N_v} \mathbb{T}_Z^{[k]}$ and for the second part define $\mathbb{T}_{Z,Z^\dagger} := \frac{1}{N_v^2} \sum_{i,j=1}^{N_v} \mathbb{T}_{Z,Z^\dagger}^{[i,j]}$ where $\mathbb{T}_{Z,Z^\dagger}^{[i,j]}$ is the transfer operator obtained by inserting an operator Z and Z^\dagger at sites i and j respectively, see Fig. 4.1.

Define C_1 and C_2 as

$$C_1 = \sum_{p=0}^{N_h-2} \text{tr} [\mathbb{T}_{Z^\dagger} \mathbb{T}^p \mathbb{T}_Z \mathbb{T}^{N_h-p-2}] , \quad (4.7)$$

$$C_2 = \text{tr} [\mathbb{T}_{Z,Z^\dagger} \mathbb{T}^{N_h-1}] . \quad (4.8)$$

This allows us to write $\sigma_{N_v, N_h}^2 = \frac{1}{N_h} \frac{C_1 + C_2}{\text{tr}[\mathbb{T}^{N_h}]}$. The factors of N_v are taken care of by the definition of \mathbb{T}_{Z,Z^\dagger} and \mathbb{T}_Z and a factor of N_h is taken care of by using translation invariance in the horizontal direction. The contribution of C_2 converges to zero in the large N_h limit. It corresponds to taking the sum over $N_v^2 N_h$ expectation values and dividing by $N_v^2 N_h^2$. The term of interest is C_1 .

From the scaling of $\frac{C_1}{N_h \text{tr}[\mathbb{T}^{N_h}]} \propto \mathcal{O}(1)$ we aim to show that the gap between $|\lambda_\alpha|$ and the largest eigenvalue λ_0 decreases with increasing N_h . A first step in the proof is that for large N_h , $\mathbb{T}^{N_h} \rightarrow |r_0\rangle\langle l_0|$, where r_0 is the eigenvector of \mathbb{T} corresponding to the eigenvalue λ_0 and l_0 the corresponding left eigenvector (ie. eigenvector of \mathbb{T}^*). We use round brackets to emphasize that, although r_0 and l_0 are eigenvectors, they are also operators. The dressed transfer operator \mathbb{T}_Z maps r_0 into the symmetry sector $\alpha = 1$ due to

$$\begin{aligned} U \mathbb{T}_Z(r_0) U^\dagger &= \mathbb{T}_{u^\dagger Z u}(U r_0 U^\dagger) \\ &= \omega \mathbb{T}_Z(r_0) . \end{aligned} \quad (4.9)$$

More explicitly, if $U U^\dagger = \omega^\beta l$, then $\text{tr} [l^\dagger \mathbb{T}_Z(r_0)] \neq 0$ only if $\beta = \alpha$. The main idea is that the factor \mathbb{T}^p will give rise to an exponential suppression, the

leading term being proportional to $|\lambda_\alpha|^p$. So $|\lambda_\alpha| < 1$ will result in zero long-range order. However, as N_v increases, the dimension of the space on which \mathbb{T} acts also increases exponentially as D^{2N_v} , where D is the bond dimension of the PEPS tensor A . Without any other assumptions, large Jordan blocks could prevent exponential suppression. As an example, consider a map \mathbb{T} in Jordan form with a single Jordan block of size D and corresponding eigenvalue $\lambda < 1$. Then for $v = (0, \dots, 0, 1)^T$, $\|\mathbb{T}^p v\|^2 = \sum_{q=0}^{\min(p,D)} \lambda^{2(p-q)} \binom{p}{q}^2$. For large p this sum scales as $\lambda^{2p} p^{2D}$, which for constant D is eventually exponentially suppressed but only at a length scale $p \propto D$. Hence, due to the exponentially increasing dimension of \mathbb{T} , correlations are only suppressed only over a length D^{2N_v} leading to a scaling of the long range order as $\sigma^2 \propto \frac{1}{N_h} D^{2N_h}$, even in the case that $|\lambda_\alpha| < 1$. It is for this reason that we need more assumptions on \mathbb{T} . We will assume for the rest of the section that the transfer operator \mathbb{T} is normal, $\mathbb{T}\mathbb{T}^* = \mathbb{T}^*\mathbb{T}$. This is in particular the case if \mathbb{T} is Hermitian, which for example can follow from Hermiticity of its Kraus operators $(B^i)^\dagger = B^i$ which physically is related to a combination of time reversal (complex conjugation) and reflection along the y -axis (transposition) symmetry.

Let us now return to Eq. (4.7). If the largest eigenvalue $\lambda_0 = 1$ of \mathbb{T} is non degenerate, then for any bounded operator O the following holds:

$$\begin{aligned} \lim_{N_h \rightarrow \infty} \sum_{p=0}^{N_h-2} \frac{\text{tr} [\mathbb{T}_{O^\dagger} \mathbb{T}^p \mathbb{T}_O \mathbb{T}^{N_h-p-2}]}{\text{tr} [\mathbb{T}^{N_h}]} &= \\ 2 \sum_{p=0}^{\infty} \text{tr} [\mathbb{T}_{O^\dagger} \mathbb{T}^p \mathbb{T}_O |r_0\rangle\langle l_0|] &. \end{aligned} \quad (4.10)$$

(The proof is quite technical, which is why we move it to the appendix.) The factor of two arises from first splitting the sum into two parts, one for which $p > N_h/2$ and one for which $p < N_h/2$. Both sums are identical (if N_h is odd) up to the position of the dagger, which can be swapped using ket-bra-hermiticity which exchanges $\mathbb{T}_O \leftrightarrow \mathbb{T}_O^\dagger$, while leaving the other terms unchanged, and thus

$\sum_{p=0}^{N_h-2} \rightarrow 2 \sum_{p=0}^{N_h/2-1}$. Using Eq. (4.10), we now have that

$$\begin{aligned}
\lim_{N_h \rightarrow \infty} N_h \sigma_{N_v, N_h}^2 &= \sum_{p=0}^{\infty} \text{tr} [\mathbb{T}_{Z^\dagger} \mathbb{T}^p \mathbb{T}_Z |r_0\rangle \langle l_0|] \\
&= \sum_{p=0}^{\infty} \langle l_0 | \mathbb{T}_{Z^\dagger} (P_\alpha \mathbb{T} P_\alpha)^p \mathbb{T}_Z |r_0\rangle \\
&\stackrel{(a)}{=} \langle l_0 | \mathbb{T}_{Z^\dagger} (1 - P_\alpha \mathbb{T} P_\alpha)^{-1} \mathbb{T}_Z |r_0\rangle \\
&\stackrel{(b)}{\leq} \| \langle l_0 | \mathbb{T}_{Z^\dagger} \|_2 \| (1 - P_\alpha \mathbb{T} P_\alpha)^{-1} \|_{\text{op}} \| \mathbb{T}_Z |r_0\rangle \|_2 \\
&\leq \frac{1}{1 - |\lambda_\alpha|} ,
\end{aligned}$$

where P_α is the projector onto the irrep sector α . It is in (a) and (b) that we have used normality of \mathbb{T} , which implies that $\|P_\alpha \mathbb{T} P_\alpha\|_{\text{op}} < 1$ such that the Neumann series converges, and $\| \mathbb{T}_Z |r_0\rangle \|_2^2 = \langle r_0 | \mathbb{T}_Z \mathbb{T}_Z |r_0\rangle \leq 1$, as $\|Z_i\|_{\text{op}} \leq 1$ and the left and right eigenvectors coincide. We now have

$$\sigma^2 = \lim_{N_h, N_v \rightarrow \infty} \sigma_{N_v, N_h}^2 \leq \lim_{N_v \rightarrow \infty} \frac{1}{N_v} \lim_{N_h \rightarrow \infty} N_h \sigma_{N_v, N_h}^2 , \quad (4.11)$$

where the inequality can be shown by coupling the l.h.s. limit such that N_h grows sufficiently faster than N_v , based on the formal definition of the limit (see appendix). It thus follows that if $\sigma^2 > 0$, for sufficiently large N_v it must hold that

$$0 < \frac{1}{N_v} \frac{1}{1 - |\lambda_\alpha|} . \quad (4.12)$$

Thus non zero long range order of an order parameter Z obeying Eq. (4.5) for some α implies that

$$|\lambda_\alpha| \geq 1 - \mathcal{O}(1/N_v). \quad (4.13)$$

At this point we have not said anything about the phase of λ_α . It is known that peripheral spectrum (eigenvalues of modulus 1) consists of roots of unity [22, Proposition 3.3] and that any eigenvalue of the form $e^{2\pi i/p}$ corresponds to a p periodic state. The degeneracy of the fixed point would then relate to a breaking of translation symmetry, as well as the global symmetry s . An example is the antiferromagnetic phase. We can remove such a phase by blocking p sites, i.e. consider T^p , yielding that $\lambda_\alpha \geq 1 - \mathcal{O}(1/N_v)$.

4.2 Stability of fixed points in the presence of degeneracy

Symmetry breaking can be understood as a situation where it is preferable for the system to collapse into states with less symmetry, when these states are favorable for some reasons or even the only ones allowed. We learned above that long-range order implies a degeneracy in the fixed point space, i.e. there exists more than one fixed point. The question we ask now is what the presence of more than one fixed point implies, when we perturb the bulk with arbitrary perturbations. We will now prove, that fixed points, that correspond to orthogonal positive-semi-definite matrices, are *stable under arbitrary perturbations*. While this is remarkable in itself, we will also learn in a moment, that this positivity requirement completely specifies the fixed point basis, which implies that the symmetry broken fixed points are given by *positive-semi-definite fixed points*.

Let us assume a perturbation on an arbitrary (finite) patch of the lattice. Observe, that everything outside this patch is given by the left and right fixed points. We compress the finite patch into one composite index and a big matrix Λ . The mixing is then given by fig. (4.2).

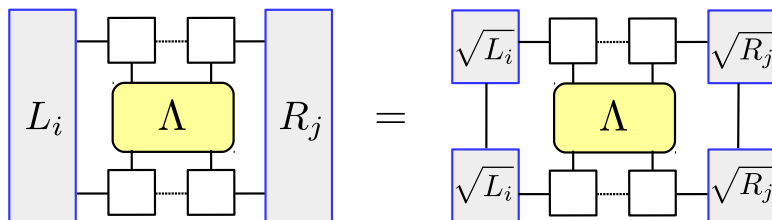


Figure 4.2: A perturbation in the bulk is represented by Λ , note that it can act on a patch of arbitrary (finite) size, indicated by dashed lines. If the fixed points are positive, we can take a unique positive square root.

We then measure the norm of the vector corresponding to the ket-layer of this diagram, see fig. 4.3. As always, the norm is computed by copying the state and contracting it from the top. We then learn, that this is equal to the (Hilbert-Schmidt) inner-product between different fixed points, which we assumed to be zero. We thus find that positive, orthogonal fixed points are stable under arbitrary perturbations. Now positivity of the fixed points implies, that we can take unique positive square roots, as explained in the diagram above.

$$\begin{aligned}
\text{norm} \left(\left(\begin{array}{c} | \\ \sqrt{L_i} \\ | \end{array} \text{---} \square \text{---} \square \text{---} \begin{array}{c} | \\ \sqrt{R_j} \\ | \end{array} \right)^2 \right) &= \begin{array}{c} \square \\ | \\ L_i \\ | \\ \square \end{array} \text{---} \begin{array}{c} \square \\ | \\ \square \\ | \\ \square \end{array} \text{---} \begin{array}{c} \square \\ | \\ R_j \\ | \\ \square \end{array} \\
= \begin{array}{c} \square \\ | \\ L_i \\ | \\ \square \end{array} \text{---} \begin{array}{c} \square \\ | \\ R_j \\ | \\ \square \end{array} &= 0 \quad i \neq j
\end{aligned}$$

Figure 4.3: Positive fixed points are stable: There exists no perturbation acting on any finite patch of the bulk, that mixes different positive fixed points, which is shown by deriving that such a state would have zero norm.

4.3 Construction of symmetry broken states

As was discussed in chapter 3, the transfer matrix is manifestly symmetric for a symmetric PEPS tensor, which is reflected in the fact that the symmetry operation commutes with the transfer matrix always. Let us abbreviate the symmetry operation by defining $S := (V_g \otimes \bar{V}_g)^{\otimes N_v}$. We now repeat eq. 3.30 here for readability:

$$[\mathbb{T}, S] = 0. \quad (4.14)$$

The vanishing commutator tells us that the eigenvectors of the transfer matrix transform under some irrep of the symmetry, which in our case are all one-dimensional, since we study finite Abelian symmetries \mathbb{Z}_N . We make the assumption, that per symmetry sector, the largest eigenvalue of \mathbb{T} is unique, also in the thermodynamic limit. We would like to characterize the fixed point space in this situation and thus uniqueness implies that we can drop the counting label on the eigenvectors, only keeping the symmetry label. For a \mathbb{Z}_N -symmetry the eigenvectors of the transfer matrix are given by

$$S r_k S^\dagger = \omega^k r_k \quad (4.15)$$

$$S l_k S^\dagger = \omega^k l_k \quad (4.16)$$

$$\text{where } k = 0..(N-1), \quad \omega = e^{2\pi i/N} \quad (4.17)$$

Note, that the zero-sector fixed point is positive, which can be seen by considering T^∞ , which was defined in equation 3.22. Its fixed points obey Eqs. 4.15 and

4.17. We then have that $T^{(\infty)}(\mathbb{1}) \geq 0$ due to the CP property of the transfer operator, and $\mathbb{1}$ is invariant under the symmetry and thus in the zero sector. Hence $T^{(\infty)}(\mathbb{1}) = r_0$ is positive as well as l_0 by analogy.

Our goal now is the following: Given the above described fixed-point set, does there exist a set of *stable fixed points* in the precise sense of fig. 4.2? As elaborated in eq. 3.10, the fixed point set of a *trace preserving* transfer operator (quantum channel) can be spanned by a set of positive semi-definite operators. The fore-mentioned transfer operator however is not necessarily trace-preserving. We will now be concerned with resolving this seeming incompatibility. Let us assume for a moment that the left fixed point in the zero-sector has full rank $l_0 > 0$, which implies that it has an inverse. This allows us to define a modified channel \tilde{T} (“isometric gauge”):

$$\tilde{T}(X) = \sum_i \left(\sqrt{l_0} A_i \frac{1}{\sqrt{l_0}} \right) X \left(\frac{1}{\sqrt{l_0}} A_i^\dagger \sqrt{l_0} \right) \quad (4.18)$$

This channel then is *trace-preserving*, which is seen by noting that the dual map \tilde{T}^* , defined via $\text{tr}(\tilde{T}^*(A)B) = \text{tr}(A\tilde{T}(B))$ is unital (i.e. $\tilde{T}^*(\mathbb{1}) = \mathbb{1}$) by the virtue of $T^*(l_0) = l_0$. We now extend this to the case, where l_0 is not full rank, by defining l_0^{-1} as the inverse on the support S of l_0 , i.e. the matrix satisfying $l_0^{-1}l_0 = l_0l_0^{-1} = \mathbb{1}_S$, the identity on S . $\tilde{T}(X)$ then is trace preserving channel on S .

To make sure that the above modification of the channel, which involves a projection onto the support of l_0 , does not change the fixed point set, let us show, that the support of any fixed point is contained in the support of l_0 . Assume some Hermitian X , then $\mathbb{1} \pm \epsilon X$ is clearly positive definite for some $\epsilon > 0$. $T^*(\mathbb{1} \pm \epsilon X) = l_0 \pm \epsilon T^*(X)$ has to be positive by definition of CP (dual maps are obviously also CP), but the r.h.s. fails to be positive as soon as $T^*(X)$ has support outside l_0 , hence $\text{supp}(l_i) \subseteq \text{supp}(l_0)$. Since the fixed point space is preserved under Hermitian conjugation ($l_i^\dagger \propto l_{N-i}$) we also have that the image of l_i is restricted to the support l_0 or in other words $P_S l_i P_S = l_i$ where P_S is the projector on the support space S of l_0 . This implies, that with respect to the original channel T , the modified trace preserving channel \tilde{T} has fixed points

$$\tilde{l}_i = \sqrt{l_0^{-1}} l_i \sqrt{l_0^{-1}}, \quad \tilde{r}_i = \sqrt{l_0} r_i \sqrt{l_0}, \quad (4.19)$$

which is not hard to verify. We start with the left fixed point, where we simply have $\tilde{T}^*(\tilde{l}_i) = \sqrt{l_0^{-1}} T^*(P_S l_i P_S) \sqrt{l_0^{-1}} = \sqrt{l_0^{-1}} T^*(l_i) \sqrt{l_0^{-1}} = \tilde{l}_i$, where we used the fact that all left fixed points are contained in the support of l_0 as shown above. For the right fixed points we similarly evaluate $\tilde{T}(\tilde{r}_i) = \sqrt{l_0} T(P_S r_i P_S) \sqrt{l_0}$, expressing the channel as $T(X) = \sum_k r_k \text{tr}(l_k^\dagger X)$, we see that $T(\Pi_S X \Pi_S) = T(X)$, from which we conclude that $\tilde{T}(\tilde{r}_i) = \tilde{r}_i$, as claimed.

Now for a *trace-preserving* channel, there exists a set of mutually orthogonal *positive-semi-definite* fixed points, which span the entire fixed point space. We thus arrive at the following key insight:

The fixed point set of a \mathbb{Z}_N -symmetric transfer-operator with long-range order is spanned by mutually orthogonal positive-semi-definite fixed points.

$$\mathbb{T}^\infty = \sum_k |\tilde{R}_k\rangle \langle \tilde{L}_k|, \quad (4.20)$$

where $\tilde{L}_k, \tilde{R}_k \geq 0$ and $\text{tr}(\tilde{L}_k^\dagger \tilde{R}_j) \propto \delta_{ij}$.

In the remainder of this section we will be tasked with first finding the basis transformation that gives these *positive* fixed points \tilde{R}_k from the irreps r_k (and the dual fixed points correspondingly) and secondly prove, that this basis does not mix under arbitrary perturbations and is thus the basis of symmetry broken states.

Hermitian \mathbb{Z}_2 -symmetry breaking transfer operator

We start with the simplest case, which requires the least technical tools. Having a Hermitian \mathbb{Z}_2 -symmetric transfer operator means that left and right fixed points coincide (which also lets us have them self-normalized) and that in our setting we have two-sectors in the transfer operator, both of which contribute with one fixed point, such that the transfer operator has the form

$$T = |r_+\rangle \langle r_+| + |r_-\rangle \langle r_-| + \dots, \quad (4.21)$$

where we omit all the other terms, which we assume to lie below some gap in the thermodynamic limit. We might naively characterize the fixed point space of this operator simply as the linear span of the two fixed points, written as

operators:

$$R(\gamma) = \frac{1}{\sqrt{1+\gamma^2}}(r_+ + \gamma r_-) \quad (4.22)$$

However, this cannot be true in general, since the resulting linear combination has to be a positive (semi-)definite matrix (operator), which first of all requires $\gamma \in \mathbb{R}$ for Hermiticity. Moreover, r_- in itself, cannot be a positive operator, since it lives in a non-trivial symmetry sector. It is invariant under the unitary conjugation with the symmetry action

$$S r_- S^\dagger = -r_-, \quad (4.23)$$

which implies that its spectrum is invariant under sign flip and thus as soon as it has a positive eigenvalue, this is accompanied by a negative partner, which renders it a non-positive matrix. This is the first indication towards the mechanism of symmetry breaking in PEPS: It is an essential ingredient for symmetry breaking, that eigenvectors, which transform non-trivially under the symmetry action, asymptotically become part of the fixed point space and positivity requirements restrict the possible states of the system. We now characterize the possible $R(\gamma)$ of equation 4.22. These are characterized by choosing γ , such that $R(\gamma) \geq 0$. Again, note that conjugation does not change the spectrum,

$$S R(\gamma) S^\dagger = R(-\gamma) \geq 0. \quad (4.24)$$

Let us now derive a useful inequality, which we will exploit repeatedly later. Given two positive operators, the trace over their product is also positive:

$$A, B \geq 0 \Rightarrow \text{tr}(AB) = \text{tr}\left(A \sum_j \lambda_j |j\rangle \langle j| \right) = \sum_j \underbrace{\lambda_j}_{\geq 0} \underbrace{\langle j| B |j\rangle}_{\geq 0} \geq 0. \quad (4.25)$$

Combined with 4.24, this inequality leads to the constraint

$$\text{tr}(R(\gamma)R(-\gamma)) = \frac{1-\gamma^2}{1+\gamma^2} \geq 0 \quad (4.26)$$

$$\gamma \leq 1 \quad (4.27)$$

Now let us assume there exist some perturbation on the transfer operator, which leads to the symmetry breaking (i.e. a splitting of the degeneracy). This perturbation then selects one state in the fixed point space. If this perturbation preserves Hermiticity, we know that the eigenbasis is orthogonal. Furthermore,

if we invert the splitting, the basis in which the perturbed transfer operator splits, will remain the same but the other state will be selected and thus also has to be positive semi-definite. The state orthogonal to $R(\gamma)$ is given by

$$R^*(\gamma) = \frac{1}{\sqrt{1 + (1/\gamma)^2}} \left(r_+ - \frac{1}{\gamma} r_- \right). \quad (4.28)$$

Now $R^*(\gamma) \geq 0$ implies

$$\gamma \geq 1 \quad (4.29)$$

by the same reasoning as above. In total, we find that

$$\gamma = 1, \quad (4.30)$$

which reduces the allowed states to

$$R = \frac{1}{\sqrt{2}} (r_+ + r_-) \quad (4.31)$$

$$R^* = \frac{1}{\sqrt{2}} (r_+ - r_-) \quad (4.32)$$

Non-Hermitian transfer operators with \mathbb{Z}_N symmetry

Starting from $T^\infty = \sum_i |\tilde{r}_i\rangle\langle\tilde{l}_i|$, we want to find the $|\tilde{R}_i\rangle$, as defined in equation 4.20. Observe, that the $|\tilde{r}_i\rangle$ are mutually orthogonal, because they reside in different sectors of the symmetry. We are free to normalize, such that $\langle\tilde{r}_i|\tilde{r}_j\rangle = \delta_{ij}$. Similarly, the $|\tilde{R}_i\rangle$ are orthogonal and if we assume them to be normalized, this already implies that the transformation must be unitary, i.e. $|\tilde{R}_i\rangle = \sum_{ij} U_{ij} |\tilde{r}_j\rangle$. The \tilde{R}_i are furthermore positive and given $A, B \geq 0$, we have $\text{tr}(AB) \geq 0$, as given in eq. 4.25. We will make use of this by deriving, that

$$\text{tr}(\tilde{R}_i S^m \tilde{R}_j (S^m)^\dagger) = \langle\tilde{R}_i|(S \otimes \bar{S})^m|\tilde{R}_j\rangle \geq 0 \quad (4.33)$$

which we reformulate as

$$\langle\tilde{r}_k|U_{ki}^\dagger(\omega^m)^l U_{jl}|\tilde{r}_l\rangle = (UW^m U^\dagger)_{ji} =: G_{ji}^{[m]} \geq 0, \quad (4.34)$$

where we used orthonormality of $|\tilde{r}_i\rangle$ and defined the diagonal matrix $W = \text{diag}\left(1 \quad \omega \quad \omega^2 \quad \dots \quad \omega^{N-1}\right)$. We note, that $G^{[m]}$ are N entry-wise non-negative matrices. Now, it can be seen that $G^{[m]-1} = G^{[N-m]}$, so the inverse of such

a matrix is also non-negative. To proceed, let us prove that

$$G_{ij} \geq 0 \text{ and } G_{ij}^{-1} \geq 0 \quad \Leftrightarrow \quad G = D \cdot P, \quad (4.35)$$

(G is then called monomial), with D (non-negative) diagonal and P a permutation matrix (i.e. exactly one 1 per row and column). To see this, take $GG^{-1} = \mathbf{1}$ and observe, that this means orthonormality of rows and columns, additionally G must have full rank thanks to the existence of the inverse. This implies, that each column of G^{-1} must be orthogonal to $N - 1$ rows of G , and thus has $N - 1$ zeros lest it has negative entries, prohibited by entry-wise non-negativity. If we push the value of this one non-zero entry into a separate matrix D , we arrive at a permutation matrix P and we are done. Note, that $W^{-1} = W^\dagger$, which implies G is unitary and thereby restricts it to a pure permutation matrix, which has to be an N -cycle, due to the fact it has all roots of unity in its spectrum. Since the label of the \tilde{R}_i is arbitrary (we cannot distinguish them in principle), there is a relabeling freedom which lets us write G as a shift operator $G = \sum |x+1\rangle \langle x|$, which we can interpret as a translation operator on a discrete position eigenbasis. G is translation invariant and thus will be diagonalized by a Fourier transformation

$$F = N^{-1/2} \sum_{px} \omega^{px} |p\rangle \langle x| \quad (4.36)$$

as

$$FGF^\dagger = \sum_p \omega^p |p\rangle \langle p|. \quad (4.37)$$

The unitary transformation we are trying to find, is therefore pinned down to $U = F \cdot C$, where C is the remaining phase freedom. The latter can be fixed by a consistency condition: We so far have, that $\tilde{R}_i = \sum_j U_{ij} \tilde{r}_j$, where we require the \tilde{R}_i to be positive (semi-)definite. Upon inversion, we thus have in particular $\tilde{r}_0 = \sum_j \tilde{c}_j \tilde{R}_j$ with the \tilde{R}_j having orthogonal support. On the other hand \tilde{r}_0 must also be positive, because it is the leading eigenvector on any finite system and thus positive on its own, which forces us to choose $c_i = +1$. We thus proved, that the basis transformation to symmetry broken states is given by the Fourier transformation $U = F = \sum_{ij} \omega^{ij} |i\rangle \langle j|$:

$$\tilde{R}_i = \sum_j F_{ij} \tilde{r}_j \geq 0. \quad (4.38)$$

For the left fixed points, the reasoning applies in complete analogy and they transform in the same fashion

$$\tilde{L}_i = \sum_j F_{ij} \tilde{l}_j \geq 0. \quad (4.39)$$

4.4 Algebraic derivation of symmetry breaking states

Since the above proof is quite involved, we would like to offer a second point of view, which is given by looking at the dual channel. It is more abstract and exploits properties about unital channels. We already showed, that it is sufficient to look at unital channels. We thus assume a unital channel with one fixed point per symmetry sector. The fixed points are given by

$$\{r_k\}_{k=0}^{N-1} \quad U r_k U^\dagger = \omega_k r_k, \quad (4.40)$$

and in particular $r_0 = \mathbb{1}$. Now, the fixed point space of a unital channel is an algebra (for proof see section 3.10). This means

$$r_i r_j = c(i, j) r_{i+j} \quad [\text{addition mod } N] \quad (4.41)$$

We assume uniqueness per symmetry sector, together with a normalization this means

$$r_k^\dagger r_k = \mathbb{1} \quad (4.42)$$

and furthermore

$$r_k^N = \mathbb{1} \quad (4.43)$$

The first equation means the r_k are unitaries. Unitaries are diagonalizable and have full rank. We denote the matrix diagonalizing r_k by $V_{(k)}$. We perform the diagonalization on the second equation:

$$r_k^N = (V_{(k)} \text{diag} [\lambda_0 \dots \lambda_{N-1}]^N V_{(k)}^\dagger) = \mathbb{1}. \quad (4.44)$$

This implies, that all eigenvalues of the r_k are N -th roots of unity.

Let us now have a closer look at the composition law

$$r_i r_j = c(i, j) r_{i+j} \quad (4.45)$$

Uniqueness tells us, that $r_i r_j \propto r_j r_i$, so we can write $r_j r_i = \beta r_i r_j$ for some $\beta \in \mathbb{C} \setminus \{0\}$. This is nothing but

$$r_i = r_j^\dagger (\beta r_i) r_j, \quad (4.46)$$

hence we learn that βr_i must have the same spectrum as r_i , which means β can only be a root of unity. We furthermore know, that

$$0 = r_i r_j - \bar{\beta} r_j r_i = [c(i, j) - \bar{\beta} c(j, i)] r_{i+j}, \quad (4.47)$$

which can only hold if

$$c(i, j) = \bar{\beta} c(j, i). \quad (4.48)$$

Evaluating this on any diagonal element leads to a contradiction for any root of unity unless $\beta = 1$. We thus have shown, that

$$[r_i, r_j] = 0 \quad (4.49)$$

The fixed points are thus all diagonal in the same basis, or expressed in the notation above, we have $V_{(i)} = V_{(j)} \forall i, j$ and can thus drop the subscript. We know (proof see section 3.10), that for a unital channel, we can always write any fixed point as a (complex) linear combination of positive fixed points. Let us call the positive fixed points R_i . There can at most be N positive matrices R_i . We are looking for the transformation

$$R_i = \sum_j M_{ij} r_j \quad (4.50)$$

Now we can diagonalize both sides simultaneously:

$$V R_i V^\dagger = \sum_j M_{ij} V r_j V^\dagger. \quad (4.51)$$

We can find at least N distinct R_i this way, since r_j has at least N distinct eigenvectors. However, there can also at most be N linear independent R_i . R_i are thus the rank-1 projectors, we construct from the r_j which is accomplished

by a Fourier transform: $M_{ij} = \omega^{ij}$. We thus arrive at the same result on a more abstract level of reasoning.

The fixed point space of a \mathbb{Z}_N symmetry breaking transfer operator is given by the Fourier transform of the irrep fixed points.

$$\boxed{\{R_i\} = \mathcal{F}(\{r_i\})} \tag{4.52}$$

Chapter 5

Numerical methods

It is in general not possible to compute the spectrum of the transfer operator for a given model analytically, let alone the corresponding eigenstates. In order to extract the signatures of symmetry breaking from PEPS models, we therefore need numerical methods. We devote this chapter to review the most important algorithms we will work with [26].

5.1 Contractions of tensor networks

As layed out in the PEPS chapter 3, our approach is to start with the definition of the local tensor and study the global properties, that follow from it, which are usually expectation values or fixed points. As explained in chapter 3, the contraction of a matrix product state is simple: We just construct the transfer matrix and find its eigenstates, which allows us to compute any property of the MPS. In the case of two-dimensional PEPS, the situation is quite different, because there is no local tensor like the MPS transfer matrix, which just repeats itself but instead we have an object growing with the system size (the PEPS transfer matrix), it is hence non-trivial to extrapolate the large system behavior of this. There has been extensive work on the computational hardness of doing such a contraction in general (in theory [68]) and on finding efficient (approximative) algorithms to do it in numerical practice [66].

5.2 The power method and the Arnoldi algorithm

In the above mentioned algorithm, the bottleneck is the memory we need for storing T , which is a matrix of size $D^{2N_v} \times D^{2N_v}$, i.e. its size grows exponentially with the system size. We can save memory by only storing vectors from the domain and image of T , which are of size D^{2N_v} “only”. Let us show how to apply the transfer operator iteratively on some vector in its domain. To do this, we can exploit the modular structure of PEPS by contracting one tensor on one site only, then storing this new vector and then iterate by applying the tensor consecutively on the next (neighboring) index. We use the NCON library [52] (i.e. MATLAB), where one can conveniently define contraction schemes. We show the contraction scheme diagrammatically in fig. 5.1. Counting the maximum number of open indices during the iteration, we see that we “only” have to store an object of size D^{2N_v+4} .

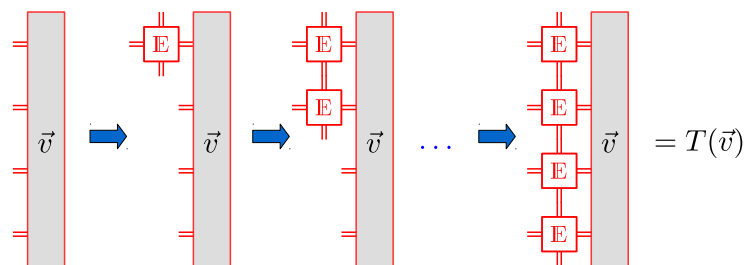


Figure 5.1: By contracting the double-tensor \mathbb{E} locally and iteratively, we gain a memory advantage of $\sim D^{2N_v}$.

Our principal interest is to find the dominant eigenvector of T . The naive method would be to iteratively apply T to a (random) initial vector

$$T|v\rangle, T(T|v\rangle), T(T(T|v\rangle)), \dots, T^\infty(|v\rangle). \quad (5.1)$$

It is clear that the resulting vector is part of the eigenspace corresponding to the largest eigenvalue, since any contribution with lower eigenvalue is projected out in the process, provided that the initial (e.g. random) vector has some overlap with that space. This method is more efficient in terms of memory cost and is known as the power method eigensolver. Based on this naive ansatz is the best known method to approximate the largest eigenvalues and corresponding

eigenvectors of a matrix, which is called the Arnoldi method. (We have noticed, that it is sometimes colloquially attributed as Lanczos method, which is incorrect since the latter only works for the case of Hermitian matrices, which is not the case for transfer operators.) The computation is the same, we again build powers of T exactly as in eq. (5.1), however now we store the n vectors. These vectors span the so called Krylov subspace

$$K_r(T, |v\rangle) = \{|v\rangle, T|v\rangle, T^2|v\rangle, \dots, T^{r-1}|v\rangle\} =: \{|v_1\rangle, |v_2\rangle, \dots, |v_r\rangle\}. \quad (5.2)$$

Let us denote the change-of-basis matrix by $Q = \{|q_1\rangle, \dots, |q_r\rangle\}$. It maps the raw power method vectors to an orthonormal basis. This Q is algorithmically found by a Gram-Schmidt process, which iteratively constructs the orthonormal basis by choosing one vector and then recursively constructing the next vector by subtracting the overlap with the previous vectors from the respective candidate of the non-orthonormal basis we started with. This implies that Q is by construction upper triangular, since the first vector is orthogonal to $r - 1$ (all other) vectors, the second one is orthogonal to $r - 2$ vectors and so on. Since Q constructs an orthonormal basis, we also know that

$$Q_{ij} = 0 \quad \forall i > j \quad (5.3)$$

$$Q^\dagger Q = \mathbb{1}_r \quad (5.4)$$

$$Q^\dagger T Q = H. \quad (5.5)$$

In this basis, the projection of T is Hessenberg (upper triangular plus the first lower diagonal), which is due to the fact that in the Gram-Schmidt procedure the $|q_k\rangle$ vectors are linear combinations only of the first k vectors of the Krylov space. Let us now show, how we arrive at the Hessenberg property. (In the following, the coefficients c_l are not relevant for the argument, but of course they eventually give the entries of the Hessenberg matrix)

$$|q_k\rangle = \sum_{l=1}^k c_l |v_l\rangle \quad (5.6)$$

$$T|q_k\rangle = \sum_{l=1}^k c_l |v_{l+1}\rangle = \sum_{l=1}^k c_l \sum_{m=1}^{l+1} \tilde{c}_m |q_m\rangle \quad (5.7)$$

$$\langle q_j | T | q_k \rangle = \sum_{l=1}^k c_l \sum_{m=1}^{l+1} \tilde{c}_m \delta_{mj} = \begin{cases} h_{qk} \\ 0 \end{cases} \quad j > k + 1, \quad (5.8)$$

which concludes the proof that it is of Hessenberg form. It is computationally cheap to find the eigenvalues of H , e.g. by a QR decomposition. The key point is that the eigenvalues of H approximate the extreme eigenvalues of T , already for moderate sizes of the Krylov subspace. To the knowledge of the author, this has not been understood rigorously and is still an open problem. There are however heuristic arguments, why this is what happens. In order to make statements about the quality of an approximation, we need to have an expression on the error we make. Let us denote the complete eigen-decomposition of T as

$$T = \sum_i \lambda_i |x_i\rangle \langle x_i| \quad (5.9)$$

Assuming that the operator is diagonalisable implies that this is a complete basis. We can therefore also expand the starting vector in that basis as

$$|v\rangle = \sum_i \alpha_i |x_i\rangle. \quad (5.10)$$

We now measure the difference between the true eigenvector and the best eigenvector approximation possible in the Krylov subspace (taken from [60, 34]). The following quantity then measures, how much of an exact eigenvector $|x_i\rangle$ lies outside the Krylov subspace:

$$\delta(Q_k, x_i) = \| |x_i\rangle - Q_k Q_k^\dagger |x_i\rangle \| = \| (\mathbb{1} - Q_k Q_k^\dagger) |x_i\rangle \|. \quad (5.11)$$

It is identically zero if $|x_i\rangle \in \mathcal{K}_k$, since this implies that $|x_i\rangle = Q |z\rangle$ for some $|z\rangle$. If this is not the case, we expect δ to be small for good approximations to $|x_i\rangle$. Any element of the Krylov subspace, and in particular the approximation to $|x_i\rangle$, which we are seeking here, can be written as a polynomial in the operator T applied to the starting vector $|v\rangle$, where the degree of the polynomial is given by the size of the Krylov subspace:

$$Q_k Q_k^\dagger |x_i\rangle = p(T) |v\rangle \quad p \in \mathbb{P}_{k-1} \quad (5.12)$$

Finding the best approximation in the Krylov subspace then amounts to finding the optimal polynomial q of a given degree. We now want to bound the error δ we make in this approximation to see what we can learn about the convergence behaviour of the Arnoldi process. To that end, let us look at

$$\begin{aligned} \|(\mathbb{1} - Q_k Q_k^\dagger) \alpha_i |x_i\rangle\| &= \min_q \|\alpha_i |x_i\rangle - q(T) |v\rangle\| \\ &= \min_q \|\alpha_i |x_i\rangle - \sum_j \alpha_j q(\lambda_j) |x_j\rangle\|. \end{aligned} \quad (5.13)$$

where we used the expansion of the starting vector $|v\rangle$ in the eigenbasis of T (eq. 5.10). Instead of minimising over all $q(\lambda_j)$ we fix one of them to $q(\lambda_i) = 1$, which might slightly degrade the upper bound but lets us continue with finding a useful expression for the error. This leads to

$$\begin{aligned} \text{eq. (5.13)} &= \min_q \|\alpha_i |x_i\rangle - \sum_j \alpha_j q(\lambda_j) |x_j\rangle\| \leq \min_{q(\lambda_i)=1} \left| \sum_{j \neq i} q(\lambda_j) \alpha_j |x_j\rangle \right| \\ &\leq \min_{q(\lambda_i)=1} \sum_{j \neq i} |\alpha_j| |q(\lambda_j)| \leq \left(\sum_{j \neq i} |\alpha_j| \right) \min_{q(\lambda_i)=1} \max_{j \neq i} (q(\lambda_j)) \end{aligned} \quad (5.14)$$

The upper bound on $\delta(Q_k, x_i)$ (eq. 5.11) is given by dividing everything by the factor $|\alpha_i|$:

$$\delta(Q_k, x_i) \leq \xi_i \epsilon_i^{(k)} := \left(\sum_{j \neq i} \frac{|\alpha_j|}{|\alpha_i|} \right) \min_{q(\lambda_i)=1} \max_{j \neq i} (q(\lambda_j)) \quad (5.15)$$

The quantity ξ_i measures the dependency of the convergence on the starting vector and the quantity $\epsilon_i^{(k)}$ measures the dependency of the convergence on the eigenvalues of T . For the former, it is straightforward to see that a large overlap of the starting vector with $|x_i\rangle$ will lead to a small error and hence a faster convergence. The eigenvalue dependency is less straightforward and we give the following instructive example of [34]: Suppose we can find a disc in the complex plane, such that all eigenvalues except for λ_1 lie within that disc. Let $C(\rho, c)$ denote that disc with radius ρ and center $c \in \mathbb{C}$, such that $\lambda_i \in C(\rho, c) \quad \forall i \geq 2$,

then (for a proof, see [34])

$$\epsilon_1^{(k)} \leq \left(\frac{\rho}{|\lambda_1 - c|} \right)^{k-1}, \quad (5.16)$$

which shows that if there is an isolated eigenvalue, separate from the rest of the spectrum, then the Arnoldi method converges this eigenvalue very quickly (exponentially fast in the size k of the Krylov subspace).

5.3 The infinite matrix product state (iMPS) algorithm

The following algorithm allows us to find an MPS representation of the fixed point of a MPS or PEPS directly in the thermodynamic limit [76, 44]. Owing to the gauge degree of freedom in a matrix product state, it is always possible to transform an MPS F into its so called left or right canonical form, where

$$F_{\alpha\beta}^i = \sum_{\gamma} (Q_R)_{\alpha\gamma}^i R_{\gamma\beta} \quad (5.17)$$

$$F_{\alpha\beta}^i = \sum_{\gamma} L_{\alpha\gamma} (Q_L)_{\gamma\beta}^i \quad (5.18)$$

with $\sum_{i\alpha} (Q_R)_{\alpha\gamma}^i (\bar{Q}_R)_{\alpha\mu}^i = \delta_{\gamma\mu}$ and $\sum_{i\alpha} (Q_L)_{\alpha\gamma}^i (\bar{Q}_L)_{\beta\gamma}^i = \delta_{\alpha\beta}$. Computationally, this is known as the QR decomposition, where $Q^\dagger Q = \mathbb{1}$ holds and R is an upper triangular matrix.

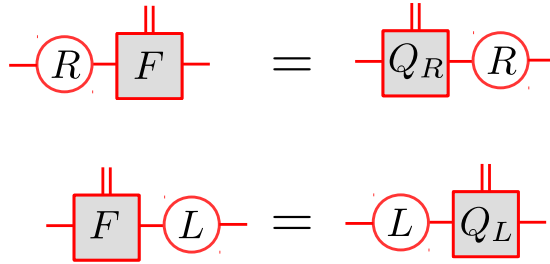


Figure 5.2: Given an MPS F , we can find matrices R (and L), such that commuting them through F brings the tensor into left (or right) canonical form

If we want to repeat this decomposition on the adjacent (in this case right) side again, the left index has another matrix sitting on it, which means the QR

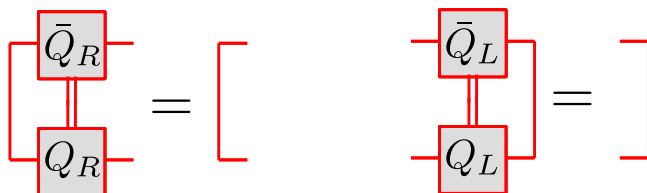


Figure 5.3: Q_R is in the left canonical gauge: The contraction over the left virtual and the physical index results in a delta tensor, i.e. the delta-tensor is invariant under the transfer matrix when coming from the left. Q_L similarly is in right canonical gauge. R and L can be found by a recursive QR-decomposition.

decomposition is changed towards

$$\sum_{\gamma} R_{\alpha\gamma} F_{\gamma\beta}^i = \sum_{\gamma} \tilde{Q}_{\alpha\gamma}^i \tilde{R}_{\gamma\beta} \quad (5.19)$$

with new Q and R matrices. The key observation is the following: This iteration has a fixed point, which is that as soon as Q and R do not change anymore upon the above transformation, we have found the fixed point behavior of the state. We will implement this simply by repeated QR decomposition. So far, we described how to find the canonical form of an MPS, which is a one-dimensional setup. However, we will now adapt it to the two-dimensional problem we face throughout this thesis. Suppose, we are given a local tensor $A_{\alpha\beta\gamma\delta}^i$, which defines the model we want to study. We thus would like to compute the fixed point of this two-dimensional model. We will make the assumption that the fixed point has some MPS description. To find this MPS, we start with some initial ansatz MPS, call it F . This MPS has two virtual indices (which take care of the entanglement in the fixed point) with some arbitrary bond dimension χ and one physical index, which in this case is a double index of size D^2 describing the vertical (virtual) direction of the PEPS transfer operator. We then apply the local double tensor \mathbb{E} on the physical (double-)index of the initial MPS. This gives yet another MPS, however with increased bond dimension χD^2 . Of this we compute the iMPS representation as detailed above. If we repeated this application of the \mathbb{E} tensor, the bond dimension would run out of control, therefore we have to truncate. This is done by truncating the singular values across the virtual index. The index of the original problem is sitting between R

and L . We therefore perform an SVD on

$$RL = USV^\dagger, \quad (5.20)$$

and decompose this across the singular values into

$$USV^\dagger = U\sqrt{S}\sqrt{S}V^\dagger, \quad (5.21)$$

which we can truncate according to

$$P_L = \sqrt{S^{-1}}U^\dagger R \quad (5.22)$$

and

$$P_R = LV\sqrt{S^{-1}}, \quad (5.23)$$

where we assume the singular values to be in decreasing order and can then truncate according to our choosing. Overall, this again gives an update procedure, applying \mathbb{E} and truncating back to a smaller bond dimension. We depict this recursion in fig. 5.4.

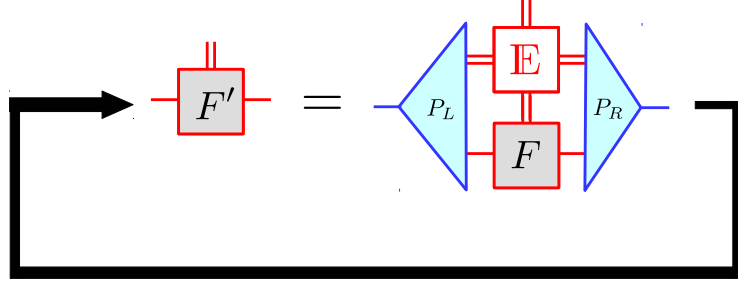


Figure 5.4: Recursion formula for finding the iMPS description of the fixed point of a two-dimensional PEPS model.

The convergence criterion is to ask, whether the updated MPS and its predecessor describe the same quantum state, which is equivalent to measuring the fidelity of the state, that is in turn given by the (mixed) transfer operators.

$$\langle \psi' | \psi \rangle = \frac{\text{tr}(\sum_i F^{i'} \otimes \bar{F}^i)^N}{\sqrt{\text{tr}(\sum_i F^{i'} \otimes \bar{F}^{i'})^N} \sqrt{\text{tr}(\sum_i F^i \otimes \bar{F}^i)^N}} \quad (5.24)$$

In practice, we measure the fidelity per site, which is the ratio of the dominant

eigenvalues corresponding to eq. (5.24):

$$\delta' = \frac{\lambda_{\max}(T_{F',F}^{\text{mixed}})}{\sqrt{\lambda_{\max}(T_{F'})\lambda_{\max}(T_F)}}. \quad (5.25)$$

If this quantity converges, we have good confidence, that we have found the optimal MPS representation of the fixed point of the respective model. The next task is to compute expectation values within the iMPS framework. Extracting the expectation value of an observable \mathcal{O} is straightforward: we simply put \mathcal{O} on one site (or a block of sites as long as \mathcal{O} has finite support), which gives us a dressed site. We extend the lattice in both directions to infinity with undressed sites. Then we apply the iMPS algorithm both from the top and from the bottom, which will give us the optimal MPS from both directions. We are then left with a one-dimensional problem with three rows. The top row is one (infinitely extended) line of the optimal MPS from the top, the middle line has the initial model tensor, which carried the operator \mathcal{O} on its physical index on one site. The bottom row is again the optimal MPS tensor. This structure is infinitely extended to left and right, except for the site where \mathcal{O} is sitting. We exploit this and find the left and right fixed point of this three-layered transfer operator [41]. This allows us to evaluate the expectation value on the iMPS as

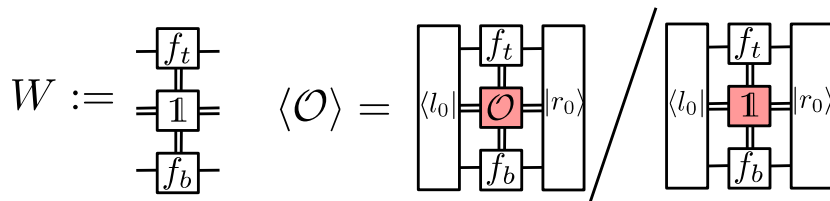


Figure 5.5: Computation of expectation values in iMPS framework: We first compute the iMPS fixed points from bottom f_b and from the top f_t (infinite plane). We then define a (“channel-”) matrix W with three layers: the optimized MPS on top and bottom and one unmodified layer with the original tensor (no operator on the physical index, indicated by $\mathbf{1}$). Evaluating the left and right dominant eigenvectors of this with a dressed channel matrix, where we put the observable \mathcal{O} on the physical index gives the expectation value on the infinite plane, where we normalize by dividing by the value of the same diagram without putting the observable on the center site.

Since the wave-function is, as always, unnormalized, we also have to compute the corresponding quantity where we replace \mathcal{O} by $\mathbf{1}$. The expectation value is thus given by the ratio of the diagrams in Fig. 5.5.

Since we will only need on site expectation values later, let us just make the side-remark, that higher order correlation functions are a bit more involved. If the two non-trivial operators act close enough to each other on the lattice, one can still use the above method by enlarging the unit-cell, however this quickly becomes intractable and one has to resort to different methods. For recent advances on building so called environment channels, see [73].

Chapter 6

Prototype models: Ising, AKLT and q -state Potts PEPS

In the previous chapter, we accomplished a complete characterization the fixed point space of the PEPS transfer operator in symmetry breaking phases. In order to verify these findings, which in particular involve assumptions about the properties of the transfer operator, we now would like to study the symmetry breaking mechanism numerically to see what we learn from our analytic results in realistic models. To find suitable PEPS models for this, we use the Rokhsar-Kivelson ansatz presented in chapter 3.4. Remarkably, we can simply use a classical Hamiltonian and construct a (quantum-) PEPS model from it. We will use the classical Ising and Potts models and hence call the corresponding PEPS models the “Ising PEPS” and the “Potts PEPS”. To test our results in a setting beyond the RK ansatz, we will furthermore study the AKLT model with a nematic field.

The Ising model [33] was the first statistical mechanics model that was shown to have a (\mathbb{Z}_2 -) symmetry breaking phase transition in two dimensions [48], before later being famously solved analytically by Onsager [43], including an unsubstantiated claim for the formula of its spontaneous magnetization, which was later derived by Chen-Ning Yang [81]. An accessible analytical solution, relying on the application of transfer operators and the Jordan-Wigner transformation,

was later given by Schultz, Mattis and Lieb [69]. The Potts model [55] can be seen as a generalization of the Ising model and hosts a \mathbb{Z}_N -symmetry breaking transition [80].

6.1 Ising PEPS

The Ising PEPS was defined in chapter 3.4 and is given by

$$A^0 = |0\rangle \langle \theta|^{\otimes 4} \quad A^1 = |1\rangle \langle \bar{\theta}|^{\otimes 4}, \quad (6.1)$$

where

$$|\theta\rangle = \cos(\theta) |0\rangle + \sin(\theta) |1\rangle \quad (6.2)$$

$$|\bar{\theta}\rangle = X |\theta\rangle = \sin(\theta) |0\rangle + \cos(\theta) |1\rangle. \quad (6.3)$$

The tensor manifestly has a \mathbb{Z}_2 -symmetry for any parameter value θ , given simply by the Pauli matrix X on both virtual and physical indices:

$$X_{ij} A_{\alpha\beta\gamma\delta}^j = A_{\mu\nu\rho\sigma}^i X_{\mu\alpha} X_{\nu\beta} X_{\rho\gamma} X_{\sigma\delta}. \quad (6.4)$$

Furthermore, due to the mapping to the square lattice Ising model we know that it has a critical point at $\theta_c \approx 0.35$ and we expect a degeneracy in the transfer operator for $\theta < \theta_c$. To verify this, we take the model and put it on a finite cylinder, where we can diagonalize the transfer operator exactly, as was described in detail in chapter 5.

$$T = \sum_{k,\alpha} \lambda_{k,\alpha} |r_{k,\alpha}\rangle \langle l_{k,\alpha}| \quad (6.5)$$

We diagonalize the transfer operator by an Arnoldi method, which gives the largest eigenvalues for moderate cylinder sizes. We first study (Fig. 6.1), how the largest eigenvalues vary with θ and find a clear indication for the phase transition at $\theta_c \approx 0.35$, which was expected from the exact value of the critical point, which lies at $\theta_c = \frac{1}{2} \arcsin[(1 + \sqrt{2})^{-\frac{1}{2}}]$. The plot shows, that the second largest eigenvalue is gapped out in the trivial phase (right hand side) and becomes part of the degenerate ground state subspace (left hand side), which is an indication for a phase transition. The two eigenstates are numerically distinct due to the splitting, which is far above machine precision. We can thus resolve

them individually to confirm that the leading eigenvector lives in the positive symmetry sector and the sub-leading one in the negative symmetry sector:

$$(X \otimes X)^{\otimes N_v} |r_{\pm}\rangle = \pm |r_{\pm}\rangle. \quad (6.6)$$

To study the way in which the degeneracy arises, we make a finite size scaling of the splitting between $\lambda_0 - \lambda_1$ against the system size N (Fig. 6.2). We find that the splitting closes exponentially fast in N_v , $\lambda_0 - \lambda_1 = \mathcal{O}(e^{-cN_v})$

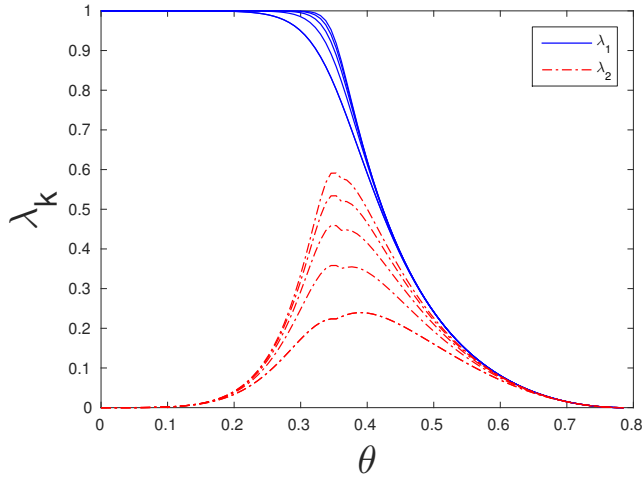


Figure 6.1: Spectrum of the Ising PEPS transfer operator for increasing system size. Blue: second largest eigenvalue, Red: third largest eigenvalue. Both for $N_v = 4, 6, \dots, 12$ (bottom to top)

Validity of the subspace approximation: fidelity measurement

We would like to test the validity of our results on symmetry broken states (cf. chapter 4.3). According to the explicit construction, the asymptotic channel of the Ising PEPS is

$$T = |r_+\rangle\langle r_+| + |r_-\rangle\langle r_-| \quad (6.7)$$

with the symmetry broken states

$$R_{\uparrow\downarrow} = \frac{1}{\sqrt{2}}(r_+ \pm r_-) \quad (6.8)$$

In order to verify this numerically, we construct these states explicitly from the exact diagonalization result. We compare these states with the fixed point of a

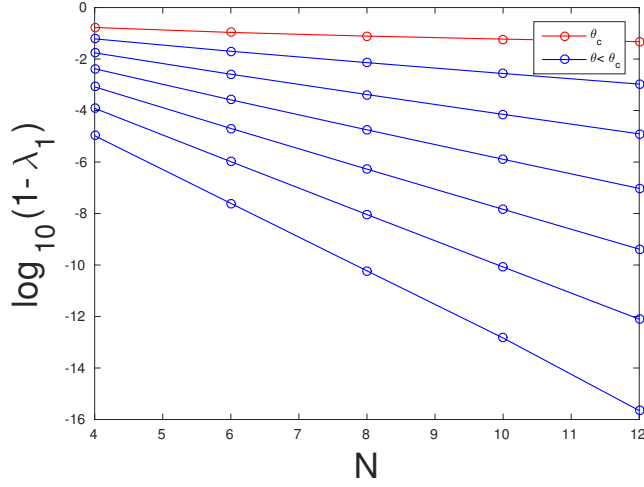


Figure 6.2: Scaling of the second largest eigenvalue in the Ising PEPS transfer operator. We plot $\log(1 - \lambda_1)$ vs. N_v for varying parameter $\theta = (0.15..0.35)$ (bottom to top), a straight line with negative slope indicates a splitting of the form $\exp(-cN_v)$

perturbed system, where we explicitly break the symmetry by applying a local perturbation on the physical index of the PEPS tensor of the form

$$A^i \rightarrow (\mathbf{1} + \epsilon Z)A^i. \quad (6.9)$$

As was described in chapter 3.3, the perturbation lifts the degeneracy if the matrix element $(r_-|T_Z|r_+)$ is non-zero. The diagonal elements are zero due to the symmetry:

$$(r_+|T_Z|r_+) = (r_+|X^{\otimes 2N_v}T_ZX^{\otimes 2N_v}|r_+) = -(r_+|T_Z|r_+) = 0 \quad (6.10)$$

This means that the matrix we have to diagonalize a symmetric off-diagonal 2×2 matrix,

$$M = \begin{pmatrix} 0 & (r_-|T_Z|r_+) \\ (r_+|T_Z|r_-) & 0 \end{pmatrix} \quad (6.11)$$

which leads to correction in the eigenvalues of

$$\lambda_{\pm}(\epsilon) = 1 \pm \epsilon(r_-|T_Z|r_+) \quad (6.12)$$

Since the perturbation lifts the degeneracy, this perturbed model will have a unique fixed point, which we again compute with an exact diagonalization (Arnoldi eigensolver). Let us call the fixed point of the perturbed model $|R_\epsilon\rangle$. We measure the difference between the two states by computing the residue of the fidelity, given by

$$\delta = 1 - \min_{k \in \uparrow \downarrow} |(R_\epsilon | R_k)|^2 \quad (6.13)$$

In order to compare different system sizes, we normalize by the number of sites used in the respective calculation $\delta(\epsilon)/N_v$. The result of the calculation for some parameter choice in the symmetry broken phase $\theta = \pi/16$ is shown in Fig. (6.3), where we plot the fidelity per site against the perturbation strength ϵ and find a straight line with slope 1.97 ± 0.02 on the log-log scale. This is in very good agreement with our expectation from perturbation theory point of view (see A.18): What we measure, is how much of the fixed point lies outside the “true” (analytic) fixed point space. As explicated in chapter 3.3, the correction to the state in first order in ϵ is orthogonal to the “ground state” subspace (adapted to our case, the fixed point subspace), hence only in second order in the perturbation to we expect a change in the fixed point, which explains the nearly perfect ϵ^2 behavior in the fidelity per site scaling.

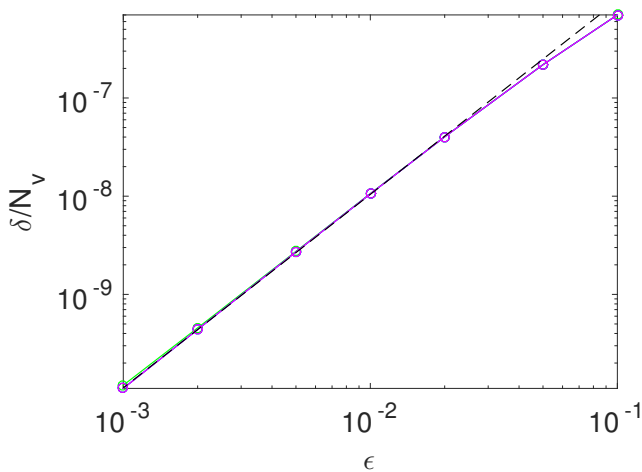


Figure 6.3: Scaling of the residual fidelity $\delta = 1 - |(f(\epsilon)|g)|^2$ against ϵ for different $N_v = 9, 11, 13, 15$, the lines almost exactly coincide. $\theta = 0.25\pi/4$ Dashed: linear fit (log/log-scale) with slope $p = 1.97 \pm 0.02$

Connection to “usual” symmetry breaking with order parameters: Ising PEPS

In order to make the connection to the more common way of detecting symmetry breaking, we measure the order parameter in the Ising PEPS fixed points. The order parameter is the dressed transfer operator T_Z , which is in direct correspondence with the order parameter Z of the Ising model (which acts on the physical indices). It is clear from symmetry considerations, that this is identically zero on the symmetric fixed points $|r_{\pm}\rangle$. We measure

$$\langle T_Z \rangle(\theta) = |(R_{\uparrow}(\theta)|T_Z|R_{\uparrow}(\theta))| \quad (6.14)$$

by exact diagonalization and a single application of an (implicitly constructed) T_Z . The result is plotted in 6.4. The failure of the order parameter to drop

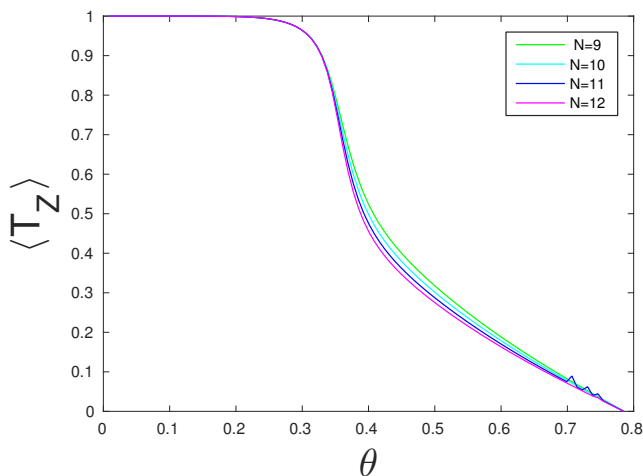


Figure 6.4: Order parameter measured on the analytic symmetry broken states $R_{\uparrow\downarrow}$ for finite system sizes (Exact diagonalization). The phase transition lies at $\theta_c \approx 0.35$. We can see a clear indication, that the order parameter significantly drops around the critical point, however it remains finite in the disordered phase.

to zero in the disordered phase is due to the fact that our assumptions for the construction of the states $R_{\uparrow\downarrow}$ are only valid in the symmetry broken phase. Once the phase transition happens, the contribution of r_- is incorrect. It therefore only makes sense, to talk about the behavior of the order parameter on the symmetry broken side of the transition. We will demonstrate, that one can extract remarkably accurate information from the finite size fixed points about

the infinite lattice limit by making a mild assumption about correlations in the system. Around the phase transition, the system tends towards an infinite correlation length, our finite cylinder setting therefore leads to an artificial cutoff as soon as the correlation length approaches the system size. Let us assume, that the finite size correction is exponential in the circumference of the cylinder:

$$m(\theta, N_v) = m(\theta, \infty) + a \exp(-bN_v) \quad (6.15)$$

with unknowns $m(\theta, \infty)$ a and b , which are functions of θ (and potentially also N_v).

This in particular gives an (inverse) correlation length $\xi^{-1} := b$, which we plot against θ in Fig. 6.5. We observe a linear dependence, which we extrapolate further to the critical point by fitting it linearly (with quadratic correction)

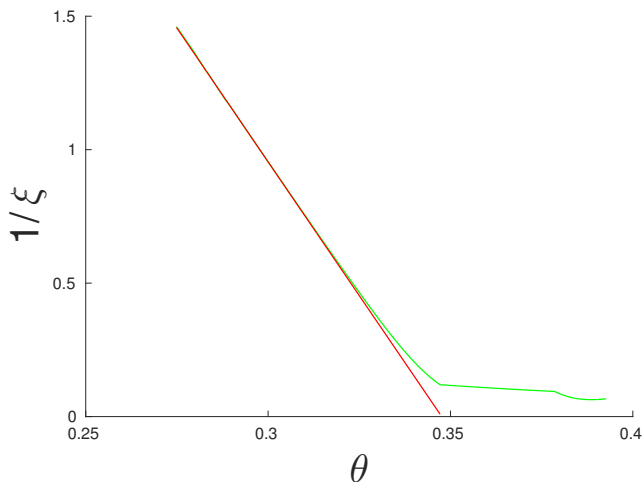


Figure 6.5: Correlation length from the finite size scaling of the order parameter (green) and linear fit (red)

The final step is to then feed the fitted correlation length $\xi(\theta)$ back into eq. 6.15, where we now also model the prefactor as $a = c(N_v)^g$, to account for short-range effects close to criticality. We compare the result to the formula for the magnetization analytically derived by Yang [81],

$$m = [1 - \sinh^{-4}(2\beta J)]^{1/8}, \quad (6.16)$$

where $\beta J = -\log \sin(2\theta)$. We are able to extract the spontaneous magnetization

by the described two-step fitting method to remarkably high accuracy.

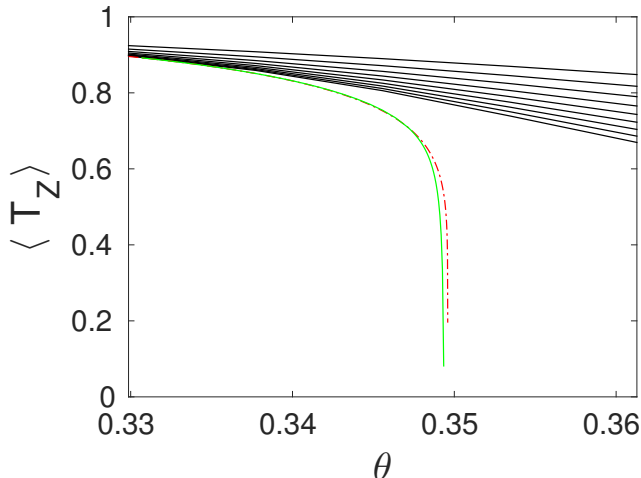


Figure 6.6: Order parameter, zoomed in around the critical point. We plot the finite size values (black), the final extrapolation curve (green) and the analytic function (Yang’s formula) of the magnetization, (red, dot/dashed). Remarkably, the finite size extrapolation is very close to the analytic curve.

Let us summarize what we learned by studying the Ising PEPS model. We started by identifying a phase transition from the spectrum of the PEPS transfer operator, including a finite size scaling of the splitting in the quasi-degenerate subspace. The transition point coincides with a mapping of the Ising PEPS to the exact result of the square lattice Ising model. We then introduced fidelity measurements as a tool to test our analytical results about how to define symmetry breaking in the PEPS environment, which were presented in chapter 4. These fidelity measurements confirm that we found the correct description of the fixed points of PEPS models with spontaneous symmetry breaking. We were furthermore able to extract remarkably accurate information about the phase transition from the finite size PEPS data by measuring the order parameter on the symmetry broken fixed points.

6.2 AKLT model with “nematic” field

We would like to test our results on a model that does not come from a classical model. To that end, we take the well known AKLT model (invented by Affleck Kennedy Lieb and Tasaki [1, 2]) with a “nematic” field [16]. This model was

invented before matrix product states were discovered and is thus an early example where it was possible to construct a model with a non-trivial ground state which could be exactly formulated (“exactly solved”). The Hamiltonian of the model turns out to be an approximation to the spin-1 Heisenberg Hamiltonian, which to this day is a research focus in quantum magnetism. It furthermore lies in what is now known as the Haldane phase and hosts symmetry protected topological order.

The AKLT model is constructed by forming $SU(2)$ -singlet-pairs from spin- $\frac{1}{2}$ particles, which we then use as bonds on a square lattice. On every vertex, four particles meet, and we thus get several representations (with multiplicities) on each vertex:

$$\left(\frac{1}{2}\right)^{\otimes 4} = \underline{2} \oplus (3)\underline{1} \oplus (2)\underline{0}. \tag{6.17}$$

We now project the vertices, onto the spin-2 subspace. The local tensor of the square lattice AKLT A is thus of the form

$$A_{\alpha\beta\gamma\delta}^i = \langle i | [\Pi_{S=2} \cdot (\mathbf{1} \otimes \mathbf{1} \otimes Y \otimes Y)] | \alpha, \beta, \gamma, \delta \rangle, \tag{6.18}$$

with respect to the computational basis and the conventionally used maximally entangled state $|\omega\rangle = |00\rangle + |11\rangle$.

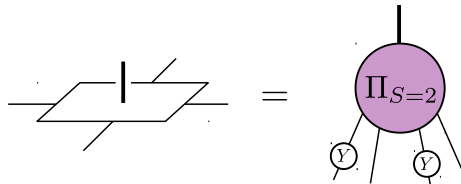


Figure 6.7: Definition of the AKLT model via the local tensor as a map from four virtual qubits to the physical (5-dimensional) Hilbert-space. The Pauli matrix Y is applied once in both lattice directions on the qubits and the map to the physical space is the spin-2 projection.

The AKLT model has a unique ground state for integer spin [1]. The symmetry of the tensor is given by the fact that it is a map between representations of $SU(2)$ (an “intertwiner”), hence any symmetry action on the physical index is related to some symmetry action on the virtual particles. The spin operators

on the physical spin can be constructed from the ladder operators via

$$S_x = \frac{1}{2}(S^+ + S^-) \quad (6.19)$$

$$S_y = \frac{1}{2i}(S^+ - S^-) \quad (6.20)$$

In particular, we can pull the virtual Pauli- Y operators through to the physical index on every second site due to

$$\exp(i\pi S_y) = \exp(i\pi \sum_{i=1}^4 Y_i/2) = (e^{i\pi Y/2})^{\otimes 4} = Y^{\otimes 4} \quad (6.21)$$

Since the corresponding operator acts on a sub-lattice of the original lattice, this is called a sub-lattice-rotation. It is a computational trick, which we exploit in order to have a ferromagnetic model as opposed to the original AKLT, which would tend towards anti-ferromagnetism due to the singlet bonds and we would then have to deal with staggered order parameters. Note that this equivalence only works on a lattice with even sites, otherwise one of the sub-lattices is dangling on one side. So far, we just have a particular state. In order to have a phase, we deform the state by acting with a particular field of the form

$$N(\alpha) = \exp(\alpha(S_z)^2), \quad (6.22)$$

which has been dubbed a “nematic” [16] field, since it constrains the particles in some degrees of freedom while others remain unaffected, analogous to nematic crystals, which are crystals that have some liquid degrees of freedom. In our case, because we explicitly have a S_z term, the generators S_x and S_y no longer commute and thus the nematic field explicitly breaks the $SU(2)$ invariance of the AKLT down to a semi-direct product of $\mathbb{Z}_2 \ltimes U(1)$. By semi-direct product we mean, that the \mathbb{Z}_2 symmetry has the usual composition, while the $U(1)$ composition is contingent on the \mathbb{Z}_2 part (because the \mathbb{Z}_2 generator reverses the rotations of the $U(1)$ group). The nematic field will eventually favor high value of S_z^2 , i.e. $S_z = \pm 2$. We hope to deform the model into a phase, where the \mathbb{Z}_2 symmetry will break spontaneously. To that end, we study the transition numerically, the spectrum of the transfer operator (exact diagonalization) is given in figure 6.8.

We see the onset of a twofold degeneracy in the transfer operator. Even though there are finite size effects, that smooth out the shape of the onset, we can

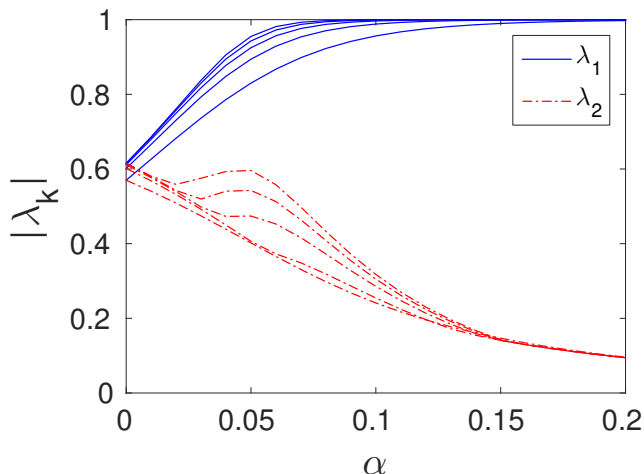


Figure 6.8: Spectrum of the nematic AKLT PEPS transfer operator against the nematic field strength, plotted for increasing system sizes. Blue: second largest eigenvalue, Red: third largest eigenvalue. Both for $N_v = 4, 6, \dots, 12$ (bottom to top)

guess the transition to lie somewhere around $\alpha \approx 0.05$, consistent with the behavior of the lower eigenvalues, which peak around the same value. We find an exponentially closing degeneracy in the second eigenvalue for high α (Fig. 6.9). While it is in general hard to tell, where exactly the slope of the lines turn “significantly” negative, we see that the degeneracy scaling is consistent with our expectation from fig. 6.8.

In order to confirm, that we have a symmetry breaking transition, we again measure the fidelity per site and the order parameter. The conjectured correct fixed points are again

$$R_{\uparrow\downarrow} = \frac{1}{\sqrt{2}}(r_0 \pm r_1) \quad (6.23)$$

and the residual fidelity per site is again given by

$$\frac{\delta}{N_v} = \frac{1 - \min_{k \in \uparrow\downarrow} [(R_\epsilon | R_k)|^2]}{N_v}. \quad (6.24)$$

We measure the fidelity by computing the eigenvectors for a finite cylinder with exact diagonalization, where for $|R_\epsilon\rangle$, we perturb the tensor infinitesimally with $\mathbb{1} + \epsilon S_z$, which removes the degeneracy, such that the corresponding fixed point is unique. The results are given in Fig. 6.10. We again observe, that the residual fidelity decreases with decreasing perturbation strength, where we find an ϵ^2

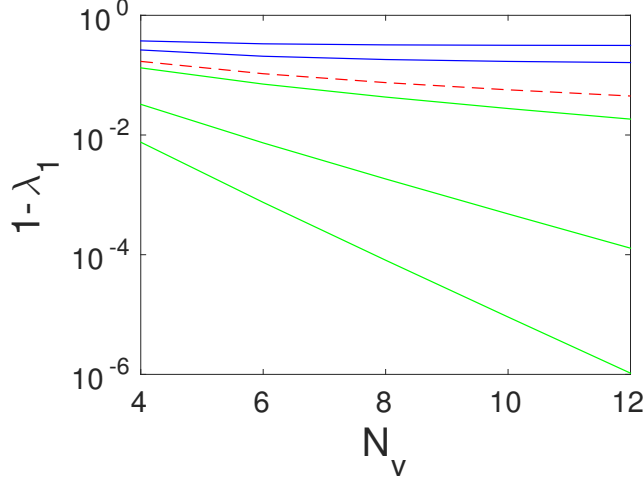


Figure 6.9: Scaling of the second largest eigenvalue in the nematic AKLT PEPS transfer operator. We plot $(1 - \lambda_1)$ logarithmically against cylinder size N_v for varying parameter $\alpha = (0.01, 0.03, 0.05, 0.06, 0.11, 0.16)$ (top to bottom), a straight line with negative slope indicates a splitting of the form $\exp(-cN_v)$

scaling, which corroborates that these states Eq. 6.23 are indeed the symmetry breaking fixed points. Upon a closer look, we notice that for large enough ϵ , all lines practically coincide. However, for small enough perturbations, δ/N_v starts to increase again. This behavior is explained by the finite size of the system, which leads to a finite splitting, which is diagonal in the irrep basis $\{r_0, r_1\}$. As soon as the perturbation strength drops below the strength of this finite splitting, which is diagonal in the irrep basis, the fixed point of the perturbed system drifts away from the symmetry broken state (eq. 6.23).

As a second test for symmetry breaking, which will show us how the conventional symmetry breaking and our approach to symmetry breaking are related, we measure the order parameter of the system. In the case of the nematic AKLT, the order parameter is the spin operator S_z . If the system is symmetric, the average should be zero and the operator would detect a spontaneous breaking of that symmetry, which favors a particular S_z direction. We measure the expectation value of the dressed transfer operator T_{S_z} on the symmetry broken states:

$$\langle T_{S_z} \rangle = (L_\uparrow | T_{S_z} | R_\uparrow) / (L_\uparrow | T | R_\uparrow) \quad (6.25)$$

The results are plotted in Fig. 6.11. We find, that for low values of α , the

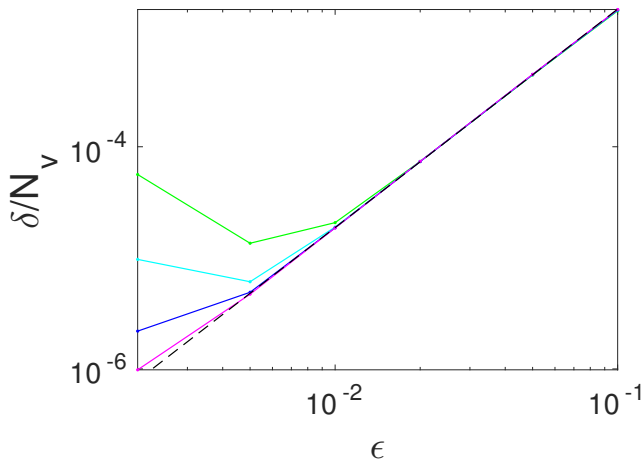


Figure 6.10: Residual fidelity per site of the nematic AKLT model, $\alpha = 0.145$, $N = 9..12$ (top to bottom), dashed line: fitted line with slope $p = 1.97 \pm 0.03$. We thus have ϵ^2 -scaling

order parameter changes significantly with system size. Since this is before the expected transition point, we expect that in this region the true value should be zero and we are dealing with substantial finite size effects. As soon as we approach the expected transition point, the lines approach each other and appear to converge for increasing α , eventually coinciding. We perform a finite size extrapolation, following our ansatz for the Ising PEPS model (eq. 6.15), which we write again for reference:

$$m(\theta, N_v) = m(\theta, \infty) + a \exp(-bN_v) \quad (6.26)$$

The extrapolation to the thermodynamic limit $N_v \rightarrow \infty$ is given by the red curve in fig. 6.11.

In the extrapolation process, we have access to a correlation length $\frac{1}{b}$ in the finite size correction $a \exp(-bN_v)$. Away from the critical point, this is finite and as long as it is smaller than the system size, it should coincide with the true correlation length. By making a scaling ansatz for this quantity $b = \frac{1}{\xi}$, we can extrapolate the critical point. Our method allows us to find it to be

$$\alpha_c \approx 0.0447, \quad (6.27)$$

which has not been determined before.

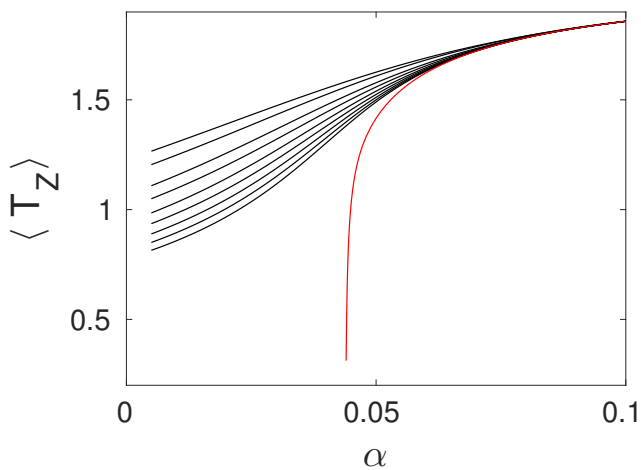


Figure 6.11: Black: Order parameter $\langle T_{S_z} \rangle$ of the Nematic AKLT model, measured on the explicitly constructed symmetry broken state R_0 for increasing system size $N_v = 4..12$ (top to bottom). Red: finite size extrapolation with exponential correction ansatz (details see text)

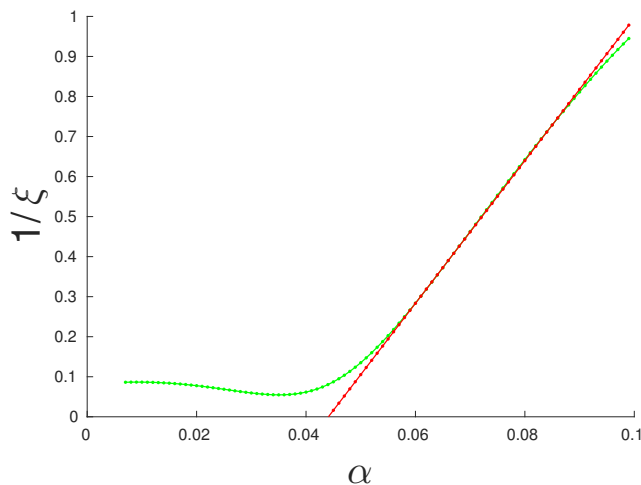


Figure 6.12: Nematic AKLT, correlation length of the order parameter finite size extrapolation fit. Green: Result of the finite size fit, Red: now we fit a straight line to the correlation length, which gives us a clear indication for the true critical point (where $\xi = \infty$)

Let us sum up our findings about the nematic AKLT model. We first identified a phase transition from the spectrum of the transfer operator. This gave us an estimate for the transition point. We confirmed that the phase for large α

is \mathbb{Z}_2 symmetry breaking and that this is reflected in the PEPS environment by constructing the fixed points explicitly and comparing this to perturbatively breaking the symmetry in the bulk. We furthermore were able to extract detailed properties about the transition directly from the finite size PEPS data, characterizing the transition.

6.3 Potts PEPS

Having gained confidence from two instances of \mathbb{Z}_2 symmetry breaking, we now would like to turn to higher symmetries. To that end, the so called Potts model is the natural candidate. The Potts model was suggested to its namesake Renfrey Potts by his advisor Cyril Domb and is an intensely studied model in various fields of physics [55]. It is a generalization of the Ising model to “spins”, which can have more than two configurations. There exist two variants of the Potts model. Both are defined over local variables (“spins” or “colors”), taking one of q possible values. The simpler one is called the *standard* q -state Potts model and is defined with a nearest neighbor interaction that only gives an energy contribution if both neighbors are in the same state and is otherwise zero:

$$H_{\text{SP}} = - \sum_{\langle s_i s_j \rangle} J_{ij} \delta_{s_i s_j}, \quad i, j \in \{1..q\} \quad (6.28)$$

The second version is called the planar, vector or clock q -state Potts model, where the interaction strength is not simply zero in case of a mismatch but depends on the difference. It is defined via the Hamiltonian

$$H_c = - \sum_{\langle s_i s_j \rangle} \cos \left(\frac{2\pi(s_i - s_j)}{q} \right) \quad (6.29)$$

An extensive review (including both versions) can be found in [80]. In the two-dimensional case, all Potts models host a phase transition and have a long-range ordered and a disordered phase. For $q < 4$, both models can be easily mapped onto each other and are thus equivalent. The nature of the $q = 4$ transition is still under some debate, while for higher q the situation becomes clearer again. In that case the vector Potts model additionally hosts a quasi-long-range order phase and in particular converges towards the famous XY-model used by Kosterlitz and Thouless to demonstrate the transition named after them. We will construct a 3-state Potts PEPS model. This will have interesting new

features, which are absent in the Ising case, in particular the symmetry will be described by complex phases.

We define the PEPS in the following way: We take a delta tensor of bond and physical dimension three, on which we want to host a Potts model. To that end, we apply a matrix on two of the virtual bonds, corresponding to the two directions of the square lattice.

$$A_{\alpha\beta\gamma\sigma}^i(\theta) = \delta_{\alpha\beta\mu\nu}^i M(\theta)_{\mu\gamma} M(\theta)_{\nu\sigma}, \quad (6.30)$$

where δ is the usual Kronecker delta, which is equal to one if all (including the physical) indices coincide and else zero. The matrix M encodes the weights between adjacent spins on the lattice and is given by

$$M(\theta) = \begin{pmatrix} 1 & \sin(\frac{\pi}{2}\theta) & \sin(\frac{\pi}{2}\theta) \\ \sin(\frac{\pi}{2}\theta) & 1 & \sin(\frac{\pi}{2}\theta) \\ \sin(\frac{\pi}{2}\theta) & \sin(\frac{\pi}{2}\theta) & 1 \end{pmatrix}, \quad (6.31)$$

where $0 < \theta < 1$. This matrix in particular commutes with the shift matrix

$$X = \begin{pmatrix} 0 & 1 & 0 \\ 0 & 0 & 1 \\ 1 & 0 & 0 \end{pmatrix}, \quad (6.32)$$

which is a generator of \mathbb{Z}_3 with $X^3 = \mathbb{1}$. Together with the fact, that the Kronecker delta is invariant under an application of X on all three indices, we thus learn that the Potts PEPS tensor has a \mathbb{Z}_3 symmetry by construction, as desired.

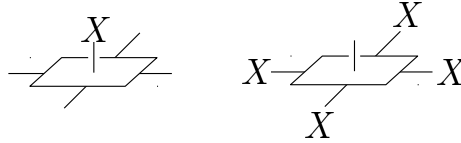


Figure 6.13: Symmetry of the Potts PEPS tensor.

This in particular implies, that the transfer operator of this model commutes with the symmetry operation on an entire column,

$$S := (X \otimes \bar{X})^{\otimes N_v} \quad (6.33)$$

$$[\mathbb{T}, S] = 0, \quad (6.34)$$

which allows us to label eigenvectors of the transfer operator by their eigenvalue with respect to the \mathbb{Z}_3 symmetry, i.e. they are all (spanned by) eigenstates of

$$S|r_{i,\kappa}\rangle = \kappa|r_{i,\kappa}\rangle, \quad (6.35)$$

where $\kappa \in \{1, \omega, \bar{\omega}\}$, $\omega = e^{2\pi i/3}$ (left eigenvectors likewise). This helps us computationally, since we can construct projectors into the three respective symmetry sectors:

$$P_\kappa = \frac{1}{3}(\mathbb{1} + \kappa S + \bar{\kappa} S^\dagger) \quad (6.36)$$

The next thing we need, is to find a phase where we have an asymptotic degeneracy in the transfer operator. For that, let us first compare the matrix M to the nearest neighbor weights of the partition function of the standard Potts Hamiltonian.

$$e^{-\beta h_{ij}} = e^{\beta \delta_{ij}} \begin{cases} e^\beta & i = j \\ 1 & i \neq j \end{cases} \quad (6.37)$$

We can freely normalize the weights, similarly to the partition function, which only ever appears in ratios, when calculating physical quantities, such that its normalization is a matter of convenience. We thus arrive at a mapping between the temperature in the classical standard Potts model and the parameter θ in our PEPS tensor:

$$e^{-\beta} = \sin^2\left(\frac{\pi}{2}\theta\right). \quad (6.38)$$

The critical point of the thermal phase transition in the classical standard Potts model is known to be at [80]

$$e^{\beta_c} = 1 + \sqrt{3}, \quad (6.39)$$

which carries over to

$$\theta_c = \frac{2}{\pi} \arcsin\left(\frac{1}{\sqrt{1+\sqrt{3}}}\right) \approx 0.4137 \quad (6.40)$$

Let us look at the extremal cases: At $\theta = 0$, we have the superposition of three orthogonal states and are hence in a GHZ-type situation, where $|r\rangle \propto |0\rangle^{\otimes N} + |1\rangle^{\otimes N} + |2\rangle^{\otimes N}$. On the other side of the interval, we have the $\theta = 1$

case, which is a complete mixture of all possible lattice configurations, which corresponds to $|r\rangle \propto [|0\rangle + |1\rangle + |2\rangle]^{\otimes N}$. Our hope, that these are the extreme cases of a ferromagnetic and a paramagnetic phase respectively, is corroborated by the analysis of the spectrum of the corresponding PEPS transfer operator, shown in figs. 6.14,6.15.

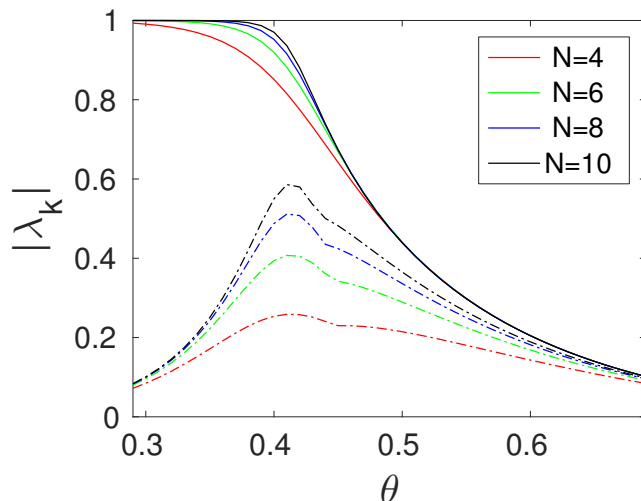


Figure 6.14: Spectrum of the Potts PEPS transfer operator. Solid lines: second and third largest (for which we observe an exact degeneracy). Dashed: fourth largest eigenvalue, both for different system size N_v (see legend). The exact critical point ($N_v \rightarrow \infty$) is $\theta_c \approx 0.4137$

We calculate the spectrum with exact diagonalization, where we use the above defined projectors (6.36), and compute the spectrum per sector. We find that the leading eigenvector is in the (trivial) 1-sector, the two onsetting eigenvectors are in the $(\omega, \bar{\omega})$ -sectors respectively. In the ferromagnetic phase the two subleading eigenvalues approach the dominant eigenvalue exponentially fast in the system size (fig. 6.15). We conclude that we have an asymptotic degeneracy with one eigenstate per symmetry sector and thus a prerequisite for symmetry breaking in the Potts PEPS state.

The next question is whether the transition has a (local) order parameter. Since the on-site symmetry is a shift matrix, its natural partner is the so called clock matrix

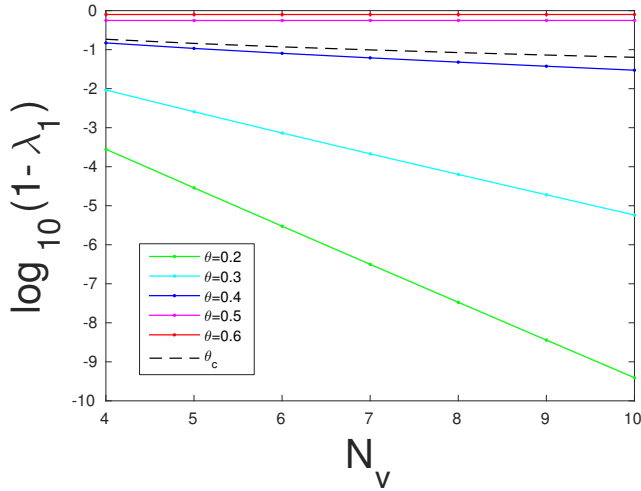


Figure 6.15: Splitting between first and second eigenvalue against system size N_v , plotted for different values of θ in the Potts PEPS. The dashed line is at criticality (of the infinite system). In the ferromagnetic phase $\theta < \theta_c$ we observe an exponentially small splitting of the form $\exp(-cN_v)$

$$Z = \begin{pmatrix} 1 & 0 & 0 \\ 0 & \omega & 0 \\ 0 & 0 & \bar{\omega} \end{pmatrix} \quad (6.41)$$

They obey a graded anticommutativity:

$$ZX = \omega XZ. \quad (6.42)$$

This means two things: Firstly, it tells us that Z has zero expectation value on a symmetric state:

$$\langle Z \rangle_{\text{sym.}} = \langle \psi_\kappa | Z | \psi_\kappa \rangle = \langle \psi_\kappa | \psi_{\kappa+1} \rangle = 0. \quad (6.43)$$

Secondly, this implies that the transfer operator dressed with a single Z , T_Z has matrix elements between the symmetry sectors and can thus lead to a new, symmetry broken eigenbasis, if we use it as a perturbation of the original, degenerate model. To test this, we perturb the Potts PEPS with a physical perturbation of the form $\mathbb{1} + \epsilon Z$. According to our findings in chapter 3.3, we have to find the basis that diagonalizes the perturbation in the degenerate fixed point subspace

$|r_1\rangle, |r_\omega\rangle, |r_{\bar{\omega}}\rangle$. This is equivalent to the matrix problem

$$(l_i|T_\epsilon|r_j) = \begin{pmatrix} 1+\gamma & 0 & 0 \\ 0 & 1 & 0 \\ 0 & 0 & 1 \end{pmatrix} + \epsilon \begin{pmatrix} 0 & \chi & \bar{\chi} \\ \bar{\chi} & 0 & \chi \\ \chi & \bar{\chi} & 0 \end{pmatrix} + \mathcal{O}(\epsilon^2), \quad (6.44)$$

where $\chi = N_v(l_1|T_Z|r_\omega)$ and γ is the finite exponentially small splitting. This equation tells us, that on a finite system we will have a competition between γ and ϵ : For $\gamma \gg \epsilon$, the largest eigenvector is simply $|r_1\rangle$, however if we choose $\epsilon \gg \gamma$, we can effectively neglect γ , such that we should diagonalize just the perturbation term in eq. 6.44. This term is a cyclic matrix and thus diagonalized by the Fourier transform, such that we get three eigenstates

$$|R_0^{[3 \times 3]}\rangle = \frac{1}{\sqrt{3}}\{|r_1\rangle + |r_\omega\rangle + |r_{\bar{\omega}}\rangle\} \quad (6.45)$$

$$|R_1^{[3 \times 3]}\rangle = \frac{1}{\sqrt{3}}\{|r_1\rangle + \omega|r_\omega\rangle + \bar{\omega}|r_{\bar{\omega}}\rangle\} \quad (6.46)$$

$$|R_2^{[3 \times 3]}\rangle = \frac{1}{\sqrt{3}}\{|r_1\rangle + \bar{\omega}|r_\omega\rangle + \omega|r_{\bar{\omega}}\rangle\}, \quad (6.47)$$

which are indeed the ones we found in our analytic fixed point analysis for general \mathbb{Z}_N symmetry breaking. (Note that, crucially, this is independent of the specific values ϵ and $|\chi|$, it only matters that they are non-zero.)

In total, we now have three candidates that describe the fixed point of the perturbed PEPS model. The first candidate is the (unique) fixed point of the fully perturbed model, which we find by exact diagonalization and call $|R_\epsilon\rangle$. The second candidate is the fixed point, that we get on the degenerate subspace eq. 6.47, which is incorporating ϵ to first order and the finite size splitting γ . We denote this fixed point by $|R^{[3 \times 3]}\rangle$, which is again found by exact diagonalization. As a third candidate, we compute the iMPS of the perturbed model, which gives a matrix product state representing the fixed point in the thermodynamic limit, as was explained in chapter 5.

We then compare these three to the fixed point we analytically constructed (see 4.38) ($\omega = e^{2\pi i/3}$) as

$$|R_i\rangle = \frac{1}{\sqrt{3}} \sum_j \omega^{ij} |r_j\rangle. \quad (6.48)$$

Finite size effects in fidelity measurement

For all three cases, we measure the remainder of the fidelity (“infidelity”) per site

$$\frac{\delta}{N_v} = \min_{|R_i\rangle} \left(\frac{1 - |\langle a | R_i \rangle|^2}{N_v} \right) \quad (6.49)$$

where $|a\rangle$ is the placeholder for the respective candidate fixed point. We plot this quantity in fig. 6.16, where we use system sizes $N_v = 6, 8, 10$ (and “infinite” for the iMPS data). This plot contains several effects which teach us about the limitations of the perturbative treatment and symmetry breaking on a finite system. We identify two regimes, which are given by the ratio of the finite-size splitting γ and the perturbation strength ϵ .

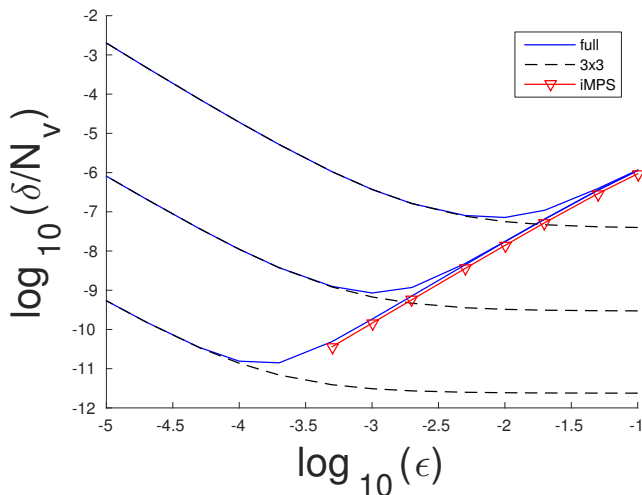


Figure 6.16: Fidelity per site in the 3-state Potts model, measuring the difference between the solution of the full transfer matrix and the solution on the fixed point subspace projection. Solid lines: Exact diagonalization for specified N_v , dashed line iMPS ansatz (“infinite” N_v), $\theta = 0.25$.

The regime $\epsilon \gg \gamma$ corresponds to the right hand side of the plot in fig. 6.16. Here we observe that for the “full” perturbation case of $(R_i | R_\epsilon)$ (solid blue lines), δ/N_v falls off as a power law $\delta/N_v \sim \epsilon^\kappa$, thus tending towards 0. This is a strong indication that we capture the correct fixed point and we furthermore measure an exponent of 1.91 ± 0.09 . Looking at the perturbation expansion of the perturbed fixed point eq. 3.35, we see that the first order correction is orthogonal to the fixed-point subspace, which implies that the correction in

the fidelity per site, we are measuring here, only enters in second order, which corresponds to an exponent of 2, explaining the exponent in the power-law behavior. In contrast to this, the data for the infidelity of the 3×3 -subspace solution ($R_i|R^{[3 \times 3]}$) (dashed black lines) suggests that this is independent of ϵ on the right hand side of the plot, where all lines for different systems sizes seem to be constant. This is in agreement with eq. 6.47, where we found that the states do not depend on the strength of ϵ . The higher order correction that we see in the full problem does not enter here because we truncated the state correction at first order. For increasing system size, the three lines saturate at decreasing infidelity, which is explained by the finite size of the system, where the symmetry broken fixed points (eq. 6.48) are not exactly orthogonal.

We identify the transition to a different regime, $\gamma \gg \epsilon$, which sets in for smaller ϵ if we increase the system size. This is indicated by a minimum of the infidelity, after which decreasing ϵ leads to the approximation of the symmetry broken fixed points actually getting worse, since the infidelity is increasing again. While this might seem surprising, it is explained remarkably well by the finite size effect. On a finite system, the degeneracy between the three fixed points is not exact. This means that in order to mix the three states, the perturbation has to have some sufficient strength. If $\epsilon \ll \gamma$, the perturbative fixed points do not capture the symmetry breaking correctly, but just give the fixed point in the trivial symmetry sector (which is always the leading one as explained above). Now the value of the splitting depends on the system size, it scales as $\gamma \sim e^{-N_v}$, which explains the observation that this effect kicks in for smaller ϵ , if we increase the system size N_v . This effect is completely captured on the fixed point subspace, which is incorporated into the infidelity we get from ($R_i|R^{[3 \times 3]}$) (dashed lines), which explains why on the left hand side these exactly coincide with the full problem fixed point.

The iMPS fixed point fits very nicely into this picture: We measure the infidelity per site between the symmetry broken iMPS describing $|R_i\rangle$ and the perturbed iMPS, which corresponds to an “infinite” version of the full problem fixed point $|R_\epsilon\rangle$. In the regime $\epsilon \gg \gamma$ the infidelities match with the finite size systems, however we do not observe a transition to the regime $\gamma \gg \epsilon$, because there is no finite size splitting γ .

iMPS for symmetry breaking fixed points

We observe a numerical problem, when we are in the symmetry broken phase and start with a random initial MPS. In that case, the convergence time drastically increases and the resulting fixed point has complex eigenvalues, when put on a finite ring. This is likely due to the degeneracy in the transfer operator in that phase. The convergence time vastly decreases, if we make a smarter choice on the initial MPS, which is somewhat with hindsight: Note that the symmetry broken fixed points have orthogonal support. If we start with an MPS that has only support in one of the sectors, the method quickly converges to an optimal MPS, which is also only supported in that support region and has real non-negative eigenvalues when put on a finite circle. We confirm this in the Potts case by computing the maximal eigenvalue of the mixed transfer matrix of a converged MPS sandwiched with the physical symmetry operation. The largest eigenvalue of this is far below 1, which tells us that the two states are orthogonal on a large system.

To confirm that we get the correct states, we measure the order parameter on the iMPS (cf. 5.5) $\langle Z \rangle$ against θ . The result is shown in Fig. 6.17. As we can see, the lines quickly coincide, which gives us confidence that the iMPS correctly captures the thermodynamic limit. To confirm this, we go one step further and do a scaling analysis in the vicinity of the critical point. Here we expect a power law behavior, as is well known in the study of critical phenomena. The exponent of the power law for the order parameter is known as β , i.e. $\langle Z \rangle \sim (\theta_c - \theta)^\beta$. By fitting the values close to the transition point to a straight line, we estimate the exponent to be $\beta \approx 0.10$, which is close to the known value $\beta = 1/9$ [80]. We now compute the correlation length, which is present in the fixed point MPS, we found with the iMPS method. It is given by the ratio of the largest eigenvalues of the MPS transfer matrix:

$$\xi = -\frac{1}{\log(\lambda_1/\lambda_0)} \quad (6.50)$$

The result is given in Fig. 6.18a). We then make a scaling analysis to extract the critical exponent of the correlation length, which we find to be $\alpha \approx 0.80$, which is in good agreement with the literature value $\alpha = 8/9$.

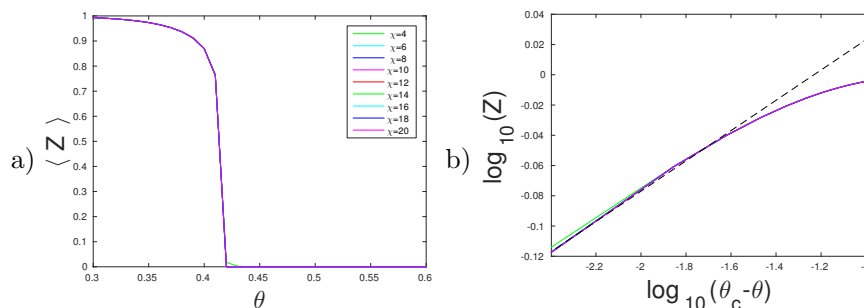


Figure 6.17: Order parameter of the 3-Potts PEPS for increasing bond dimension. a) We see that the order parameter detects the continuous symmetry breaking transition already with moderate bond dimension. b) critical exponent extrapolation: we find $\beta \approx 0.10$

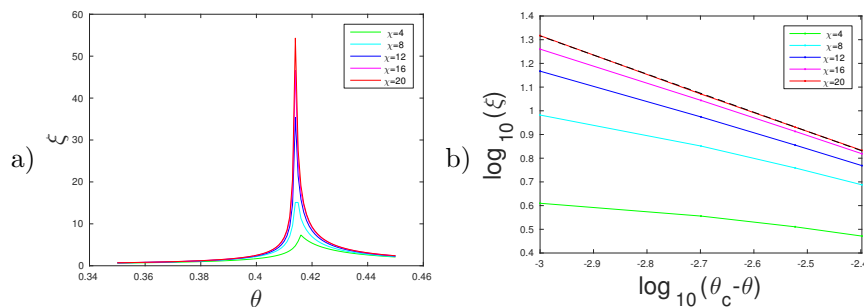


Figure 6.18: a) Correlation length in the fixed point, for increasing bond dimension we capture the divergence increasingly well. b) Scaling analysis in the vicinity of the critical point, the slope of the dashed line is $\alpha \approx 0.80$.

Summary

Let us summarize our findings about the Potts PEPS and this entire chapter, which was about numerical study of three concrete models, which we all found to be PEPS models with spontaneous symmetry breaking. By studying the 3-state Potts PEPS we confirmed that our description of symmetry breaking in the fixed point space is correct also for higher symmetry groups. We identified the relevant degrees of freedom for understanding symmetry breaking in a finite size PEPS model: (1) the presence of long-range order, which implies an asymptotic degeneracy in the transfer operator; (2) the finite-size splitting

in this quasi-degeneracy on finite systems and (3) the existence of symmetry breaking matrix elements, which eventually lift the degeneracy and which (4) then “collapse” to (positive-semi-definite) symmetry broken fixed points. We laid out a complete understanding of the interplay between these ingredients. We furthermore demonstrated that iMPS are suitable for the study of symmetry breaking PEPS models by showing that they fit into this picture. The PEPS fixed point, which are then themselves described by an MPS, furthermore carry the full information about the symmetry breaking in the bulk, which we demonstrated by measuring the order parameter and the correlation length on the iMPS fixed point.

We will continue in the next chapter, where we will study the entanglement properties of the symmetry broken fixed points.

Chapter 7

Entanglement Hamiltonians

It was recently discovered, that the entanglement structure of two-dimensional systems can be captured by a (pseudo-)Hamiltonian. This Hamiltonian is therefore called the entanglement Hamiltonian [37, 11]. It has proven a useful tool to characterize model wave-functions in different contexts [83, 51, 23, 12]. Remarkably, in the PEPS framework, we can formulate an exact “holographic” mapping from the bulk to a boundary state, which is given by the fixed points of the transfer operator, we have been dealing with in all of the previous chapters. Non-surprisingly, entanglement Hamiltonians are used regularly in PEPS models [54, 16, 78].

In this chapter, we introduce the concept of Entanglement Hamiltonians and how they can be realized exactly in the PEPS framework. We will be concerned with the question under what conditions this entanglement Hamiltonian is physical and therefore describes a physical “edge theory”. This condition will be a notion of locality of the Hamiltonian and we will present the tools to determine the locality properties of N -body Hamiltonians.

7.1 The Li-Haldane conjecture

As described in chapter 2, entanglement is what is “non-classical” about quantum theory. Tools have to be developed to measure, characterize and understand entanglement, which is a field with many open questions. We are particularly interested in ways to characterize entanglement in many body systems. One way,

that has been put forward recently, is the method of entanglement Hamiltonians, which takes the bipartite reduced state and interprets it as a thermodynamic quantity. This way, we get access to a (quasi-)Hamiltonian, whose structure might tell us something about the state and its phase. In a seminal paper [37], Li and Haldane observed a remarkable connection between Gibbs states and entanglement properties: The density matrix resulting from the reduced state after an entanglement bipartition can be described by the Gibbs state of some Hamiltonian $\rho(H) = e^{-\beta H}$. They suggested, that instead of just computing the real number $S(\rho)$, one can take a step back and look at the operator ρ . This state is in general a mixed state (it is pure if and only if there is no entanglement between A and B) and following Haldane, we make the claim, that this mixed state is the Gibbs state of an underlying Hamiltonian. Since $\rho \geq 0$, this mapping is in principle always possible

$$\rho = \sum_k p_k |k\rangle \langle k| \quad (7.1)$$

$$\rho_A =: \exp(-H_E) \quad (7.2)$$

$$H_E = -\log(\rho) = -\sum_k \log(p_k) |k\rangle \langle k|, \quad (7.3)$$

with the restriction that the logarithm is only defined on the positive real axis, i.e. we might get infinite energies for singular ρ . Furthermore, the role of β is not clearly defined, since there is no clear concept of temperature and we can absorb it into H . The entanglement entropy of the system is then equivalent to the thermal entropy of this Hamiltonian. The study of the spectrum of this entanglement Hamiltonian is the subject of the field of entanglement spectroscopy, which has the major goal of discovering measures for characterizing phases of many body systems based on their entanglement [56]. The analogy between Hamiltonians and entanglement is not accidental: It hints towards the hope, that entanglement properties can be used to describe and discern phases. For the more familiar case of Hamiltonians, not only the ground state itself but also its low energy excitations characterize the phase. Similarly, the analogy suggests that there is a “low-entanglement” theory above the ground-state, which is captured by the entanglement spectrum and the entanglement Hamiltonian [37].

7.2 Bulk-boundary isometry, Boundary Hamiltonians

Given the PEPS structure in the (physical) quantum state, one can make a connection to a virtual boundary state of the system [16, 17, 82, 67]. We again start with a PEPS (or MPS) on a cylinder (chain), where we assume the cylinder to be extended long enough in the horizontal direction. We then perform an entanglement cut along the vertical line of the cylinder. Our goal is to compute the reduced state on region A (we called it R for region in chapter 2, but now the notion of left and right will enter, which is why we resort to the original bipartite formulation in terms of A and B of chapter 2).

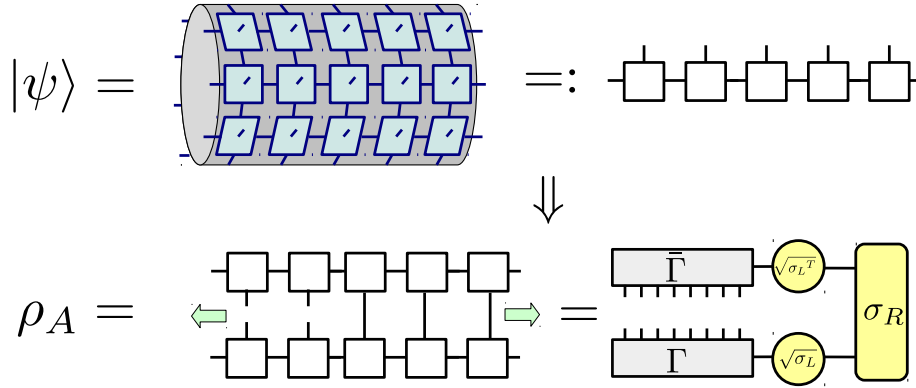


Figure 7.1: The reduced density matrix in a bipartition is isometric to a virtual density matrix $\sigma = \sqrt{\sigma_L} \sigma_R \sqrt{\sigma_L^T}$, if we assume the horizontal system size to be large ($N_h \rightarrow \infty$).

In the computation of the reduced state ρ_A , we trace out over bra and ket layer of part B , which for a large system just gives the right fixed point. The non-trivial part is to compute the left hand side of the reduced state, which has open physical indices. In order to do that, we view the entire left half of the bipartition as one big matrix M : The left index of M is a composite index with all physical indices of $|\psi\rangle$ on system A and the right composite index consists of all the virtual indices along the entanglement cut. We now employ the polar decomposition: For every rectangular matrix M , there exists a decomposition of the form

$$M = \Gamma \cdot P, \quad (7.4)$$

where $P = \sqrt{M^\dagger M} \geq 0$ is a positive semi-definite matrix and $\Gamma^\dagger \Gamma = \mathbb{1}$, i.e. Γ

is an isometry. The polar decomposition can be seen as an implication of the more familiar singular value decomposition (eq. 2.6) by identifying

$$\Gamma = UV^\dagger \quad P = VSV^\dagger, \quad (7.5)$$

which shows that it always exists. We thus learn, that the reduced state can be written as

$$\rho_A = \sum M_\alpha^{\{I_{\text{ket}}\}} \sigma_{R\alpha\beta} (M_\beta^{\{I_{\text{bra}}\}})^\dagger, \quad (7.6)$$

where I is the composite physical index and α (β) the composite virtual index. We now use the polar decomposition and arrive at

$$\rho_A = \Gamma P \sigma_R P \Gamma^\dagger. \quad (7.7)$$

We find a more familiar expression for P , by evaluating the norm of the state $\langle \psi | \psi \rangle = \text{tr}(\sigma_L \sigma_R) = \text{tr} M^\dagger M \sigma_R$, from which we learn that

$$M^\dagger M = P^2 = \sigma_L \quad (7.8)$$

and finally arrive at

$$\rho_A = \Gamma \sqrt{\sigma_L} \sigma_R \sqrt{\sigma_L} \Gamma^\dagger. \quad (7.9)$$

This tells us, that, asymptotically, the spectrum of the reduced state of region A is isometric to the spectrum of a state which lives on the boundary of the system. Note that the boundary state is well defined, as it is positive (semi-)definite, due to

$$\sqrt{\sigma_L} \sigma_R \sqrt{\sigma_L} = \sqrt{\sigma_L} \sqrt{\sigma_R} (\sqrt{\sigma_L} \sqrt{\sigma_R})^\dagger \geq 0. \quad (7.10)$$

The mapping between bulk and boundary state is given by the isometry Γ .

We take eq. (7.9) in conjunction with eq. (7.2), to define the notion of the *boundary Hamiltonian*:

$$H_B = -\log(\sqrt{\sigma_L} \sigma_R \sqrt{\sigma_L}) \quad (7.11)$$

The boundary Hamiltonian is a one-dimensional object acting on the virtual degrees of freedom at the entanglement cut and therefore cannot fully reproduce the two-dimensional entanglement Hamiltonian of the bulk system. However, it is intuitively clear that the entanglement should be dominated by degrees of

freedom at the boundary of the bulk region. This intuition has been substantiated in [54], where the bulk correlation length has been identified with a thermal length at the one-dimensional boundary system. We will be concerned with the analysis of the above defined boundary Hamiltonian and studying what we can learn from it about the bulk quantum system.

7.3 Locality analysis of extended Hermitian operators

We would like to investigate, what kind of terms dominate the Hamiltonian, i.e. whether it is a (quasi-)local Hamiltonian. We define the concept of locality by expressing the Hamiltonian $H \in D^N \times D^N$ in a basis of local Hermitian $D \times D$ matrices acting on the individual N sites of the chain, which we call g_i . This is most conveniently done by finding basis elements which are orthogonal under Hilbert-Schmidt inner product

$$\text{tr}(g_i^\dagger g_j) \propto \delta_{ij} \quad (7.12)$$

The central property is to define $g_i = \mathbb{1}$ as trivial action and any other matrix as non-trivial action. A term of the Hamiltonian is then considered local, if it only acts non-trivially on a few number of neighboring sites. We quantify this notion by constructing strings of N matrices taken from this set:

$$\Omega_I = g_{i_1} \otimes g_{i_2} \otimes \dots \otimes g_{i_N} \quad (7.13)$$

Due to the fact that the trace of a tensor product is the product of traces, these strings are all orthogonal, i.e. the inner product of two strings is zero if they do not coincide,

$$\text{tr}(\Omega_I^\dagger \Omega_J) \propto \delta_{IJ}. \quad (7.14)$$

Crucially, there always exists a local basis spanning $D \times D$ Hermitian matrices and we can thus span the entire set of Hermitian $D^N \times D^N$ matrices and write

$$H = \sum_I h_I \Omega_I. \quad (7.15)$$

The number of Hermitian $N \times N$ matrices is N^2 . The identity element is special and we require it to have no overlap with any other basis element under

the Hilbert-Schmidt norm, which is equivalent to requiring all other elements of the basis to be traceless. Note that for bond dimension $D = N$ this coincides with the definition of generators of $SU(N)$. This is why we can use the Pauli matrices for qubits and the Gell-Mann matrices for qutrits (see appendix A.4 for the explicit matrices).

We now define the concept of k -localness by grouping together all operator strings, that act non-trivially on a string of length k , i.e. on the end points of the string the matrices should be anything but the identity matrix, whereas in-between it can be any operator, also including the identity matrix. Note that this should not be confused with a k -body notion, where one wonders how many operators in a set are non-trivial. The key property is the maximum distance on the string between non-trivial operators.

$$\Omega^{(k)} = \sum_{I \in k\text{-local}} \Omega_I \quad (7.16)$$

which allows us to group the terms of the Hamiltonian according to their locality:

$$H = \sum_k h^{(k)} \Omega^{(k)}. \quad (7.17)$$

It is crucial to note, that the basis set is formed such that any unitary conjugation will maintain the locality structure since it preserves the identity and only maps the non-trivial operators into each other. A k -local string will thus be still k -local under conjugation and just permute the different operators within that class:

$$U^{\otimes N} \Omega^{(k)} U^{\dagger \otimes N} = \sum_{I \in k\text{-local}} U^{\otimes N} \Omega_I U^{\dagger \otimes N} = \sum_{I \in k\text{-local}} \Omega_{\Pi(I)} = \Omega^{(k)} \quad (7.18)$$

The Hamiltonian terms can be filtered out easily thanks to the orthogonality property of the basis elements:

$$h_k(\rho) = \text{tr}(H_E(\rho) \hat{\Omega}^{(k)}) \quad (\in \mathbb{R}), \quad (7.19)$$

where we use dual elements $\text{tr}(\hat{\Omega}^{(k)} \Omega^{(l)}) = \delta_{kl}$. The h_k can be efficiently computed by vectorization. Vectorizing $\hat{\Omega}^{(k)}$ gives a matrix, where each row corresponds to a particular arrangement of putting strings of local operators with non-trivial endpoints of distance k . The columns then correspond to all permu-

tations of this string and of all possible replacements of the particular operators by other operator strings with the same k -locality. Vectorizing H_B gives just one vector. The matrix-vector product between the two then gives another vector, whose norm is the k -locality weight.

$$h_k(\rho) = M(\Omega_{(k)}) \cdot \vec{v}(H_B(\rho)), \quad (7.20)$$

which means computing a weight just consists in one matrix multiplication, making the computation of the weights numerically efficient. The main bottleneck will be the matrix logarithm, which will restrict us system size $N_v = 12$ for qubits (Ising and AKLT PEPS) and $N_v = 8$ for qutrits (Potts PEPS).

Entanglement Hamiltonians and entanglement measures

We would like to point out that the locality weights of the entanglement Hamiltonian, which we will use to make statement about the entanglement structure of PEPS, share important properties with so called entanglement measures [53]. The core ones are additivity, monotonicity and continuity. We first establish, that the matrix logarithm splits under tensor products as

$$\log(A \otimes B) = \log(A) \otimes \mathbf{1} + \mathbf{1} \otimes \log(B), \quad (7.21)$$

which can be easily seen in the eigenbasis of A and B as $\log(\sum a_i b_j |ij\rangle \langle ij|) = \sum (\log(a_i) + \log(b_j)) |ij\rangle \langle ij|$. This implies additivity in the sense that

$$h_k(\rho \otimes \sigma) = h_k(\rho) + h_k(\sigma). \quad (7.22)$$

Similarity transformations and in particular unitaries can be pulled out of the matrix logarithm,

$$\log(X\rho X^{-1}) = X \log(\rho) X^{-1}, \quad (7.23)$$

which implies that the locality weights are invariant under local unitaries

$$h_k(U^{\otimes N} \rho U^{\dagger \otimes N}) = \text{tr}(U^{\otimes N} H_E U^{\dagger \otimes N} \Omega^{(k)}) = \text{tr}(H_E U^{\dagger \otimes N} \Omega^{(k)} U^{\otimes N}) = h_k(\rho). \quad (7.24)$$

Note that here by local we mean that we are restricted to on-site unitaries, which is a stronger restriction than in usual bipartite entanglement, where any unitary on system A should be allowed. However, since we talk about the “range” of entanglement on system A , it is natural to have this stronger constraint, since

long-ranged unitaries could change this. Continuity is given by the continuity of the matrix logarithm $|\log(A + \epsilon X) - \log(A)| < \delta$, from which we take that changing the state infinitesimally leads to infinitesimal changes in the locality weights.

7.4 Entanglement Hamiltonians for symmetry broken PEPS

Entanglement Hamiltonians allow us to define a way to quantify, what could intuitively be described as the concept of the “range” of entanglement in a many body setting by relating the reduced state to an underlying (pseudo-)Hamiltonian via its Gibbs state. We state the formula for the boundary Hamiltonian again, for reference:

$$H_B = -\log(\sqrt{lr}\sqrt{l}), \quad (7.25)$$

where l and r are left and right fixed points of the transfer operator of the particular system. Mapping the quantity encoding the entanglement properties to a Hamiltonian is convenient, because for Hamiltonians, the concept of locality is clear: it’s simply the distance between sites where the Hamiltonian terms act non-trivially. The focus of this chapter is to inquire into the locality structure of entanglement in PEPS. Since this is only accessible by numerical means, we will have to rely on a set of concrete models, which are however universal in the sense of continuous phase transitions and allow us to answer this question in this setting.

Local Hamiltonians for trivial phases

It was demonstrated in [16], that the boundary Hamiltonian in a trivial phase is (quasi-)local (we will omit the prefix “quasi” in the remainder, since we always deal with tails and exponential falloffs). This appeals to the intuition, that entanglement and correlation length are related and the correlation length is finite in a trivial phase. The weights of the boundary Hamiltonian indicate that this behavior breaks down as we approach the critical point, which is again in accordance with the analogy to the (or a) correlation length, which diverges at the critical point. However, it was found, that as we drive the system away from criticality deeper into the ordered phase, the weights stay highly non-local, as depicted in Fig. 7.2. Note that this would be at odds with the above

reasoning, since also the ordered phase has a finite correlation length and for certain models, there even exist duality mappings between both sides of the transition.

Local Hamiltonians for symmetry broken phases

One of the central results of this work is the characterization of the fixed point space of transfer operators. Note, that in equation 7.25 for the boundary Hamiltonian, we deliberately did not specify what exactly we mean by “a fixed point”. This is unambiguous in a trivial phase, since by definition one only has to deal with a unique (left and right) fixed point. As we go into a symmetry breaking phase, this however becomes ambiguous: In a finite system, we typically have a splitting between the largest eigenvalue and the low lying eigenvalues. As we elaborated, this is however an artifact of a finite system. The *correct* fixed points are the ones we dubbed the symmetry breaking fixed points: the fixed points that are positive and stable under arbitrary perturbations. We thus propose to change the perspective and take these fixed points as the starting point for the boundary Hamiltonian analysis:

$$H_B = -\log(\sqrt{L_i}R_i\sqrt{L_i}). \quad (7.26)$$

We in principle get different Hamiltonians labeled by i . However, the different fixed points are all related by local unitary conjugation, which we can pull out of the square root and out of the matrix logarithm, such that also the Hamiltonians will be related by a local unitary. We developed the locality measure precisely such that it be invariant under local unitaries, from which we conclude that it suffices to study one representative H_B .

Ising PEPS

We start with the Ising PEPS, previously studied in [16]. We compute the fixed points again with exact diagonalization and for $\theta < \theta_c$ we construct the symmetry broken states explicitly on an $N_v = 12$ system. We then do the Hamiltonian analysis by choosing a local Hermitian basis, which in this case consists of the Pauli matrices (and the identity matrix). The resulting weights are plotted (semi-)logarithmically, such that straight lines with negative slope indicate exponentially falling of weights and thus a local boundary Hamiltonian. We first plot the “naïve” boundary Hamiltonian weights (Fig. 7.2), which is

computed from the fixed point r_+ disregarding the symmetry breaking. When we set the parameter θ into the symmetry broken phase of the model, the weights of these Hamiltonians clearly tend towards a horizontal line, which indicates long-range characteristics.

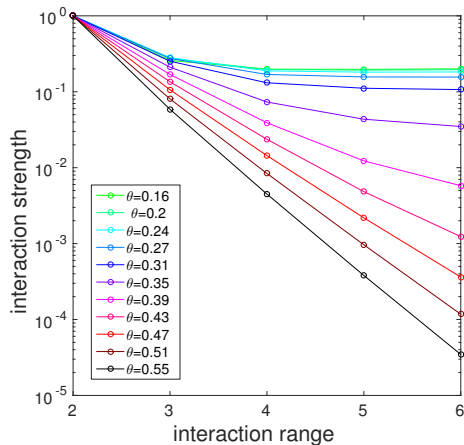


Figure 7.2: The unbroken boundary Hamiltonian of the Ising PEPS, when not taking symmetry breaking into account. Deep in the symmetry broken phase ($\theta < \theta_c = 0.35$) the boundary Hamiltonian is highly non-local, due to GHZ-type long ranged entanglement.

Now to contrast this behavior in the symmetry broken phase, we compute the weights of the symmetry broken boundary Hamiltonian $H_B = \log(r_+ + r_-)$. In fig. 7.3, we plot the weights of this Hamiltonian for several values of θ , where of course $\theta < \theta_c$. We also plot the corresponding weights of the naïve Hamiltonian (dashed lines) for comparison. Note, how the weights are “dual” to each other: the more non-local $\log(r_+)$ gets, the more local the correct symmetry broken Hamiltonian gets.

Nematic AKLT

The nematic AKLT model also hosts a \mathbb{Z}_2 phase transition and as our findings (see chapter 6) suggest, is in the Ising universality class. However the wave-function and the model do not come from a statistical model Rokhsar-Kivelson construction. Despite this, we again find that the symmetry broken fixed points lead to a local boundary Hamiltonian. The Hamiltonian analysis works analogously to the Ising PEPS case. We first plot the unbroken boundary Hamiltonian computed from the finite-size fixed point r_+ , that has the full

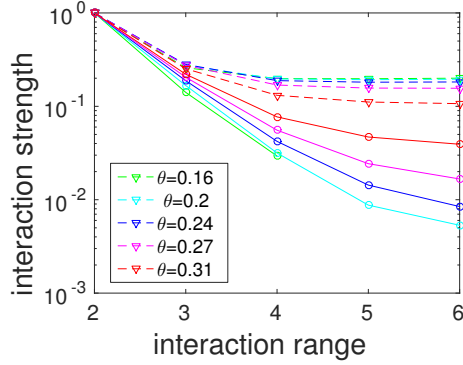


Figure 7.3: The “correct” boundary Hamiltonian of the Ising PEPS gives quasi-local interaction strength decay: Solid lines are the weights of the Hamiltonian obtained from the symmetry broken fixed points (iMPS). For comparison, we plot the unbroken Hamiltonian weights (dashed lines, matching colors, see legend), which behave in a dual way.

symmetry, see Fig. 7.4. In a second step, we then compute the Hamiltonian interaction strengths for the boundary Hamiltonian that generates the symmetry broken fixed points. In Fig. 7.5 we compare the two constructions and their scaling with the interaction range in relation to the driving parameter. We find that the symmetry broken boundary Hamiltonian becomes more local in the symmetry broken phase of the nematic AKLT model.

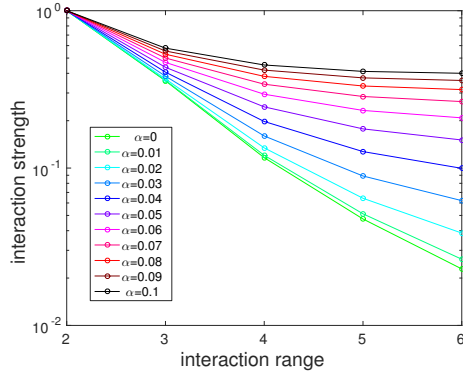


Figure 7.4: Boundary Hamiltonian, when we just take the dominant eigenvector on a finite system ($N = 12$) as the fixed point. This will generically be symmetry-unbroken due to the splitting which suppresses the symmetry breaking. Here, the weights are increasingly non-local as we drive the transition to the symmetry broken phase $\alpha_c \approx 0.045$.

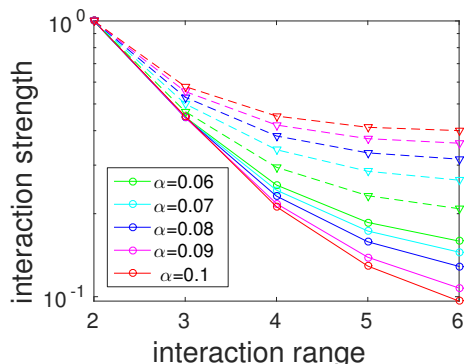


Figure 7.5: Boundary Hamiltonian weight analysis of the nematic AKLT model in the symmetry broken phase. Solid lines are the "correct" Hamiltonian from symmetry broken fixed points (iMPS), the Hamiltonians are more local as we go deeper into the symmetry broken phase. Dashed line are the weights of the Hamiltonians obtained from the unbroken (i.e. symmetric) fixed points (ED) for comparison. Note how they become more non-local for increasing α , a dual picture to the symmetry broken weights.

3-state Potts PEPS

The 3-state Potts PEPS hosts a \mathbb{Z}_3 -symmetry breaking transition at $\theta_c \approx 0.4137$. The \mathbb{Z}_3 symmetry is broken spontaneously for $\theta < \theta_c$. We want to find out, whether our observation that we can find a local boundary Hamiltonian by considering the symmetry broken fixed points is also confirmed for this symmetry class. The higher bond dimension makes the computation slightly more demanding. We employ the iMPS algorithm with a symmetry broken initial condition, which gives the MPS description for the infinite system limit. However, we are limited to small systems by the fact that we have to compute the logarithm of the fixed point density matrix, which cannot be done locally, i.e. we have to explicitly construct the density matrix as a whole. This limits us to system size $N_v = 8$. We again plot the boundary Hamiltonian, we get from the symmetry-unbroken fixed point first (Fig. 7.6) and then in a second step we compare the weights for the symmetry broken phase to the weights of the symmetry broken boundary Hamiltonian (Fig. 7.7).

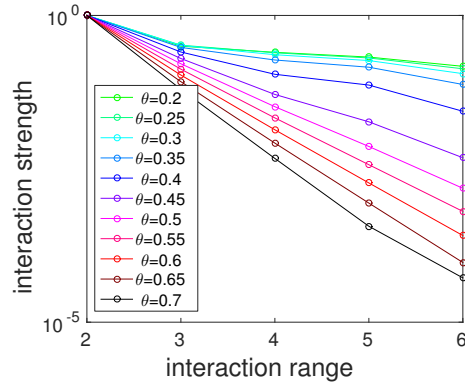


Figure 7.6: Same story for the 3-state Potts PEPS boundary Hamiltonian. We make a locality analysis, here we obtained the unbroken Hamiltonian by iMPS, where we made a twirl over the symmetry. We see again, that the locality weights increase throughout the phase and indicate that there is no local Hamiltonian generating the entanglement due to the artificial GHZ-type long range entanglement.

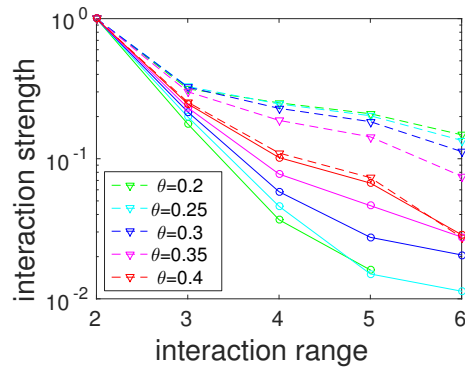


Figure 7.7: Now we compare the unbroken to the broken boundary Hamiltonian. The breaking of the symmetry clearly leads to better scaling of the interaction weights, which indicates that taking the “correct”, i.e. symmetry broken fixed point, there is a local Hamiltonian which generates it.

Summary

Let us summarize what we have done in this chapter. After introducing and motivating the study of entanglement spectra and entanglement Hamiltonians, we derived an exact holographic mapping between the bulk reduced state in a PEPS and its boundary state corresponding left and right fixed points. This led us to consider an instance of the Li-Haldane conjecture, which states that

the entanglement reduced state is a Gibbs state of an underlying Hamiltonian. While it was known before, that this relation is physical in trivial phases without symmetry breaking, we achieved to extend the notion of entanglement Hamiltonians to symmetry broken phases by using the correct symmetry breaking pattern in the PEPS fixed point space, which was derived in the previous chapters, and using the symmetry broken fixed points obtained there, to find their underlying entanglement Hamiltonians to be a *local* Hamiltonian and therefore *physical*.

Chapter 8

Conclusions and Outlook

The central result of this thesis is that *PEPS models*, where symmetries are manifestly encoded in the tensor, can host phases, in which this symmetry of the tensor is spontaneously broken on the global wave-function. We identified long-range order as the suitable criterion for detecting this in finite volume PEPS states. We proved that in a \mathbb{Z}_N -symmetric PEPS, long-range order leads to an N -fold degeneracy in the fixed point space of the PEPS transfer operator under realistic assumptions. We defined a natural notion of symmetry broken states as the ones being stable under arbitrary perturbations, after which we showed that positive fixed points naturally fulfill this stability property. We then showed that the fixed point space of these models always admits such a decomposition into positive fixed points, which we showed to be *unique*, thereby identifying the symmetry breaking mechanism in PEPS as the one *selecting positive fixed points*. We studied prototypical PEPS models, which we verified to host the above described symmetry breaking by extracting the signatures of symmetry breaking in finite PEPS data. We concluded by studying the entanglement structure of the identified “preferred basis”, i.e. the positive fixed points, by studying their entanglement Hamiltonian and analyzing its locality structure, where we found the entanglement Hamiltonian to be local, thereby establishing that symmetry broken phases have an associated *local* entanglement Hamiltonian.

We would like to give a concise perspective on the broader context of this thesis and on open questions.

The broader context of this work are general phase transitions in PEPS, which are a very active area of research. PEPS in particular provide a local description for topological phases and topological phase transitions. These transitions have recently been understood in analogy to symmetry breaking on the PEPS boundary [27, 18], where string order parameters in the bulk were found to be dual to regular order parameters on the boundary. A deep understanding of symmetry breaking in PEPS is therefore also highly relevant for the study of topological phases, which are a candidate for quantum memory and quantum computing [47].

We close with an open question: Do PEPS models with *continuous* symmetry breaking exist? As our presentation of Rokhsar-Kivelson-PEPS in section 3.4 suggested, some classes of PEPS wave-functions can be understood as *thermal* states. The famous Mermin-Wagner theorem [39] tells us, that for thermal states (i.e. at finite temperature) of local Hamiltonians, spontaneous symmetry breaking is forbidden in dimension less than three. Finding a continuous symmetry breaking PEPS would therefore probably give very deep insights on the exact relation between statistical physics and PEPS models.

Appendix A

Appendix

A.1 Perturbation theory for transfer operators

We expand a perturbed transfer operator in a series expansion. This is analogous to Rayleigh-Schrödinger perturbation theory, which we have to modify for non-Hermitian matrices. In order to appeal to intuition, we still use the terminology of “ground state” (i.e. the fixed point(s)) and “excitations” (i.e. eigenstates of the transfer operator with eigenvalue less than 1) We define the full transfer operator

$$\tilde{T} := T_{\mathbb{1}+\epsilon\Lambda} = T + \epsilon T_{[\Lambda]} + \epsilon^2 T_{[\Lambda, \Lambda]} + \dots \quad (\text{A.1})$$

$$|r_k\rangle = |r_k^{(0)}\rangle + \epsilon|r_k^{(1)}\rangle + \epsilon^2|r_k^{(2)}\rangle + \dots \quad (\text{A.2})$$

$$\langle l_k| = \langle l_k^{(0)}| + \epsilon\langle l_k^{(1)}| + \epsilon^2\langle l_k^{(2)}| + \dots \quad (\text{A.3})$$

$$\lambda_k = \lambda_k^{(0)} + \epsilon\lambda_k^{(1)} + \epsilon^2\lambda_k^{(2)} + \dots \quad (\text{A.4})$$

$$\langle l_k|r_m\rangle = \delta_{km} \quad (\text{A.5})$$

First, we are free to set $\langle l_k^{(0)}|r_k^{(0)}\rangle = 1$. In first order, this leads to $\langle l_k^{(0)}|r_k^{(1)}\rangle + \langle l_k^{(1)}|r_k^{(0)}\rangle = 0$, which we fulfill by setting $\langle l_k^{(0)}|r_k^{(1)}\rangle = \langle l_k^{(1)}|r_k^{(0)}\rangle = 0$. We then evaluate the expansion of

$$\tilde{T}|r_k\rangle = \lambda_k|r_k\rangle \quad (\text{A.6})$$

$$\langle l_k|\tilde{T} = \langle l_k|\lambda_k \quad (\text{A.7})$$

order by order. We assume all operators to be completely diagonalizable and smooth as functions of ϵ . The expansion reads

$$\tilde{T}|r_k\rangle = \lambda_k|r_k\rangle = \quad (\text{A.8})$$

$$\{T + \epsilon T_{[\Lambda]} + \epsilon^2 T_{[\Lambda, \Lambda]}\} \left\{ |r_k^{(0)}\rangle + \epsilon |r_k^{(1)}\rangle + \epsilon^2 |r_k^{(2)}\rangle \right\} = \quad (\text{A.9})$$

$$\left\{ \lambda_k^{(0)} + \epsilon \lambda_k^{(1)} + \epsilon^2 \lambda_k^{(2)} \right\} \left\{ |r_k^{(0)}\rangle + \epsilon |r_k^{(1)}\rangle + \epsilon^2 |r_k^{(2)}\rangle \right\}, \quad (\text{A.10})$$

where $T_{[\Lambda, \Lambda]}$ denotes a transfer operator dressed with two matrices on any two sites. The expansion has to be true in any order in ϵ separately:

$$T|r_k^{(0)}\rangle = \lambda_k^{(0)}|r_k^{(0)}\rangle \quad (\text{A.11})$$

$$T|r_k^{(1)}\rangle + T_{[\Lambda]}|r_k^{(0)}\rangle = \lambda_k^{(1)}|r_k^{(0)}\rangle + \lambda_k^{(0)}|r_k^{(1)}\rangle \quad (\text{A.12})$$

We now act with the left eigenvector from the left and find, that (given smoothness and diagonalizability), the standard statement, that the first order eigenvalue correction is given by the matrix element of the perturbation operator in the unperturbed ground state remains true also for non-Hermitian operators:

$$\lambda_k^{(1)} = \langle l_k^{(0)} | T_{[\Lambda]} | r_k^{(0)} \rangle \quad (\text{A.13})$$

In case of a degeneracy, the equation is not uniquely defined, instead we have to diagonalize in the degenerate subspace, which we denote by S :

$$M_{k, \alpha \beta}^{(1)} = \langle l_{k, \alpha}^{(0)} | T_{[\Lambda]} | r_{k, \beta}^{(0)} \rangle = U \lambda_{k, \gamma}^{(1)} V^\dagger \quad (\text{A.14})$$

We will implicitly assume in the following that we are in this ‘‘correct’’ basis. Using, that $\mathbb{1} = \sum_m |r_m^{(0)}\rangle \langle l_m^{(0)}|$, we can rewrite

$$T_{[\Lambda]}|r_{k, \alpha}^{(0)}\rangle = \lambda_{k, \alpha}^{(1)}|r_{k, \alpha}^{(0)}\rangle + \sum_{m \notin S} |r_m^{(0)}\rangle \langle l_m^{(0)} | T_{[\Lambda]} | r_{k, \alpha}^{(0)} \rangle, \quad (\text{A.15})$$

which transforms the first order equation into

$$(\lambda_k^{(0)} - T)|r_{k, \alpha}^{(1)}\rangle = \sum_{m \notin S} |r_m^{(0)}\rangle \langle l_m^{(0)} | T_{[\Lambda]} | r_{k, \alpha}^{(0)} \rangle \quad (\text{A.16})$$

We substitute

$$T = \sum_m \lambda_m^{(0)} |r_m^{(0)}\rangle \langle l_m^{(0)}| \quad (\text{A.17})$$

and have

$$|r_{k,\alpha}^{(1)}\rangle = \sum_{m \notin S} \frac{1}{\lambda_k^{(0)} - \lambda_m^{(0)}} |r_m^{(0)}\rangle \langle l_m^{(0)} | T_{[\Lambda]} | r_{k,\alpha}^{(0)} \rangle, \quad (\text{A.18})$$

which we can do due to the fact that the $|r_m^{(0)}\rangle \langle l_m^{(0)}|$ form a complete basis and the inverse is only problematic for $m \in S$, but this case leads to a zero on both sides and we just have to exclude it from the sum. The correction to the eigenstate is thus in first order given by the matrix elements of the perturbation evaluated between the ground state(s) of the unperturbed model and its excited states, suppressed by the “energy” gap between the two.

A.2 Formal definition of the limit in a two-dimensional PEPS with long-range order

In eq. 4.11, we deal with the double limit $N_h, N_v \rightarrow \infty$. This can be done as follows. Let $\tau_{N_v} = \lim_{N_h} N_h \sigma_{N_h, N_v}^2$, and let $S := \lim_{N_v} \tau_{N_v}$. Then, for any $\epsilon > 0$,

$$\begin{aligned} \exists N_v^0 \forall N_v \geq N_v^0 : \left| \frac{1}{N_v} \tau_{N_v} - S \right| < \frac{\epsilon}{2} \quad \text{and} \\ \exists N_h^0(N_v) \forall N_h \geq N_h^0(N_v) : \frac{1}{N_v} \left| N_h \sigma_{N_h, N_v}^2 - \tau_{N_v} \right| < \frac{\epsilon}{2}. \end{aligned}$$

Thus,

$$\left| \frac{N_h}{N_v} \sigma_{N_h, N_v}^2 - S \right| \leq \epsilon,$$

and finally

$$\sigma^2 = \lim_{N_h, N_v \rightarrow \infty} \sigma_{N_h, N_v}^2 \leq \frac{N_h}{N_v} \sigma_{N_h, N_v}^2 = S,$$

as long as we couple the limits such that both $N_h \geq N_h^0(N_v)$ and $N_h \geq N_v$. (If $S = \infty$, the inequality (4.11) holds trivially.) Let us note that for normal \mathbb{T} , the convergence in Eq. (4.10), Ref. [57], yields a scaling $N_h^0(N_v) \propto N_v / (1 - |\lambda_\alpha(N_v)|)$, such that a non-zero σ^2 for all isotropically coupled limits $N_h/N_v = \text{const.}$ is sufficient to infer that $|\lambda_\alpha| \rightarrow 1$ as $N_v \rightarrow \infty$.

A.3 Taking the thermodynamic limit in the long-range order expression

In this appendix, we give a derivation of eq. 4.10, which was the claim that the following holds:

$$\lim_{N_h \rightarrow \infty} \sum_{p=0}^{N_h-2} \frac{\text{tr} [\mathbb{T}_{O^\dagger} \mathbb{T}^p \mathbb{T}_O \mathbb{T}^{N_h-p-2}]}{\text{tr} [\mathbb{T}^{N_h}]} = 2 \sum_{p=0}^{\infty} \text{tr} [\mathbb{T}_{O^\dagger} \mathbb{T}^p \mathbb{T}_O |r_0\rangle \langle l_0|] .$$

Clearly, without the limit, we can cut the sum in half, i.e.

$$\sum_{p=0}^{N_h-2} \frac{\text{tr} [\mathbb{T}_{\hat{Z}} \mathbb{T}^p \mathbb{T}_{\hat{Z}} \mathbb{T}^{N_h-p-2}]}{\text{tr} [\mathbb{T}^{N_h}]} = S(0, N_{\text{cut}}) + S(N_{\text{cut}} + 1, N_h - 2) ,$$

where $N_{\text{cut}} = \lfloor \frac{N_h}{2} \rfloor - 1$, and

$$S(a, b) := \sum_{p=a}^b \frac{\text{tr} [\mathbb{T}_{\hat{Z}} \mathbb{T}^p \mathbb{T}_{\hat{Z}} \mathbb{T}^{N_h-p-2}]}{\text{tr} [\mathbb{T}^{N_h}]} .$$

Due to cyclicity of the trace, $S(N_{\text{cut}} + 1, N_h - 2) = S(0, N_{\text{cut}} + \kappa)$, where $N_{\text{cut}} + \kappa = N_h - 2 - (N_{\text{cut}} + 1)$ and thus $\kappa = -1, 0$, depending whether N_h is even or odd.

We will now show that

$$\lim_{N_h \rightarrow \infty} S(0, N_{\text{cut}} + \kappa) = \sum_{p=0}^{\infty} \text{tr} [\mathbb{T}_{\hat{Z}} \mathbb{T}^p \mathbb{T}_{\hat{Z}} |r_+\rangle \langle l_+|] .$$

To this end, we use that [72]

$$\|\mathbb{T}^M - |r_+\rangle \langle l_+|\|_{\text{tr}} \leq c\Gamma^M \quad (\text{A.19})$$

where $\Gamma < 1$, as well as

$$|\text{tr} [\mathbb{T}_{\hat{Z}} \mathbb{T}^p \mathbb{T}_{\hat{Z}} X]| \leq \|\mathbb{T}_{\hat{Z}}\|_{\text{op}} \|\mathbb{T}^p\|_{\text{op}} \|\mathbb{T}_{\hat{Z}}\|_{\text{op}} \|X\|_{\text{tr}} \leq \zeta \|X\|_{\text{tr}} \quad (\text{A.20})$$

with $\zeta := (c + 1)\|\mathbb{T}_{\hat{Z}}\|_{\text{op}}^2$, which can be shown using Hölder's inequality, the

submultiplicativity of the operator norm, and

$$\|\mathbb{T}^p\|_{\text{op}} \leq \|\mathbb{T}^p - |r_+\rangle\langle l_+|\|_{\text{op}} + \||r_+\rangle\langle l_+|\|_{\text{op}} \leq \|\mathbb{T}^p - |r_+\rangle\langle l_+|\|_{\text{tr}} + 1 \stackrel{(A.19)}{\leq} c\Gamma^{p+1} \leq c+1,$$

and finally

$$|\text{tr}[\mathbb{T}^{N_h}]| \geq |\text{tr}[|r_+\rangle\langle l_+|]| - |\text{tr}[\mathbb{T}^{N_h} - |r_+\rangle\langle l_+|]| \geq 1 - \|\mathbb{T}^{N_h} - |r_+\rangle\langle l_+|\|_{\text{tr}} \geq 1 - c\Gamma^{N_h}. \quad (\text{A.21})$$

We now have

$$\begin{aligned} \Delta_p &:= \left| \frac{\text{tr}[\mathbb{T}_{\hat{Z}} \mathbb{T}^p \mathbb{T}_{\hat{Z}} \mathbb{T}^{N_h - p - 2}]}{\text{tr}[\mathbb{T}^{N_h}]} - \text{tr}[\mathbb{T}_{\hat{Z}} \mathbb{T}^p \mathbb{T}_{\hat{Z}} |r_+\rangle\langle l_+|] \right| \\ &\leq \left| \frac{\text{tr}[\mathbb{T}_{\hat{Z}} \mathbb{T}^p \mathbb{T}_{\hat{Z}} \mathbb{T}^{N_h - p - 2}]}{\text{tr}[\mathbb{T}^{N_h}]} - \frac{\text{tr}[\mathbb{T}_{\hat{Z}} \mathbb{T}^p \mathbb{T}_{\hat{Z}} |r_+\rangle\langle l_+|]}{\text{tr}[\mathbb{T}^{N_h}]} \right| + \left| \frac{\text{tr}[\mathbb{T}_{\hat{Z}} \mathbb{T}^p \mathbb{T}_{\hat{Z}} |r_+\rangle\langle l_+|]}{\text{tr}[\mathbb{T}^{N_h}]} - \frac{\text{tr}[\mathbb{T}_{\hat{Z}} \mathbb{T}^p \mathbb{T}_{\hat{Z}} |r_+\rangle\langle l_+|]}{\text{tr}[|r_+\rangle\langle l_+|]} \right| \\ &\stackrel{(A.20, A.21)}{\leq} \zeta \frac{\|\mathbb{T}^{N_h - p - 2} - |r_+\rangle\langle l_+|\|_{\text{tr}}}{1 - c\Gamma^{N_h}} + \zeta \||r_+\rangle\langle l_+|\|_{\text{tr}} \left| \frac{\text{tr}[|r_+\rangle\langle l_+|] - \text{tr}[\mathbb{T}^{N_h}]}{\text{tr}[\mathbb{T}^{N_h}] \text{tr}[|r_+\rangle\langle l_+|]} \right| \\ &\stackrel{(A.19, A.21)}{\leq} \zeta \frac{c\Gamma^{N_h - p - 2}}{1 - c\Gamma^{N_h}} + \zeta \||r_+\rangle\langle l_+|\|_{\text{tr}} \frac{c\Gamma^{N_h}}{1 - c\Gamma^{N_h}} \\ &\leq 2\zeta c\nu \Gamma^{N_h - p - 2}, \end{aligned}$$

where in the last step we have assumed that N_h is sufficiently large such that $1 - c\Gamma^{N_h} \geq \frac{1}{2}$, and have introduced $\nu := 1 + \||r_+\rangle\langle l_+|\|_{\text{tr}}$. It follows that

$$\left| S(0, N_{\text{cut}} + \kappa) - \sum_{p=0}^{N_{\text{cut}} + \kappa} \text{tr}[\mathbb{T}_{\hat{Z}} \mathbb{T}^p \mathbb{T}_{\hat{Z}} |r_+\rangle\langle l_+|] \right| \leq \sum_{p=0}^{N_{\text{cut}} + \kappa} \Delta_p \leq \frac{N_h}{2} \times 2\zeta c\nu \Gamma^{N_h/2 - 1}$$

where we have used $N_{\text{cut}} + \kappa \leq \frac{N_h}{2} - 1$ and $N_h - p - 2 \geq N_h/2 - 1$. Clearly, the r.h.s. goes to zero as $N_h \rightarrow \infty$, and thus,

$$\lim_{N_h \rightarrow \infty} S(0, N_{\text{cut}} + \kappa) = \sum_{p=0}^{\infty} \text{tr}[\mathbb{T}_{\hat{Z}} \mathbb{T}^p \mathbb{T}_{\hat{Z}} |r_+\rangle\langle l_+|]$$

as claimed.

A.4 Gell-Mann matrices for locality analysis

In order to meaningfully speak about locality of an N -body operator in chapter 7, we write the operators in terms of a local Hermitian basis (equation 7.15). For bond-dimension $D = N$, these coincide with the generators of the special unitary group $SU(N)$, which are defined as the matrices G , whose exponential leads to a special unitary $N \times N$ matrix, $U = \exp(iG)$. There, unitarity leads to $G^\dagger = -G$ and $\det(U) = 1$ requires $\text{tr}(G) = 0$. When studying the 3-state Potts PEPS, we hence use the well known Gell-Mann matrices, which we list here for completeness:

$$\lambda_1 = \begin{pmatrix} 0 & 1 & 0 \\ 1 & 0 & 0 \\ 0 & 0 & 0 \end{pmatrix} \quad \lambda_2 = \begin{pmatrix} 0 & -i & 0 \\ i & 0 & 0 \\ 0 & 0 & 0 \end{pmatrix} \quad (\text{A.22})$$

$$\lambda_3 = \begin{pmatrix} 1 & 0 & 0 \\ 0 & -1 & 0 \\ 0 & 0 & 0 \end{pmatrix} \quad \lambda_4 = \begin{pmatrix} 0 & 0 & 1 \\ 0 & 0 & 0 \\ 1 & 0 & 0 \end{pmatrix} \quad (\text{A.23})$$

$$\lambda_5 = \begin{pmatrix} 0 & 0 & -i \\ 0 & 0 & 0 \\ i & 0 & 0 \end{pmatrix} \quad \lambda_6 = \begin{pmatrix} 0 & 0 & 0 \\ 0 & 0 & 1 \\ 0 & 1 & 0 \end{pmatrix} \quad (\text{A.24})$$

$$\lambda_7 = \begin{pmatrix} 0 & 0 & 0 \\ 0 & 0 & -i \\ 0 & i & 0 \end{pmatrix} \quad \lambda_8 = \frac{1}{\sqrt{3}} \begin{pmatrix} 1 & 0 & 0 \\ 0 & 1 & 0 \\ 0 & 0 & -2 \end{pmatrix}. \quad (\text{A.25})$$

Acknowledgements

This work would not have been possible without contributions from many people. First and foremost, I would like to express my gratitude towards Norbert Schuch for the supervision of my PhD, I have learned a lot from you and am thankful that you made this project and these years possible. Along the course of this dissertation, I have had the pleasure to meet many brilliant and gentle people and to work at two great institutions. It was both a pleasure and an honor to be part of the Institute for Quantum Information in Aachen, I would like to thank Barbara Terhal, David DiVincenzo and Fabian Hassler as well as H el ene Barton for welcoming me to the group. I am indebted to Kasper Duivendoorn, thank you for your continuous advice and support in scientific and non-scientific matters and for being a good friend. I thank Nikolas, Susanne, Ben and Alessandro in particular for the nice coffee gatherings, which was my favorite pastime at IQI. Furthermore, I would like to thank Firat, Stefan, Pascal, Lauri, Shabir, Daniel, Stefano, Adri an, Christoph, Fabio and all the other people at IQI for the pleasant atmosphere. I furthermore thank Sergej Fischer for organizing the weekly physics/engineers football. The transition to MPQ was smooth, largely thanks to Andrea Kluth. I furthermore thank Ignacio Cirac for having created this amazing institution, where I met many great people. Mohsin, I will miss sharing the office with you, it was the perfect balance between calmness and focussed work and the possibility to discuss problems at basically any time, I learned a lot from you. I also thank Andreas and Ivana for being such nice fellow office mates. I thank Henrik for countless discussions, from which I learned a lot. An integral part of my MPQ routine was the table-tennis, thanks for all the fun, Henrik, Dr. Johannes, Johannes, Tao, Alessandro and Andr as. I thank Andrew and Antoine for various discussions and for organizing the Friday beers and the whole theory group for the nice time at MPQ. I thank Monika Wild for finding a house for me including my

great flatmates Nionios and Sabine. I thank my good friends who helped me at various occasions, with respect to this thesis and in other matters. Last but not least I would like to express gratitude to my family, first of all my parents Michael and Irene for being there for me. I am especially indebted to my sisters Isabelle and Valerie for encouragement and advice throughout my life in general and during the course of my PhD.

Bibliography

- [1] Ian Affleck, Tom Kennedy, Elliott H. Lieb, and Hal Tasaki. Rigorous results on valence-bond ground states in antiferromagnets. *Phys. Rev. Lett.*, 59:799–802, Aug 1987.
- [2] Ian Affleck, Tom Kennedy, Elliott H. Lieb, and Hal Tasaki. Valence bond ground states in isotropic quantum antiferromagnets. *Comm. Math. Phys.*, 115(3):477–528, 1988.
- [3] Luigi Amico, Rosario Fazio, Andreas Osterloh, and Vlatko Vedral. Entanglement in many-body systems. *Rev. Mod. Phys.*, 80:517–576, May 2008.
- [4] A. Arias, A. Gheondea, and S. Gudder. Fixed points of quantum operations. *Journal of Mathematical Physics*, 43(12):5872–5881, 2002.
- [5] R. Augusiak, F. M. Cucchietti, and M. Lewenstein. *Many-Body Physics from a Quantum Information Perspective*, pages 245–294. Springer Berlin Heidelberg, Berlin, Heidelberg, 2012.
- [6] John S Bell. On the Einstein Podolsky Rosen paradox. *Physics*, 1(3):195–290, 1964.
- [7] Robin Blume-Kohout, Hui Khoon Ng, David Poulin, and Lorenza Viola. Characterizing the Structure of Preserved Information in Quantum Processes. *Phys. Rev. Lett.*, 100:030501, Jan 2008.
- [8] Fernando G. S. L. Brandão and Michał Horodecki. Exponential Decay of Correlations Implies Area Law. *Communications in Mathematical Physics*, 333(2):761–798, 2015.
- [9] Paul Busch and Javed Singh. Lüders theorem for unsharp quantum measurements. *Physics Letters A*, 249(1):10 – 12, 1998.

-
- [10] P.M. Chaikin and T.C. Lubensky. *Principles of Condensed Matter Physics*. Cambridge University Press, 2000.
- [11] Anushya Chandran, M. Hermanns, N. Regnault, and B. Andrei Bernevig. Bulk-edge correspondence in entanglement spectra. *Phys. Rev. B*, 84:205136, Nov 2011.
- [12] Xiao Chen and Eduardo Fradkin. Quantum entanglement and thermal reduced density matrices in fermion and spin systems on ladders. *Journal of Statistical Mechanics: Theory and Experiment*, 2013(08):P08013, 2013.
- [13] Xie Chen, Zheng-Cheng Gu, and Xiao-Gang Wen. Classification of gapped symmetric phases in one-dimensional spin systems. *Phys. Rev. B*, 83:035107, Jan 2011.
- [14] Man-Duen Choi. A schwarz inequality for positive linear maps on c^* -algebras. *Illinois J. Math.*, 18(4):565–574, 12 1974.
- [15] J. Ignacio Cirac, Spyridon Michalakis, David Pérez-García, and Norbert Schuch. Robustness in projected entangled pair states. *Phys. Rev. B*, 88:115108, Sep 2013.
- [16] J. Ignacio Cirac, Didier Poilblanc, Norbert Schuch, and Frank Verstraete. Entanglement spectrum and boundary theories with projected entangled-pair states. *Phys. Rev. B*, 83:245134, Jun 2011.
- [17] J.I. Cirac, D. Pérez-García, N. Schuch, and F. Verstraete. Matrix product density operators: Renormalization fixed points and boundary theories. *Annals of Physics*, pages –, 2016.
- [18] Kasper Duivenvoorden, Mohsin Iqbal, Jutho Haegeman, Frank Verstraete, and Norbert Schuch. Entanglement phases as holographic duals of anyon condensates, 2017. arXiv:1702.08469v1.
- [19] A. Einstein, B. Podolsky, and N. Rosen. Can Quantum-Mechanical Description of Physical Reality Be Considered Complete? *Phys. Rev.*, 47:777–780, May 1935.
- [20] J. Eisert, M. Cramer, and M. B. Plenio. *Colloquium* : Area laws for the entanglement entropy. *Rev. Mod. Phys.*, 82:277–306, Feb 2010.

- [21] David E. Evans and Raphael Høegh-Krohn. Spectral Properties of Positive Maps on C^* -Algebras. *Journal of the London Mathematical Society*, s2-17(2):345–355, 1978.
- [22] M. Fannes, B. Nachtergaele, and R. F. Werner. Finitely correlated states on quantum spin chains. *Comm. Math. Phys.*, 144(3):443–490, 1992.
- [23] Lukasz Fidkowski. Entanglement Spectrum of Topological Insulators and Superconductors. *Phys. Rev. Lett.*, 104:130502, Apr 2010.
- [24] David Pérez García, F Verstraete, MM Wolf, and JI Cirac. PEPS as unique ground states of local Hamiltonians. *Quant. Inf. Comp.*, 8:0650–0663, 2008.
- [25] Yimin Ge and Jens Eisert. Area laws and efficient descriptions of quantum many-body states. *New Journal of Physics*, 18(8):083026, 2016.
- [26] Jutho Haegeman and Frank Verstraete. Diagonalizing transfer matrices and matrix product operators: a medley of exact and computational methods, 2016. arXiv:1611.08519v1.
- [27] Jutho Haegeman, Valentin Zauner, Norbert Schuch, and Frank Verstraete. Shadows of anyons and the entanglement structure of topological phases. *Nature communications*, 6, 2015.
- [28] M B Hastings. An area law for one-dimensional quantum systems. *Journal of Statistical Mechanics: Theory and Experiment*, 2007(08):P08024, 2007.
- [29] Bas Hensen, H Bernien, AE Dréau, A Reiserer, N Kalb, MS Blok, J Ruitenberg, RFL Vermeulen, RN Schouten, C Abellán, et al. Loophole-free Bell inequality violation using electron spins separated by 1.3 kilometres. *Nature*, 526(7575):682–686, 2015.
- [30] R.A. Horn and C.R. Johnson. *Matrix Analysis*. Cambridge University Press, 1990.
- [31] Ryszard Horodecki, Paweł Horodecki, Michał Horodecki, and Karol Horodecki. Quantum entanglement. *Rev. Mod. Phys.*, 81:865–942, Jun 2009.
- [32] P. Horsch and W. von der Linden. Spin-correlations and low lying excited states of the spin-1/2 Heisenberg antiferromagnet on a square lattice. *Zeitschrift für Physik B Condensed Matter*, 72(2):181–193, 1988.

- [33] Ernst Ising. Beitrag zur Theorie des Ferromagnetismus. *Zeitschrift für Physik*, 31(1):253–258, 1925.
- [34] Elias Jarlebring. Lecture notes in numerical linear algebra. *KTH Stockholm*, 2015.
- [35] Tohru Koma and Hal Tasaki. Symmetry breaking and finite-size effects in quantum many-body systems. *Journal of Statistical Physics*, 76(3):745–803, 1994.
- [36] H. A. Kramers and G. H. Wannier. Statistics of the Two-Dimensional Ferromagnet. Part I. *Phys. Rev.*, 60:252–262, Aug 1941.
- [37] Hui Li and F. D. M. Haldane. Entanglement Spectrum as a Generalization of Entanglement Entropy: Identification of Topological Order in Non-Abelian Fractional Quantum Hall Effect States. *Phys. Rev. Lett.*, 101:010504, Jul 2008.
- [38] Göran Lindblad. A General No-Cloning Theorem. *Letters in Mathematical Physics*, 47(2):189–196, 1999.
- [39] N. D. Mermin and H. Wagner. Absence of Ferromagnetism or Antiferromagnetism in One- or Two-Dimensional Isotropic Heisenberg Models. *Phys. Rev. Lett.*, 17:1133–1136, Nov 1966.
- [40] Andras Molnar, Norbert Schuch, Frank Verstraete, and J. Ignacio Cirac. Approximating Gibbs states of local Hamiltonians efficiently with projected entangled pair states. *Phys. Rev. B*, 91:045138, Jan 2015.
- [41] Alexander Müller-Hermes, J Ignacio Cirac, and Mari Carmen Bañuls. Tensor network techniques for the computation of dynamical observables in one-dimensional quantum spin systems. *New Journal of Physics*, 14(7):075003, 2012.
- [42] M.A. Nielsen and I.L. Chuang. *Quantum Computation and Quantum Information*. Cambridge Series on Information and the Natural Sciences. Cambridge University Press, 2000.
- [43] Lars Onsager. Crystal Statistics. I. A Two-Dimensional Model with an Order-Disorder Transition. *Phys. Rev.*, 65:117–149, Feb 1944.
- [44] R. Orús and G. Vidal. Infinite time-evolving block decimation algorithm beyond unitary evolution. *Phys. Rev. B*, 78:155117, Oct 2008.

- [45] Román Orús. A practical introduction to tensor networks: Matrix product states and projected entangled pair states. *Annals of Physics*, 349:117 – 158, 2014.
- [46] Tobias J Osborne. Hamiltonian complexity. *Reports on Progress in Physics*, 75(2):022001, 2012.
- [47] Jiannis K Pachos. *Introduction to topological quantum computation*. Cambridge University Press, 2012.
- [48] R. Peierls. On Ising’s model of ferromagnetism. *Mathematical Proceedings of the Cambridge Philosophical Society*, 32(3):477–481, 10 1936.
- [49] Asher Peres. Separability Criterion for Density Matrices. *Phys. Rev. Lett.*, 77:1413–1415, Aug 1996.
- [50] David Perez-Garcia, Frank Verstraete, Michael Wolf, and Ignacio Cirac. Matrix Product State Representations. *Quantum Inf. Comput.*, 7(5&6):401–430, July 2007.
- [51] Ingo Peschel and Viktor Eisler. Reduced density matrices and entanglement entropy in free lattice models. *Journal of Physics A: Mathematical and Theoretical*, 42(50):504003, 2009.
- [52] Robert N. C. Pfeifer, Glen Evenbly, Sukhwinder Singh, and Guifre Vidal. NCON: A tensor network contractor for MATLAB, 2014. arXiv:1402.0939v3.
- [53] Martin B Plenio and Shashank Virmani. An introduction to entanglement measures, 2005.
- [54] Didier Poilblanc. Entanglement Spectra of Quantum Heisenberg Ladders. *Phys. Rev. Lett.*, 105:077202, Aug 2010.
- [55] R. B. Potts. Some generalized order-disorder transformations. *Mathematical Proceedings of the Cambridge Philosophical Society*, 48(1):106–109, 001 1952.
- [56] Xiao-Liang Qi, Hosho Katsura, and Andreas W. W. Ludwig. General Relationship between the Entanglement Spectrum and the Edge State Spectrum of Topological Quantum States. *Phys. Rev. Lett.*, 108:196402, May 2012.

- [57] Manuel Rispler, Kasper Duivenvoorden, and Norbert Schuch. Long-range order and symmetry breaking in projected entangled-pair state models. *Phys. Rev. B*, 92:155133, Oct 2015.
- [58] Manuel Rispler, Kasper Duivenvoorden, and Norbert Schuch. \mathbb{Z}_N symmetry breaking in projected entangled pair state models. *Journal of Physics A: Mathematical and Theoretical*, 50(36):365001, 2017.
- [59] Daniel S. Rokhsar and Steven A. Kivelson. Superconductivity and the Quantum Hard-Core Dimer Gas. *Phys. Rev. Lett.*, 61:2376–2379, Nov 1988.
- [60] Y. Saad. *Numerical Methods for Large Eigenvalue Problems: Revised Edition*. Classics in Applied Mathematics. Society for Industrial and Applied Mathematics, 2011.
- [61] S. Sachdev. *Quantum phase transitions*. Cambridge University Press, Cambridge, second ed. edition, 2011.
- [62] Mikel Sanz. *Tensor Networks in Condensed Matter*. PhD thesis, Technische Universität München, 2011.
- [63] Ulrich Schollwöck. The density-matrix renormalization group in the age of matrix product states. *Annals of Physics*, 326(1):96 – 192, 2011. January 2011 Special Issue.
- [64] E. Schrödinger. Discussion of Probability Relations between Separated Systems. *Mathematical Proceedings of the Cambridge Philosophical Society*, 31(4):555–563, 10 1935.
- [65] Norbert Schuch, David Pérez-García, and Ignacio Cirac. Classifying quantum phases using matrix product states and projected entangled pair states. *Phys. Rev. B*, 84:165139, Oct 2011.
- [66] Norbert Schuch, Didier Poilblanc, J. Ignacio Cirac, and David Pérez-García. Resonating valence bond states in the PEPS formalism. *Phys. Rev. B*, 86:115108, Sep 2012.
- [67] Norbert Schuch, Didier Poilblanc, J. Ignacio Cirac, and David Pérez-García. Topological Order in the Projected Entangled-Pair States Formalism: Transfer Operator and Boundary Hamiltonians. *Phys. Rev. Lett.*, 111:090501, Aug 2013.

- [68] Norbert Schuch, Michael M. Wolf, Frank Verstraete, and J. Ignacio Cirac. Computational Complexity of Projected Entangled Pair States. *Phys. Rev. Lett.*, 98:140506, Apr 2007.
- [69] T. D. Schultz, D. C. Mattis, and E. H. Lieb. Two-Dimensional Ising Model as a Soluble Problem of Many Fermions. *Rev. Mod. Phys.*, 36:856–871, Jul 1964.
- [70] R. Shankar. *Principles of Quantum Mechanics*. Springer US, 2012.
- [71] Franco Strocchi. *Symmetry Breaking*, volume 732. Springer, Berlin Heidelberg, 2008.
- [72] Oleg Szehr, David Reeb, and Michael M. Wolf. Spectral Convergence Bounds for Classical and Quantum Markov Processes. *Communications in Mathematical Physics*, 333(2):565–595, 2015.
- [73] Laurens Vanderstraeten, Jutho Haegeman, Philippe Corboz, and Frank Verstraete. Gradient methods for variational optimization of projected entangled-pair states. *Phys. Rev. B*, 94:155123, Oct 2016.
- [74] F. Verstraete and J. I. Cirac. Renormalization algorithms for Quantum-Many Body Systems in two and higher dimensions, 2004. arXiv:cond-mat/0407066v1.
- [75] F. Verstraete, M. M. Wolf, D. Perez-Garcia, and J. I. Cirac. Criticality, the Area Law, and the Computational Power of Projected Entangled Pair States. *Phys. Rev. Lett.*, 96:220601, Jun 2006.
- [76] G. Vidal. Classical Simulation of Infinite-Size Quantum Lattice Systems in One Spatial Dimension. *Phys. Rev. Lett.*, 98:070201, Feb 2007.
- [77] Guifré Vidal. Entanglement monotones. *Journal of Modern Optics*, 47(2-3):355–376, 2000.
- [78] Thorsten B. Wahl, Stefan T. Haßler, Hong-Hao Tu, J. Ignacio Cirac, and Norbert Schuch. Symmetries and boundary theories for chiral projected entangled pair states. *Phys. Rev. B*, 90:115133, Sep 2014.
- [79] Michael M. Wolf. Quantum channels and operations, 2012.
- [80] F. Y. Wu. The Potts model. *Rev. Mod. Phys.*, 54:235–268, Jan 1982.

- [81] C. N. Yang. The Spontaneous Magnetization of a Two-Dimensional Ising Model. *Phys. Rev.*, 85:808–816, Mar 1952.
- [82] S. Yang, L. Lehman, D. Poilblanc, K. Van Acoleyen, F. Verstraete, J. I. Cirac, and N. Schuch. Edge Theories in Projected Entangled Pair State Models. *Phys. Rev. Lett.*, 112:036402, Jan 2014.
- [83] Hong Yao and Xiao-Liang Qi. Entanglement Entropy and Entanglement Spectrum of the Kitaev Model. *Phys. Rev. Lett.*, 105:080501, Aug 2010.